NASA TECHNICAL NOTE

NASA TN D-4343

NASA TN D-4343

WIND-TUNNEL INVESTIGATION OF LATERAL AERODYNAMIC CHARACTERISTICS OF A POWERED FOUR-DUCT-PROPELLER VTOL MODEL IN TRANSITION

by Kenneth P. Spreemann

Langley Research Center
Langley Station, Hampton, Va.

NATIONAL AERONAUTICS AND SPACE ADMINISTRATION • WASHINGTON, D. C. • FEBRUARY 1968

WIND-TUNNEL INVESTIGATION OF LATERAL AERODYNAMIC CHARACTERISTICS OF A POWERED FOUR-DUCT-PROPELLER VTOL MODEL IN TRANSITION

By Kenneth P. Spreemann

Langley Research Center
Langley Station, Hampton, Va.

NATIONAL AERONAUTICS AND SPACE ADMINISTRATION

For sale by the Clearinghouse for Federal Scientific and Technical Information
Springfield, Virginia 22151 – CFSTI price $3.00

WIND-TUNNEL INVESTIGATION OF LATERAL AERODYNAMIC CHARACTERISTICS OF A POWERED FOUR-DUCT-PROPELLER VTOL MODEL IN TRANSITION

By Kenneth P. Spreemann
Langley Research Center

SUMMARY

A wind-tunnel investigation to determine the lateral and directional aerodynamic characteristics of a powered four-duct-propeller 1/5-scale model of a VTOL airplane has been conducted in the 17-foot (5.18-meter) test section of the Langley 300-mph 7- by 10-foot tunnel. The model was tested through a sideslip-angle range at angles of attack of 0°, 8°, and 12° and with duct deflection angles from -5° to 90° at various thrust coefficients from hovering to conventional forward flight.

The initial cruise configuration had neutral directional stability in the power-off low-angle-of-attack conditions (0° and 8°) and became stable at the high-angle-of-attack condition (12°). A larger vertical tail having a higher aspect ratio than was used on the initial configuration provided a slightly stable model in the power-off condition; however, in the power-on condition, the model became unstable in the lower transition-speed range regardless of tail geometry. Tail-wing fairings of various sizes and shapes significantly increased the directional stability.

Differential deflection of the elevons (vanes) in the ducts provided large control increments in roll and yaw through the transition-speed range; however, the total requirements for trim and control will necessitate the use of both elevon deflection and differential propeller thrust throughout the transition-speed range.

INTRODUCTION

As part of a program to study the aerodynamic and control characteristics of a four-duct-propeller VTOL transport airplane configuration, an investigation has been conducted with a 1/5-scale model in the 17-foot (5.18-meter) test section of the Langley 300-mph 7- by 10-foot tunnel.

The stability tests were run in two phases. The first phase dealt principally with attempts to modify the initial configuration to provide a stable model in the longitudinal mode. (See ref. 1.) In the course of the first phase of testing, it was established that

the model had lateral and directional instabilities. The second phase of the investigation, presented in this paper, dealt primarily with the lateral and directional stability and control in transition and various types of modifications employed in attempts to reduce some of the instabilities encountered.

SYMBOLS

The positive sense of forces, moments, and angles is indicated in figure 1 for the complete model and in figure 2 for the ducts, propellers, and elevons. Moments of the complete model are referred to the assumed center-of-gravity location indicated in figure 3. The yawing moments of the propellers are referred to the individual propeller plane.

The units of measure used in this paper are given both in the U.S. Customary Units and in the International System of Units (SI). Details concerning the use of SI, together with physical constants and conversion factors, are given in reference 2.

A_t vertical-tail aspect ratio, $(\text{Span})^2/\text{Area}$

b reference wing span, 7.667 ft (2.337 m)

$C_{l,s}$ rolling-moment coefficient referred to stability axes, M_{Xs}/qSb

$C_{n,p}$ propeller yawing-moment coefficient, $M_{Z,p}/qSb$

$C_{n,s}$ yawing-moment coefficient referred to stability axes, M_{Zs}/qSb

C_P propeller power coefficient, $2\pi Qn/\rho n^3 D^5$

C_T total propeller thrust coefficient based on free-stream dynamic pressure, T_T/qS

$C_{T,1}$ individual propeller thrust coefficient based on free-stream dynamic pressure, pressure, T_p/qS

$C_{T,2}$ individual propeller thrust coefficient based on rotational speed of propeller, $T_p/\rho n^2 D^4$

C_Y side-force coefficient, F_Y/qS

$C_{Y,p}$ propeller side-force coefficient, $F_{Y,p}/qS$

c local chord, ft (m)

$\bar{c}$ mean aerodynamic chord, $\frac{2}{S}\int_0^{b/2} c^2 dy$, ft (m)

D propeller diameter, 1.40 ft (0.427 m)

F_L lift, lbf (N)

F_Y side force, positive toward right along Y-axis, lbf (N)

$F_{Y,p}$ propeller side force, lbf (N)

i_t horizontal-tail, or stabilizer, incidence angle, positive when trailing edge is down, deg

i_w wing incidence angle with respect to fuselage reference line (X-axis), deg

M_{Xs} rolling moment about the X_s-axis, positive clockwise looking forward, ft-lbf (m-N)

$M_{Z,p}$ propeller yawing moment, ft-lbf (m-N)

M_{Zs} yawing moment about the Z_s-axis, positive moment rotates nose to right, ft-lbf (m-N)

n rotational speed of propeller, rps

Q propeller shaft torque, ft-lbf (m-N)

q free-stream dynamic pressure, $\frac{1}{2}\rho V_\infty^2$, lbf/ft^2 (N/m^2)

S wing reference area, 9.0 ft^2 (0.836 m^2)

S_t vertical-tail area, ft^2 (m^2)

T_p thrust of each propeller, lbf (N)

T_T total propeller thrust, thrust plus drag (propeller off) at $\alpha = 0^o$ and $\delta_D = 0^o$, lbf (N)

V_∞ free-stream velocity, ft/sec (m/sec)

X,Y,Z model axes (fig. 1)

X_S,Y_S,Z_S stability axes (fig. 1)

y spanwise distance from plane of symmetry, ft (m)

α model angle of attack of fuselage reference line, deg

β sideslip angle, deg

δ_D duct deflection angle, deg

δ_V elevon or vane deflection angle, deg

θ model pitch angle with respect to fuselage reference line in hovering, deg

ρ mass density of air in free stream, slugs/ft^3 (kg/m^3)

Subscripts:

F front

R rear

Rt right

Lt left

Model components:

H_1,H_2 horizontal stabilizers

V_t vertical tail

MODEL AND APPARATUS

A three-view drawing of the complete four-duct-propeller VTOL model, together with pertinent dimensions, is given in figure 3. The model was mounted on a sting-supported six-component strain-gage balance for measurements of the forces and moments of the complete model. The wing reference area of 9.0 ft^2 (0.836 m^2) and the reference span of 7.667 ft (2.337 m) provided an aspect ratio of 6.54. The reference area and span included the short wing, the projected planform area and span of the rear ducts, and the outboard stabilizer on the ducts. (See fig. 3.)

Thrust was provided by the four ducted propellers, two mounted forward on the fuselage and two mounted rearward at the tips of the short wing (NACA 64A418.5 (modified) airfoil section). Four nacelles were also mounted on the wing to simulate the nacelles of the four engines, which on the full-scale airplane would power the four propellers through shafting and gearing. For the model, however, each propeller was powered by an electric motor in the center body of each duct. Therefore, the duct center bodies were actually larger than they would have been if scaled down from the full-scale airplane. The motors were mounted on strain-gage balances; the two right-hand motors were instrumented to measure the normal force and pitching moment of the propellers, whereas the two left-hand motors were instrumented to measure the side force and yawing moment of the propellers. Thrust and torque were measured on all four propellers.

Details of the ducts and modified lips are shown in figure 4. Each pair of ducts was mounted on a shaft with actuators attached so that the front and rear ducts could be rotated through angle ranges independently of each other. Duct deflection angles were varied from -5^o to 90^o. Details of the various vertical tails used on the model, elevons (vanes) used in the ducts, and horizontal stabilizers used on the rear ducts are shown in figures 5, 6, and 7, respectively. The tail-wing fairings and the vertical fins used on top or bottom of the rear ducts are shown in figures 8 and 9, respectively.

TESTS

The tests were conducted in the 17-foot (5.18-meter) test section of the 300-mph 7- by 10-foot tunnel. The arrangement and calibration of this test section are given in reference 3. The tunnel velocity and the model propeller speed were held constant throughout the sideslip-angle range for a particular run. The wing incidence angle was set at 3^o with respect to the fuselage reference line throughout the investigation. The various thrust coefficients were obtained by varying the tunnel velocity while maintaining a constant model propeller speed. The thrust coefficient C_T was based on the total thrust T_T of the propellers. The total thrust was obtained for the model by taking the difference between the longitudinal force with the propeller operating and the longitudinal

force with the propeller removed at zero angle of attack and zero duct deflection angle. The thrust coefficients of each propeller $(C_{T,1}$ and $C_{T,2})$ were based on the measured thrust of each propeller at each angle of attack.

The Reynolds numbers, based on wing chord or duct chord and free-stream velocity, for the range of thrust coefficients are given in the following table:

C_T	q		V_∞		Reynolds number based on –	
	lbf/ft^2	N/m^2	ft/sec	m/sec	Wing chord	Duct chord
0	10	478.8	91.8	27.98	9.8×10^5	4.8×10^5
.4	10	478.8	91.8	27.98	9.8	4.8
.8	7	335.2	76.7	23.38	8.16	4.0
2.1	3.5	167.6	54.3	16.55	5.8	2.85
7.1	1.3	62.2	34.5	10.52	3.5	1.72
25.0	.42	20.1	18.8	5.73	2.0	.92
60.0	.19	9.1	12.7	3.87	1.34	.66

PRESENTATION OF RESULTS

The results of the investigation are presented in the following figures:

For some tests, propeller data were recorded and are presented as parts of the appropriate figures.

DISCUSSION

Stability

Initial configuration.- Data for the initial configuration are given in figure 10, which shows that the model had neutral directional stability at low angles of attack in the power-off condition. The directional stability was increased at the high angle of attack, 12°.

Figure 11 shows that with the tail off, the model was unstable at all test angles of attack; however, $\partial C_{n,s}/\partial\beta$ was less negative at the high angle of attack. In attempts to improve the stability of the model, larger vertical tails with higher aspect ratios were tried. The results of these changes are given in figure 12, which shows that the higher aspect ratio tail (designated vertical tail 3 and made by extending the span of vertical tail 2) provided a slightly stable configuration in the power-off condition. However, with increases in power (higher values of C_T), the model became progressively less stable. (See figs. 13 and 14.) A comparison of figures 13 and 14 shows the effects of adding a tail-wing fairing (designated tail-wing fairing 1) to the model. This modification provided considerable improvement in the directional stability of the model. In addition, a set of fins (fig. 9) were installed on the rear ducts in a further effort to stabilize the model. Even though these fins were effective throughout the speed range, the model was still unstable in the low-transition-speed range ($C_T = 2.1$). (See fig. 15.)

Revised cruise configuration.- Tuft studies indicated that there was a completely stalled region at the vertical-tail—wing juncture. At this point in the test program, a tail-wing fairing (designated fairing 1 in fig. 8(a)) was adapted to the model. This addition did improve the directional stability, as shown by a comparison of figures 13(b) and 14(c), but the model was again unstable in the low-transition-speed range at $C_T = 2.1$ (fig. 14(d)).

In the second phase of the test program, a larger tail (designated vertical tail 4) with the tail-wing fairing was incorporated on the model. The results are given in figure 16 and indicate that there was some improvement in stability; however, in the high-power low-speed end of the cruise-configuration flight range, the model was neutrally stable or unstable. (See figs. 16(c) and 16(d.) This result would imply that in this speed range differential thrust or some other form of stability augmentation system will be required.

The contributions to the lateral characteristics of various components of the model can be determined from figures 17 and 18.

Transition.- The lateral and directional stability characteristics of the model tested are presented in figure 19, which shows the effects of rotating the ducts from the high-transition-speed range $(\delta_{D,F} = \delta_{D,R} = 15^{o})$ to near hovering $(\delta_{D,F} = \delta_{D,R} = 90^{o})$. From the high-transition-speed range $(C_T = 0.40, \quad \delta_{D,F} = \delta_{D,R} = 15^{o})$ to the lower range $(C_T = 7.1, \quad \delta_{D,F} = \delta_{D,R} = 60^{o})$, the model was stable between sideslip angles of -10^{o} and $+10^{o}$. In the very low transition range $(C_T = 25.0, \quad \delta_{D,F} = \delta_{D,R} = 75^{o}$ and $C_T = 60.0, \quad \delta_{D,F} = \delta_{D,R} = 90^{o})$, the model was directionally stable within a more limited sideslip-angle range.

Control

Cruise configuration.- Figures 20 to 21 show the effectiveness of differential deflection of the elevons (vanes) for roll control at various thrust coefficients. Elevon deflection angles from 0^{o} to 10^{o} or 15^{o} provided proportional increments in roll control in the power-off condition. Beyond these angles the control effectiveness drops off (figs. 20(a) and 21(a)), probably due to the stalling of the elevons at the high angles of attack. Differential deflections of the elevons were more effective in the power-on than in the power-off condition (fig. 21). This increased effectiveness can be attributed to the higher rate of mass flow over the elevons for the power-on condition as compared with that for the power-off condition in which the windmilling propellers retarded the flow through the ducts. With power on, however, large yawing moments are incurred (figs. 21(b) and 21(c)) which would require proportional cross coupling of the roll and yaw controls from differential propeller thrust.

Transition.- Lateral control characteristics in the transition-speed range in which the ducts are rotated from low angles (high speed, $C_T = 0.40$) to the vertical (hovering, $C_T = \infty$) are given in figure 22. When only elevon deflection is used, a problem arises similar to that in the cruise range, previously discussed. As the ducts are rotated up to proceed into the low-transition-speed region and eventually hovering, the differentially deflected elevon control gradually converts from primarily roll control (fig. 22(a)) to yaw control (figs. 22(b) and 22(c)) and eventually becomes all yaw control (fig. 22(f)). Thus a situation exists similar to that in the cruise condition wherein proportional cross coupling of the roll and yaw controls from differential propeller thrust and elevon deflection would be required.

A larger scale model of an earlier version of the present model was tested in the Ames 40- by 80-foot wind tunnel. (See ref. 4.) The earlier configuration had a different fuselage and tail and relatively smaller ducts than the present model. However, the results show the same trends in lateral and directional stability and control as the model of this investigation. The investigations support one another very well, showing that for

an airplane of this type programed cross coupling of controls will be necessary in the transition-speed range.

Effect of Tail-Wing Fairing Size

At the end of the second phase of testing, an investigation of the effects of reducing the size and altering the shape of the tail-wing fairing was undertaken. The lateral aerodynamic characteristics are given in figure 23, which shows that there were only small reductions in the efficiency of this modification as the size was reduced; however, even the smallest fairing provided favorable results.

CONCLUSIONS

A wind-tunnel investigation to determine the static, lateral, and directional stability and control characteristics of a powered four-duct-propeller model of a VTOL airplane indicated the following conclusions:

1. The initial cruise configuration had neutral directional stability in the power-off low-angle-of-attack conditions (0° and 8°) and became stable at the high-angle-of-attack condition (12°).

2. A larger vertical tail with a higher aspect ratio than was used on the initial configuration provided a slightly stable model in the power-off condition; however, in the power-on condition, the model became unstable in the lower transition-speed range regardless of tail geometry.

3. All the tail-wing fairings employed gave significant favorable increments in directional stability.

4. Differential deflection of the elevons (vanes) in the ducts provided large control increments in roll and yaw; however, the total requirements for trim and control will necessitate the use of both elevon deflection and differential propeller thrust throughout the transition-speed range.

5. In the cruise configuration, fins on bottom or top of the rear ducts provided significant increases in the directional stability of the model.

Langley Research Center,
National Aeronautics and Space Administration,
Langley Station, Hampton, Va., September 14, 1967,
721-01-00-23-23.

REFERENCES

1. Spreemann, Kenneth P.: Wind-Tunnel Investigation of Longitudinal Aerodynamic Characteristics of a Powered Four-Duct-Propeller VTOL Model in Transition. NASA TN D-3192, 1966.

2. Mechtly, E. A.: The International System of Units – Physical Constants and Conversion Factors. NASA SP-7012, 1964.

3. Kuhn, Richard E.; and Hayes, William C., Jr.: Wind-Tunnel Investigation of Longitudinal Aerodynamic Characteristics of Three Propeller-Driven VTOL Configurations in the Transition Speed Range, Including Effects of Ground Proximity. NASA TN D-55, 1960.

4. Giulianetti, Demo J.; Biggers, James C.; and Maki, Ralph L.: Longitudinal and Lateral-Directional Aerodynamic Characteristics of a Large-Scale, V/STOL Model With Four Tilting Ducted Fans Arranged in a Dual Tandem Configuration. NASA TN D-3490, 1966.

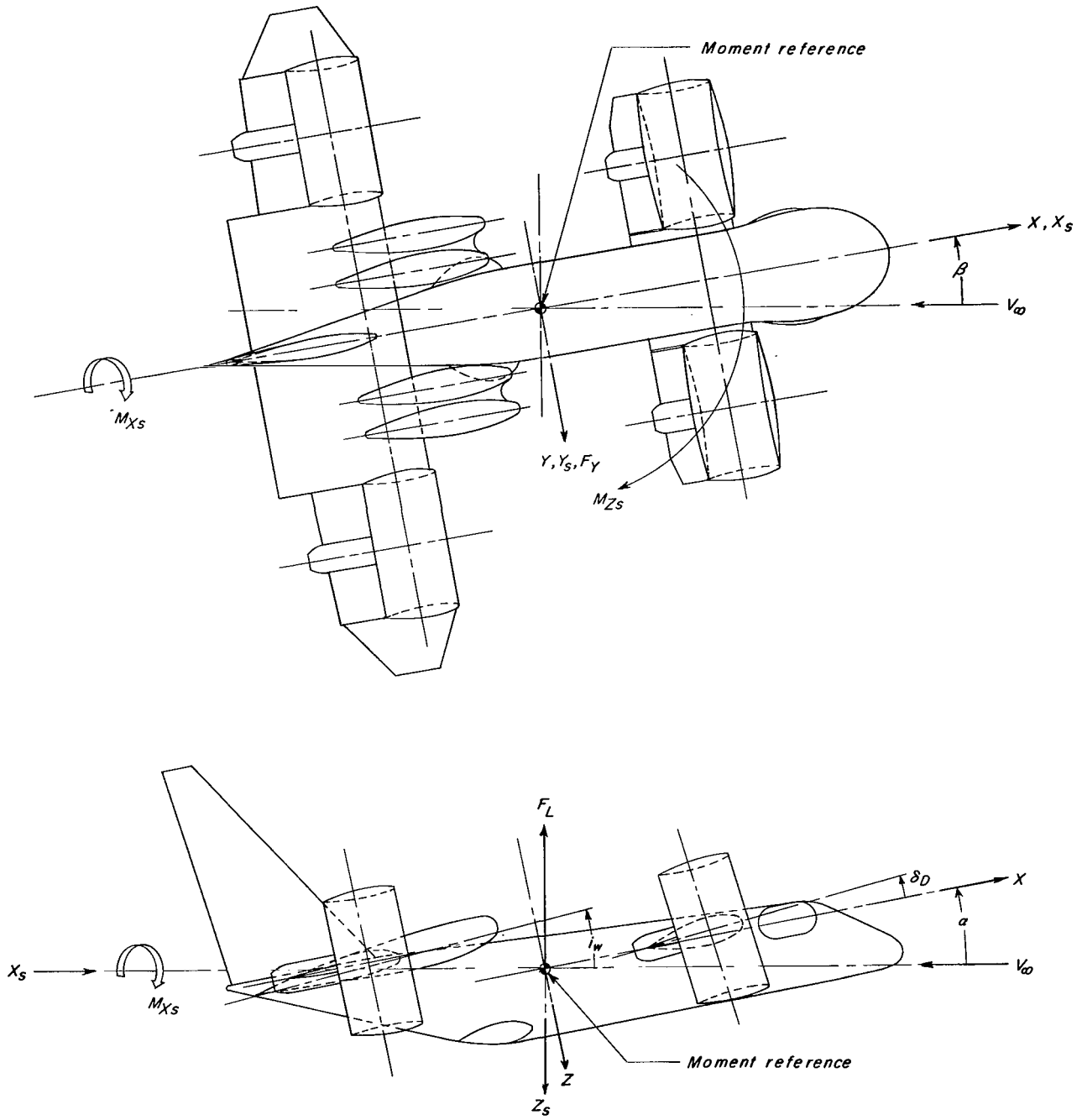

Figure 1.- Conventions used to define positive sense of forces, moments, and angles for the complete model.

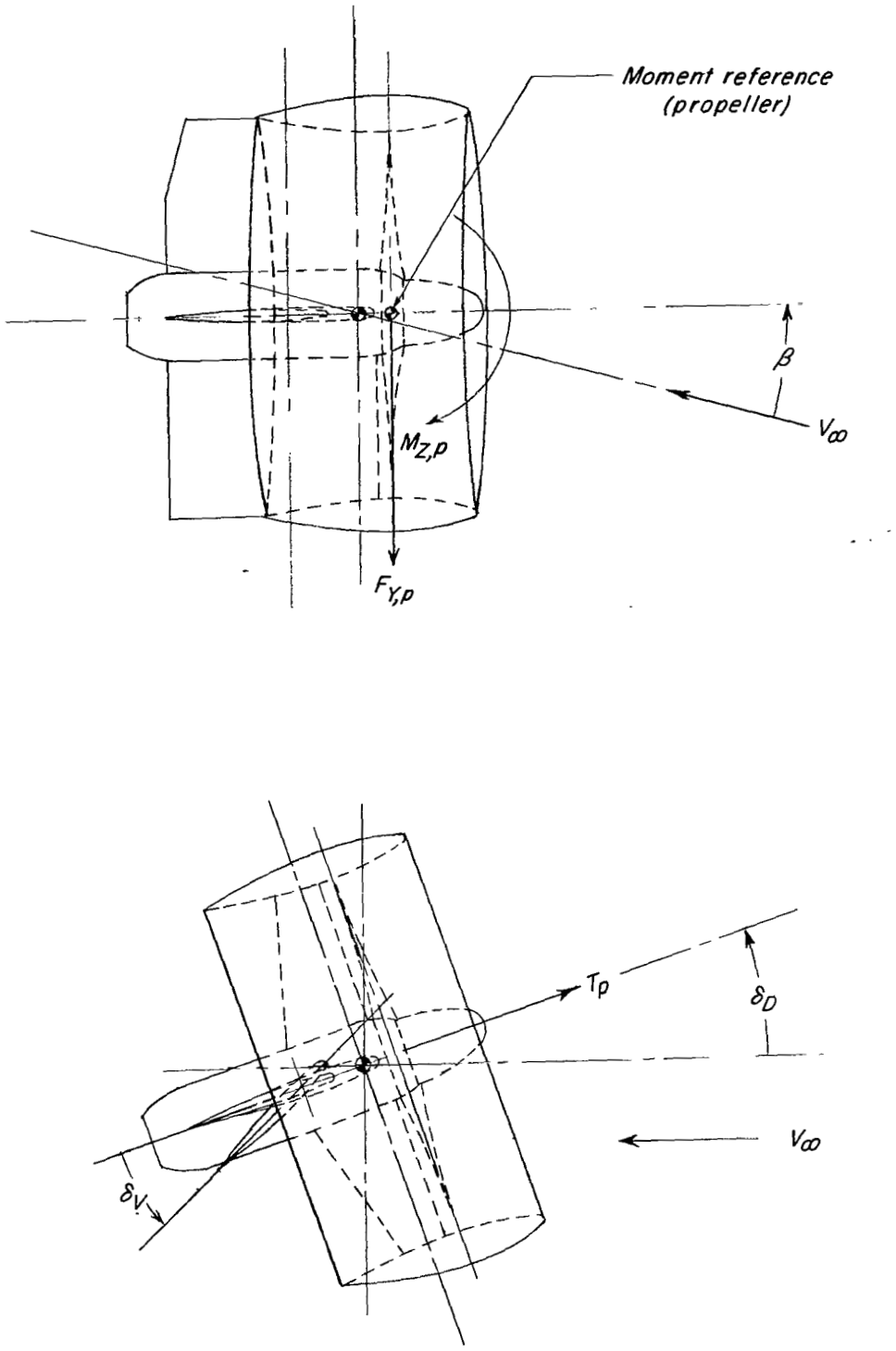

Figure 2.- Conventions used to define positive sense of forces, moments, and angles for the ducts, propellers, and elevons.

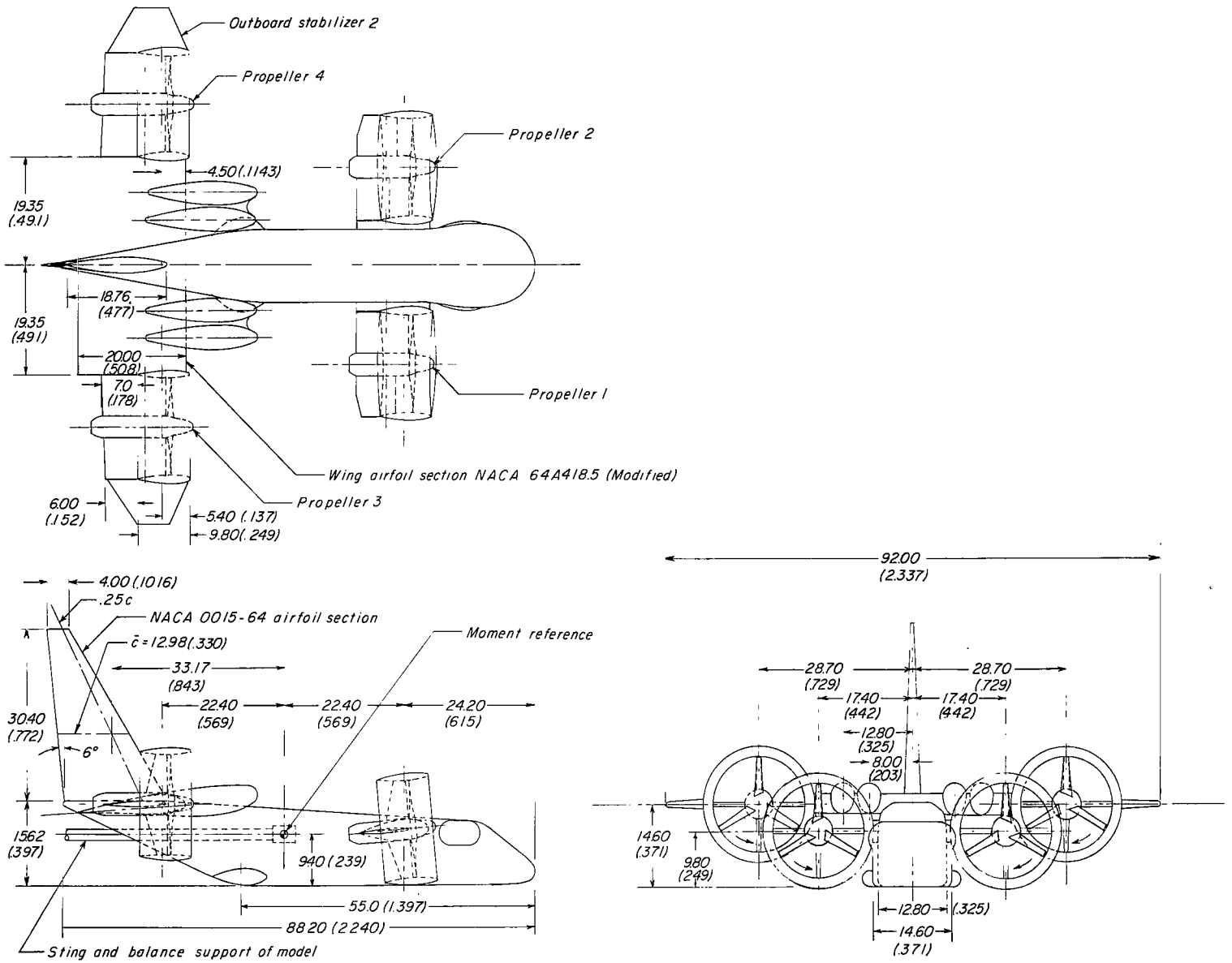

Figure 3.- Drawing of complete model. (Dimensions given first in inches and parenthetically in meters.)

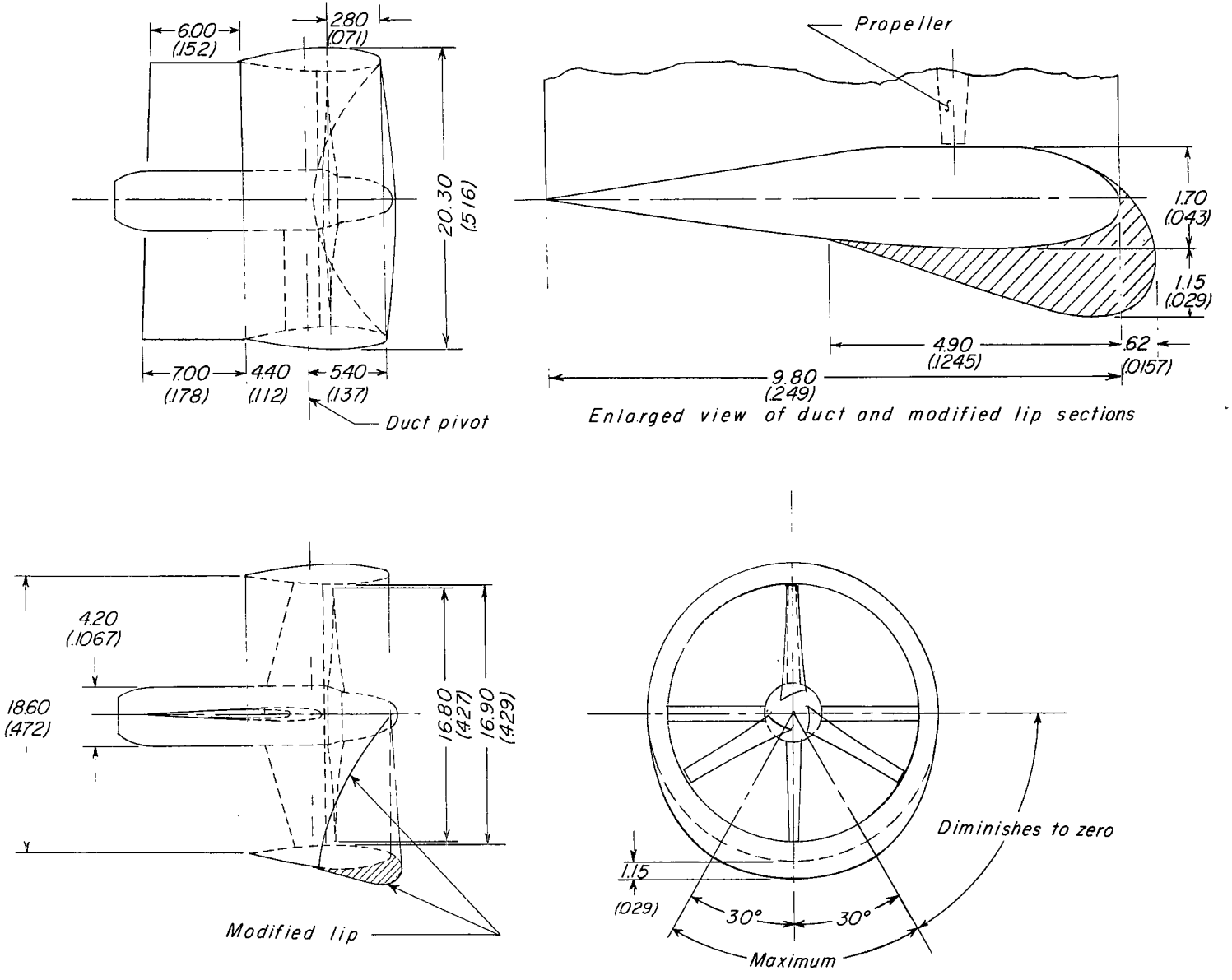

Figure 4.- Details of ducts and modified duct lips. (Dimensions given first in inches and parenthetically in meters.)

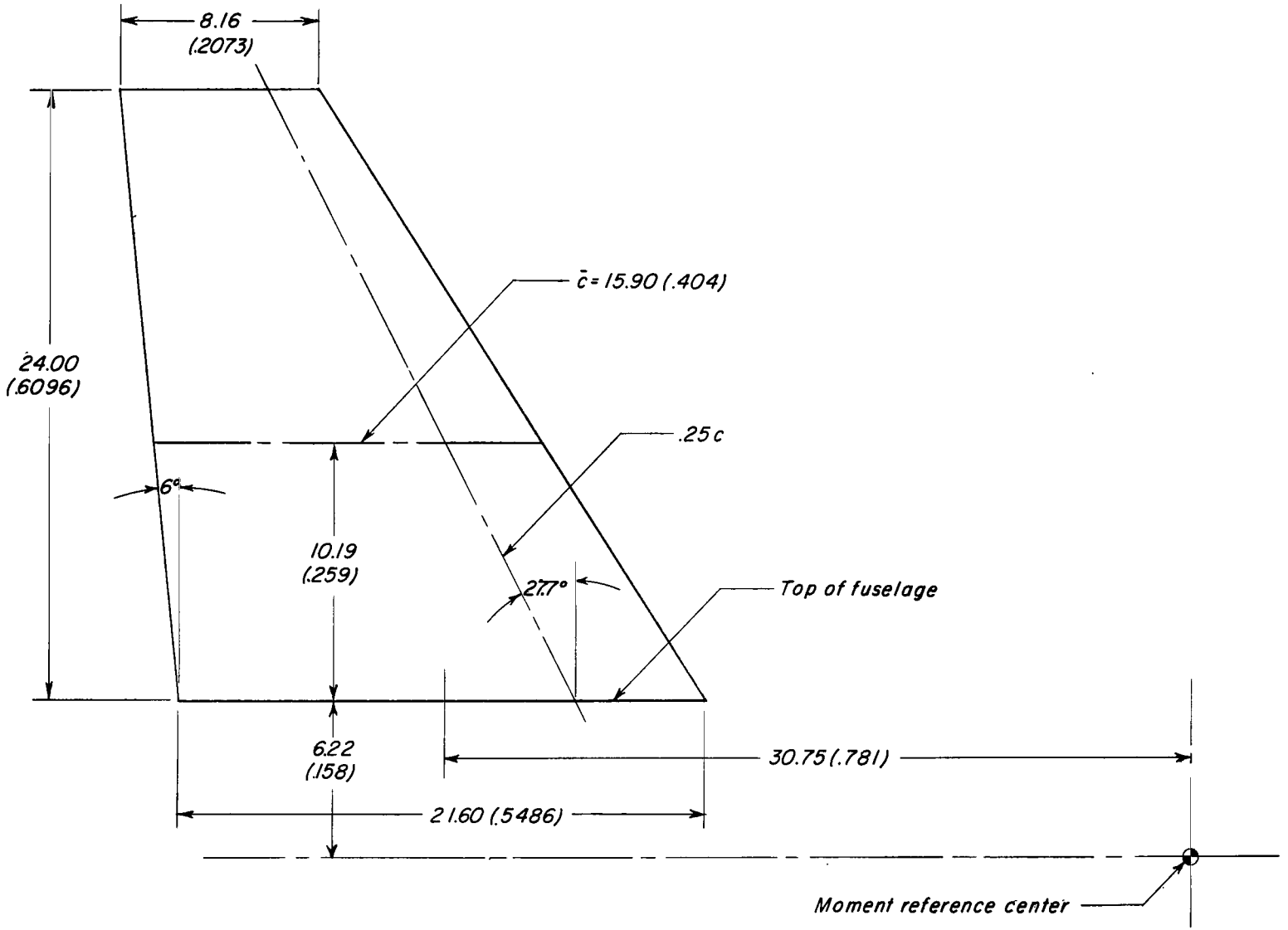

(a) Vertical tail 1; NACA 0015-64 basic airfoil section; A_t = 1.61; S_t = 2.48 ft^2 (0.230392 m^2).

Figure 5.- Details of vertical tails employed on model. (Dimensions given first in inches and parenthetically in meters.)

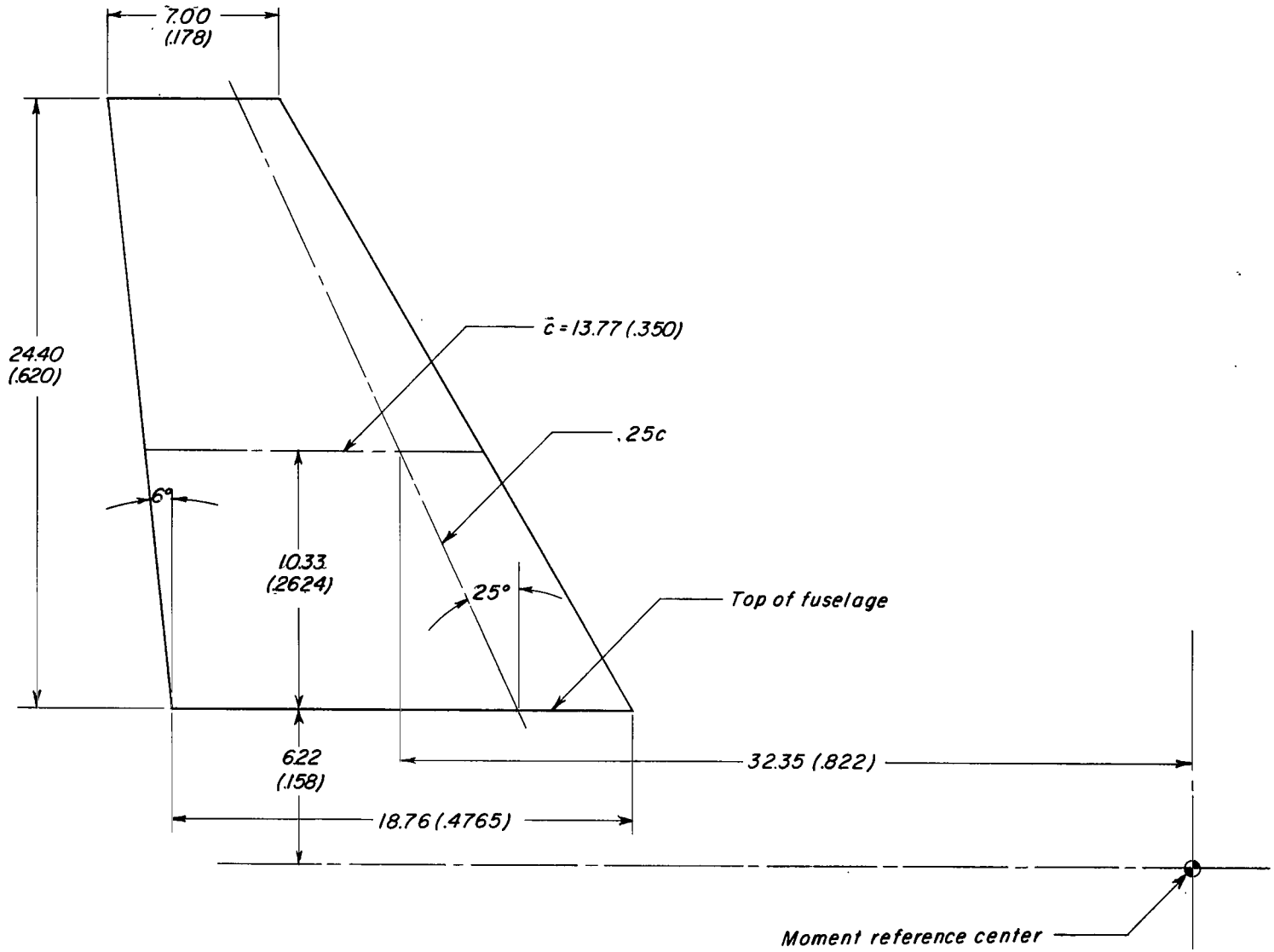

(b) Vertical tail 2; NACA 0015-64 basic airfoil section; A_t = 1.89; S_t = 2.19 ft^2 (0.203451 m^2).

Figure 5.- Continued.

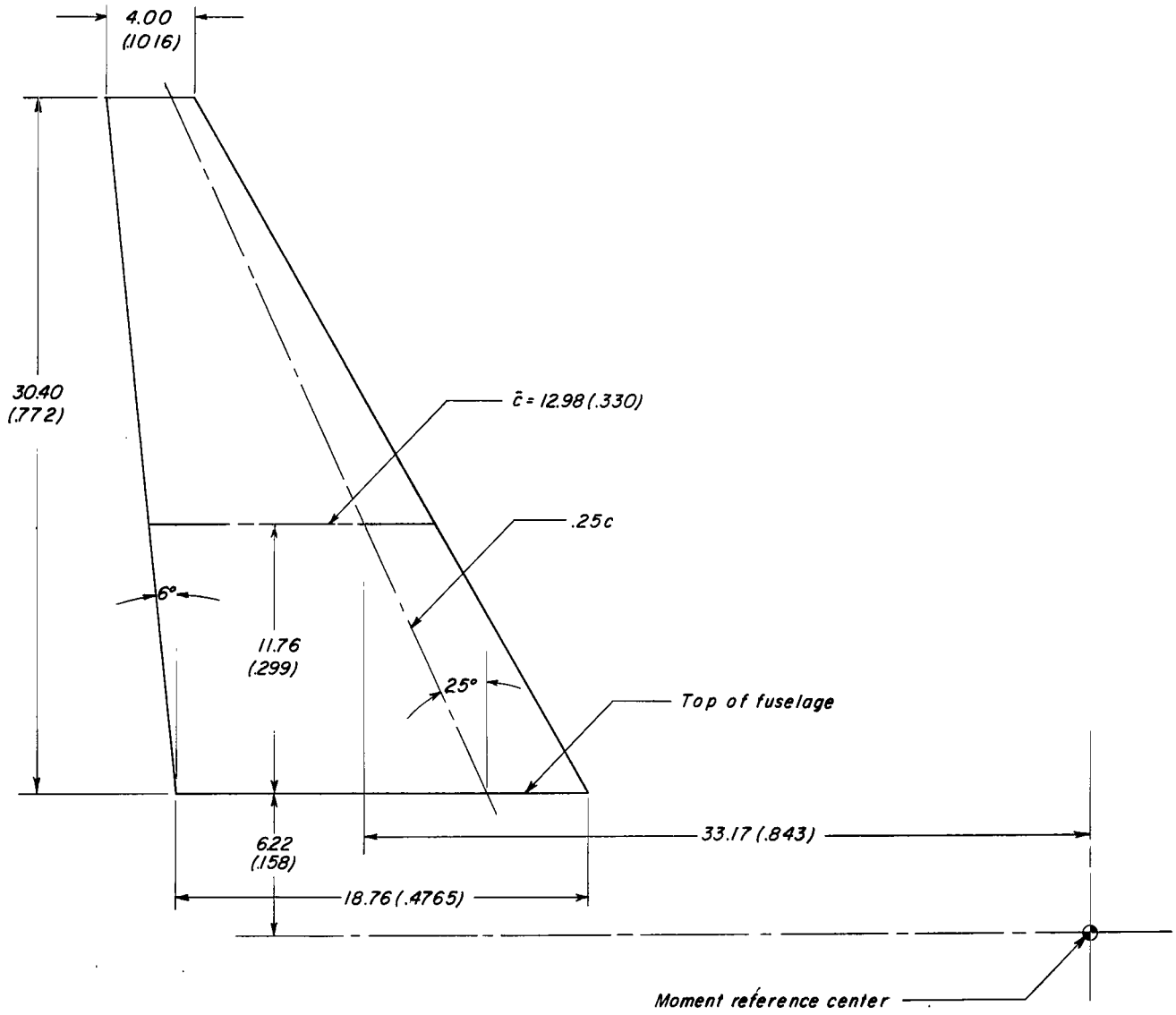

(c) Vertical tail 3; NACA 0015-64 basic airfoil section; A_t = 2.67; S_t = 2.40 ft^2 (0.222960 m^2).

Figure 5.- Continued.

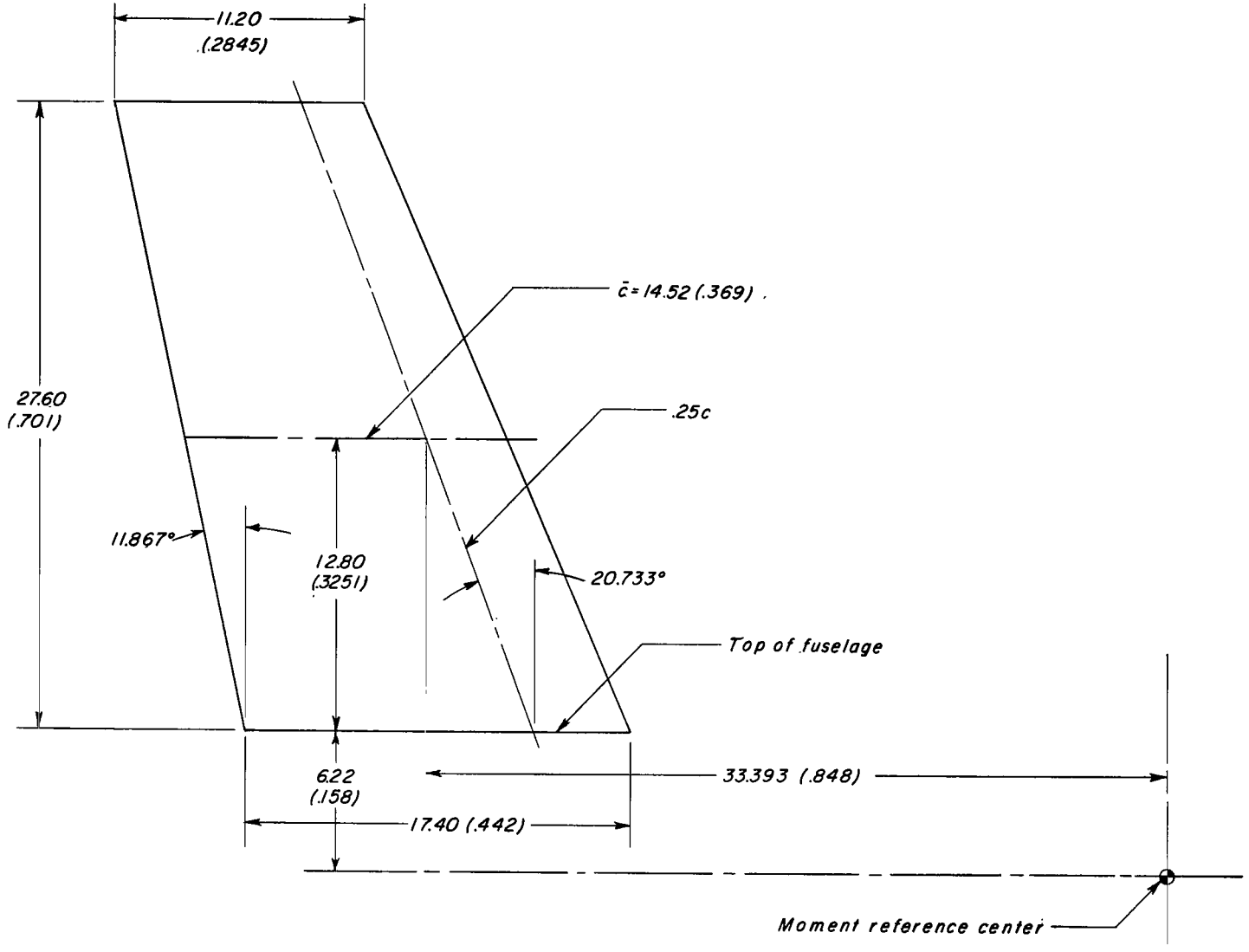

(d) Vertical tail 4; NACA 0010-64 basic airfoil section; A_t = 1.93; S_t = 2.74 ft^2 (0.254546 m^2).

Figure 5.- Concluded.

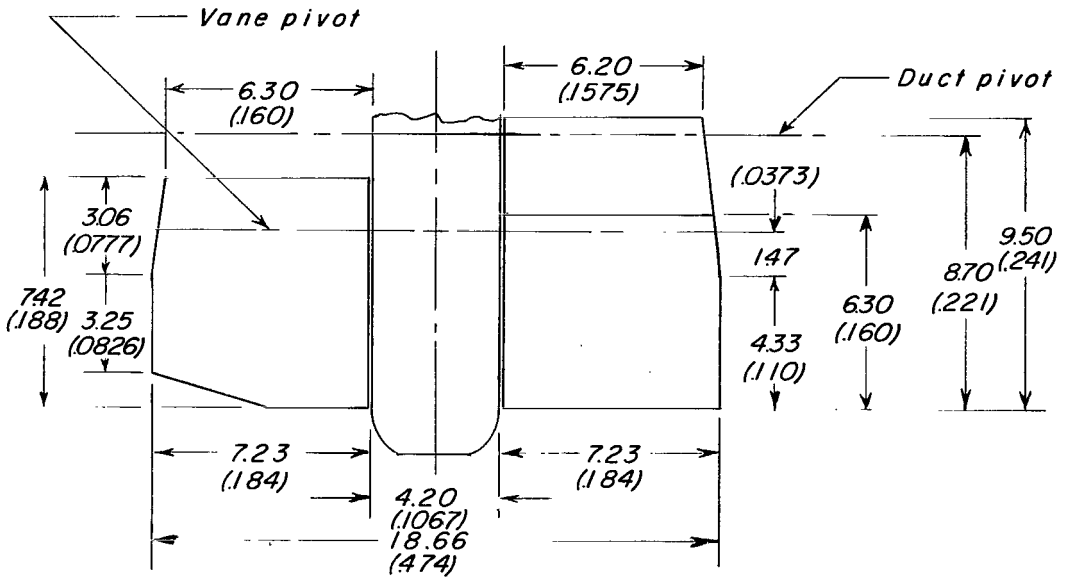

Front left vane

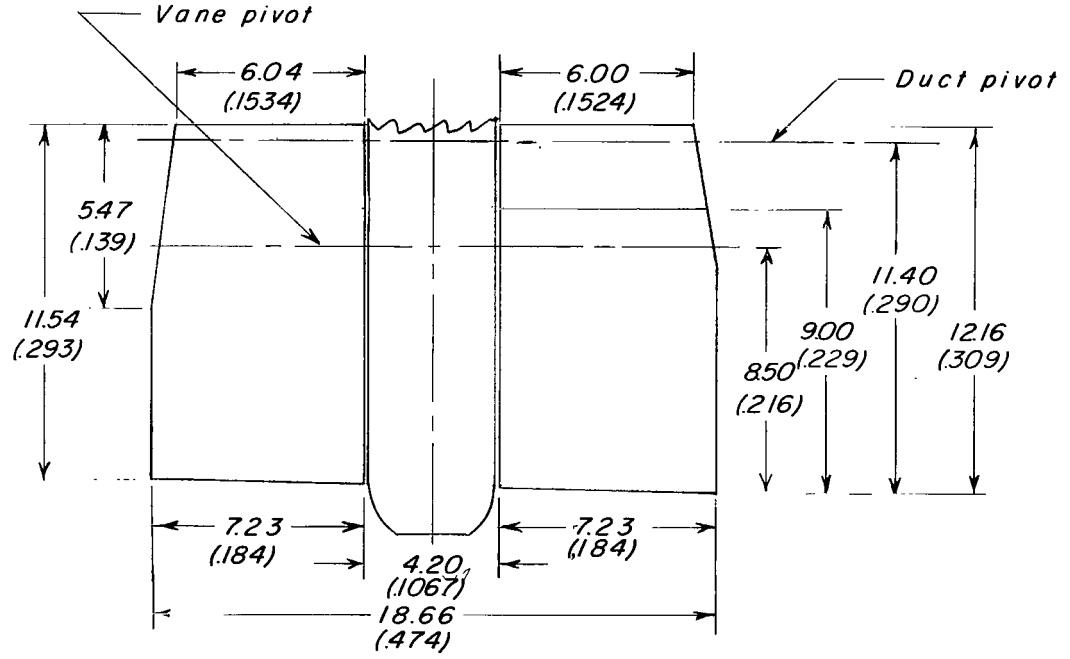

Rear left vane

Figure 6.- Details of elevons (vanes) used in ducts. (Dimensions given first in inches and parenthetically in meters.)

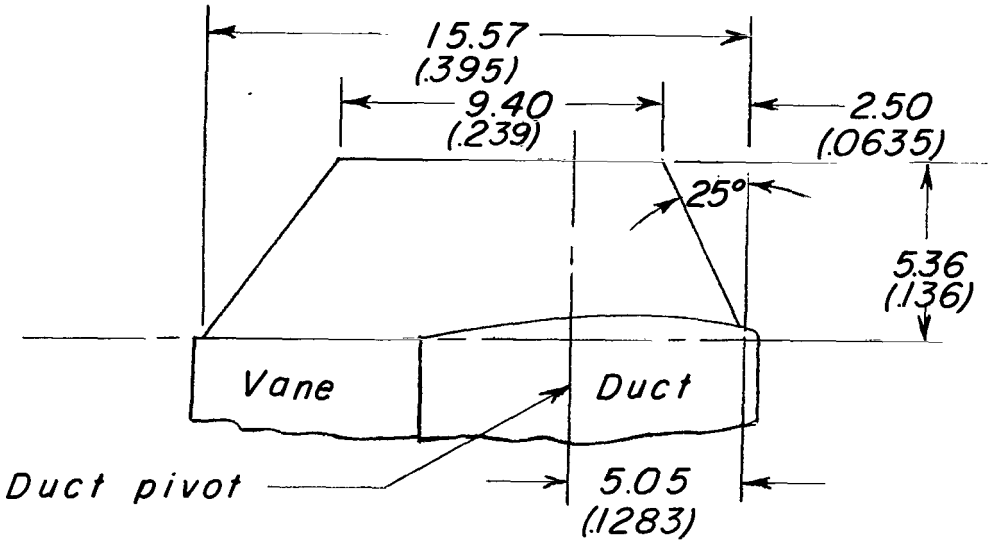

H_1 (NACA 64 A 415 section)

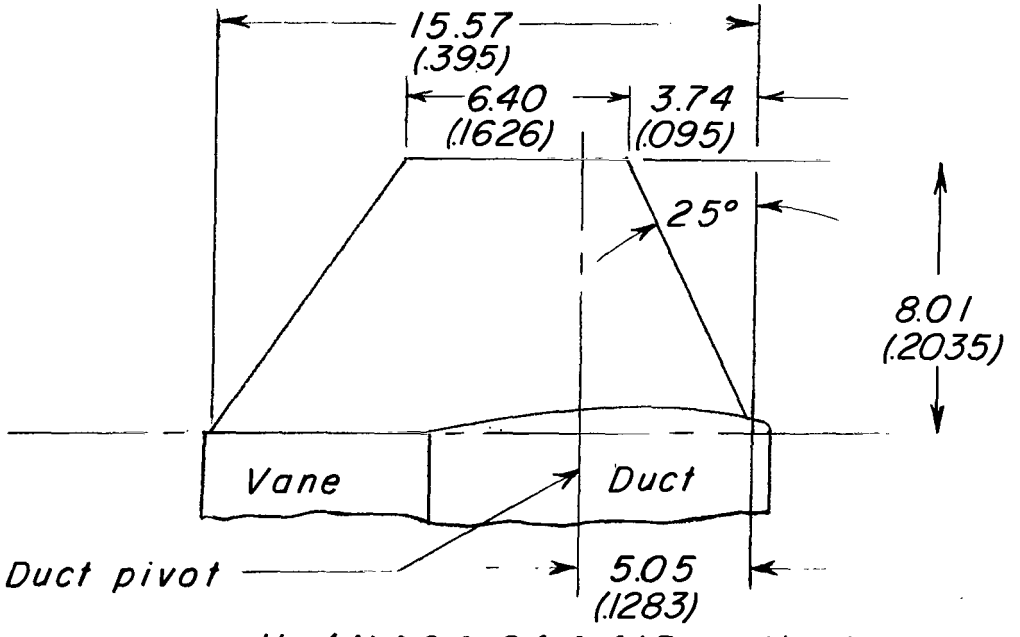

H_2 (NACA 64 A 415 section)

Figure 7.- Details of outboard stabilizers. (Dimensions given first in inches and parenthetically in meters.)

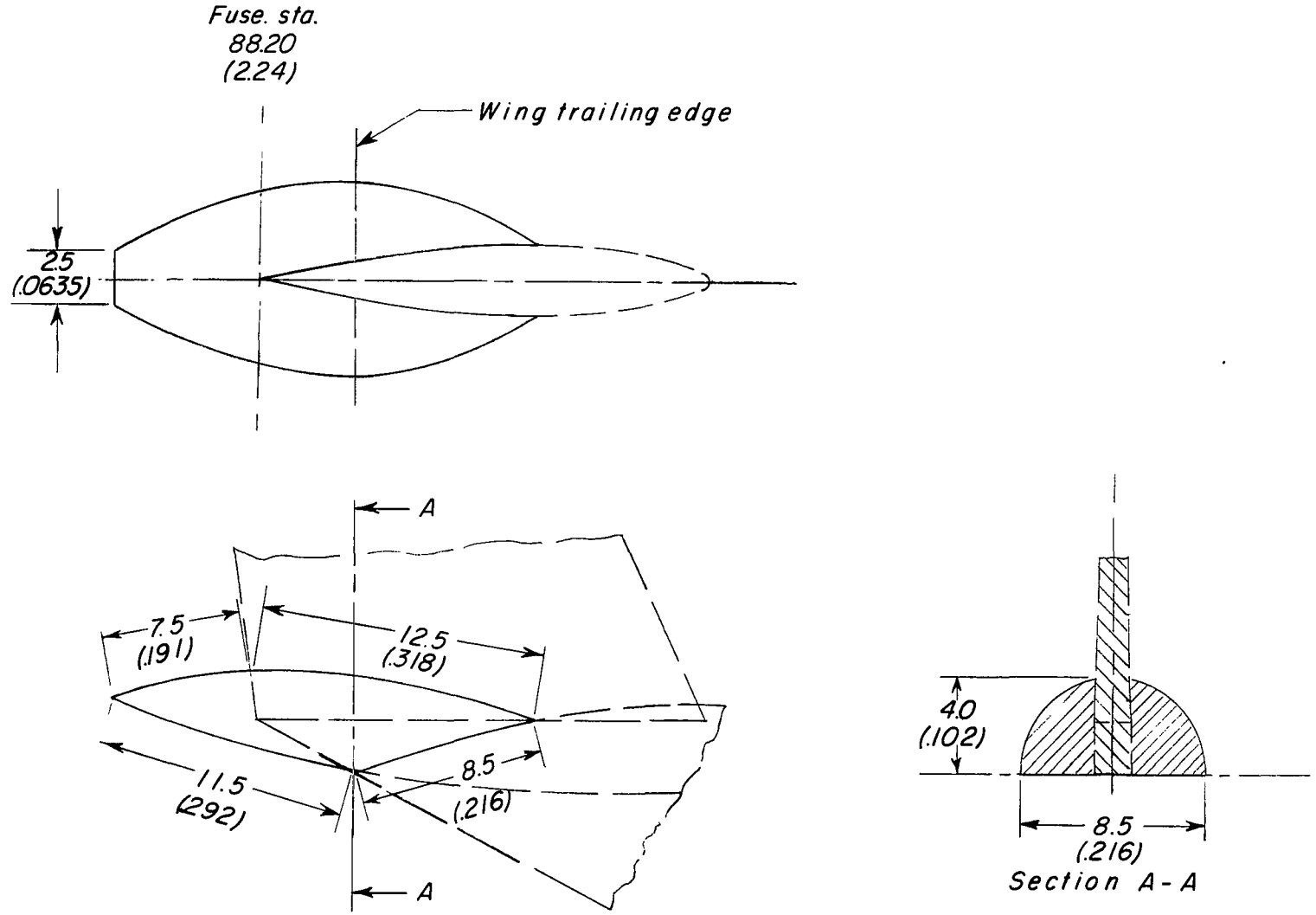

(a) Fairing 1.

Figure 8.- Drawing of tail-wing fairings. (Dimensions given first in inches and parenthetically in meters.)

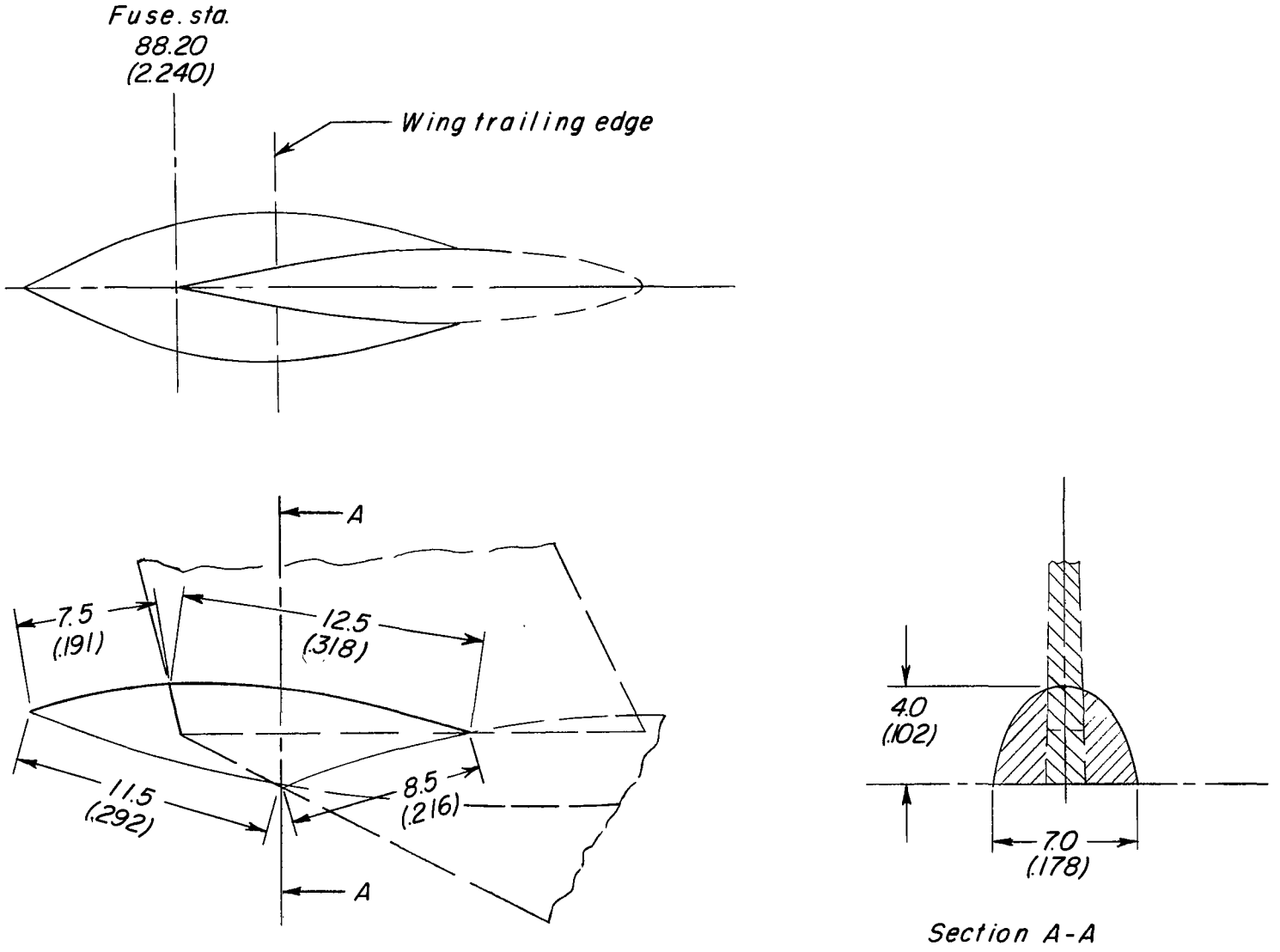

(b) Fairing 2.

Figure 8.- Continued.

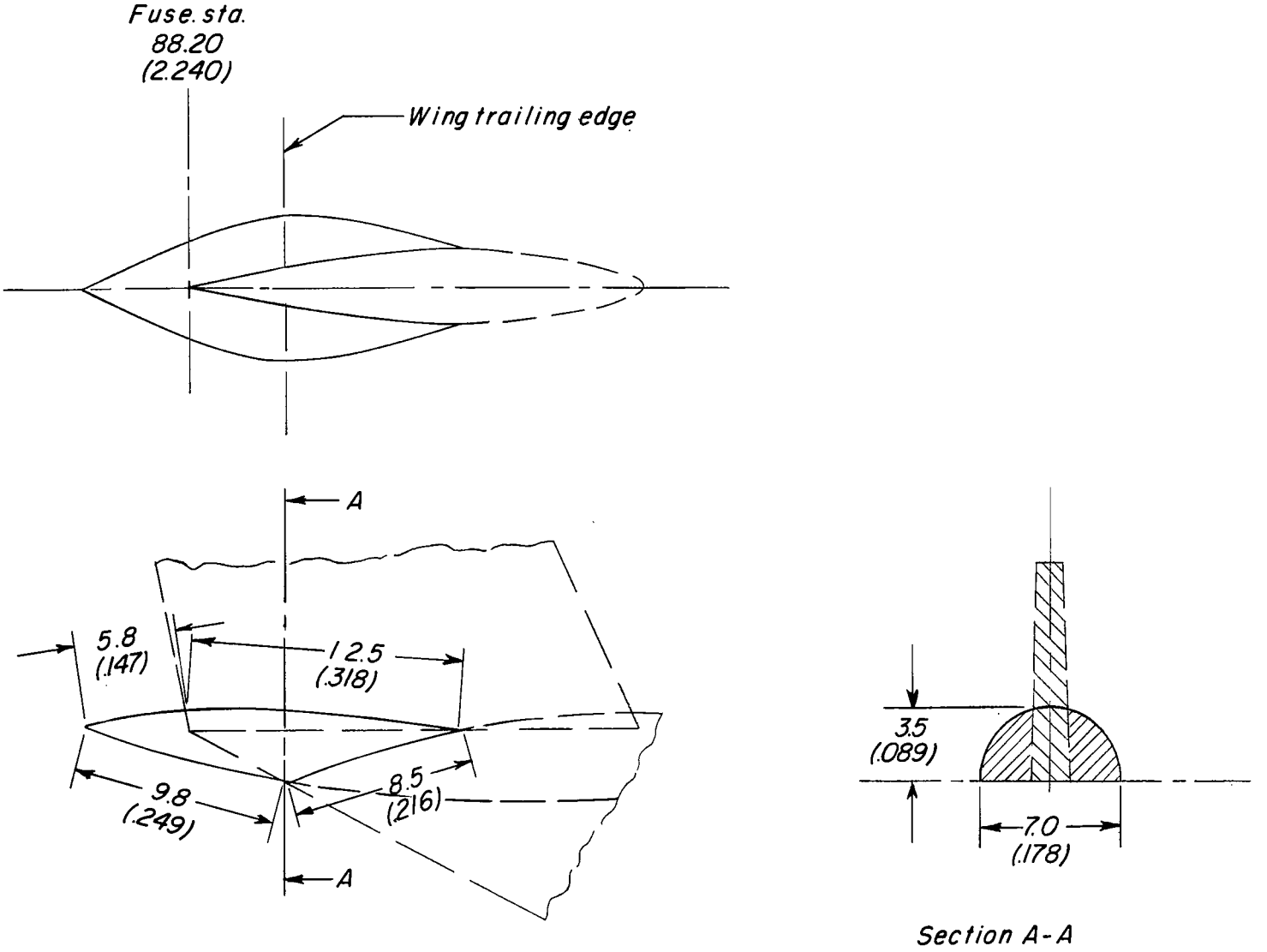

(c) Fairing 3.

Figure 8.- Continued.

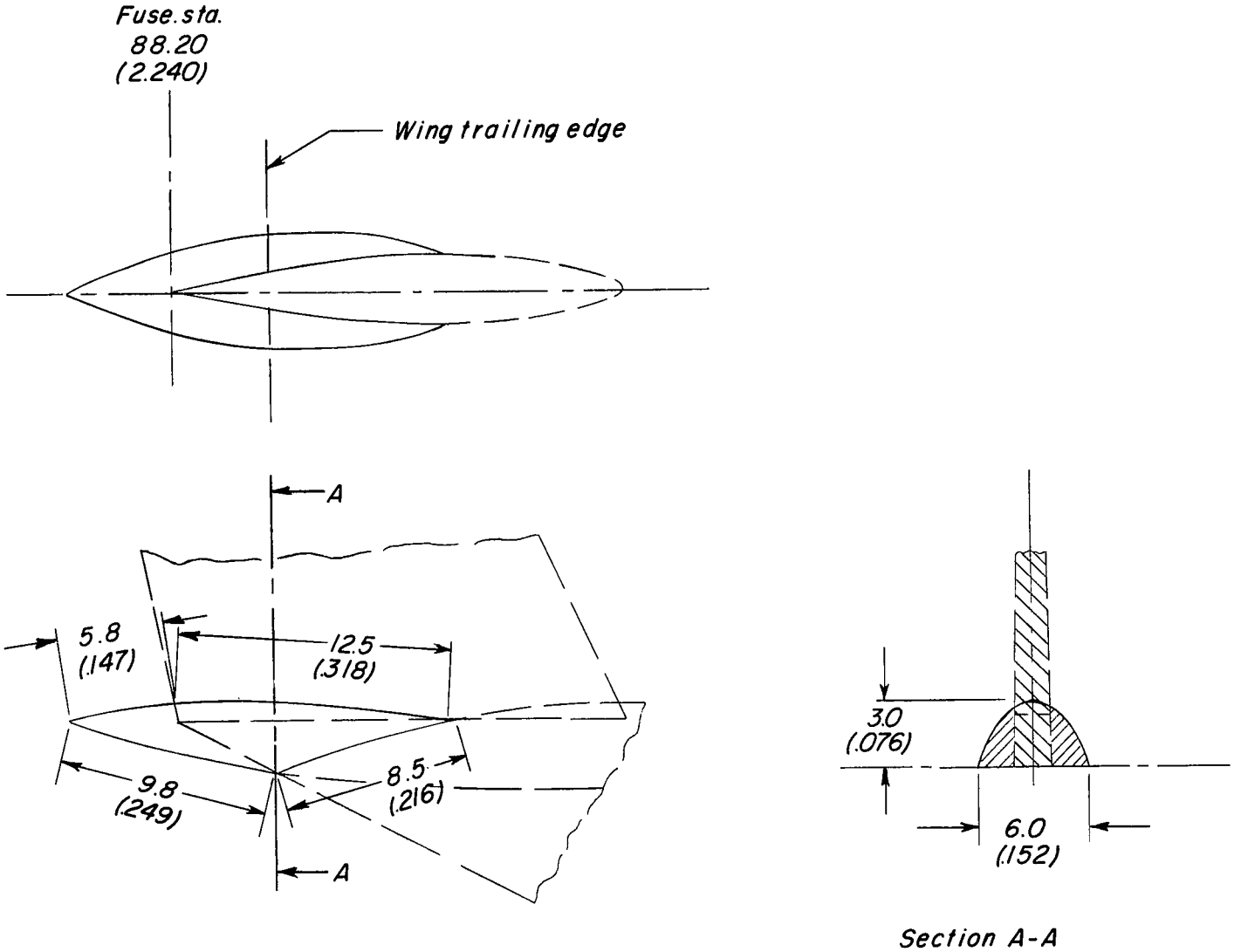

(d) Fairing 4.

Figure 8.- Continued.

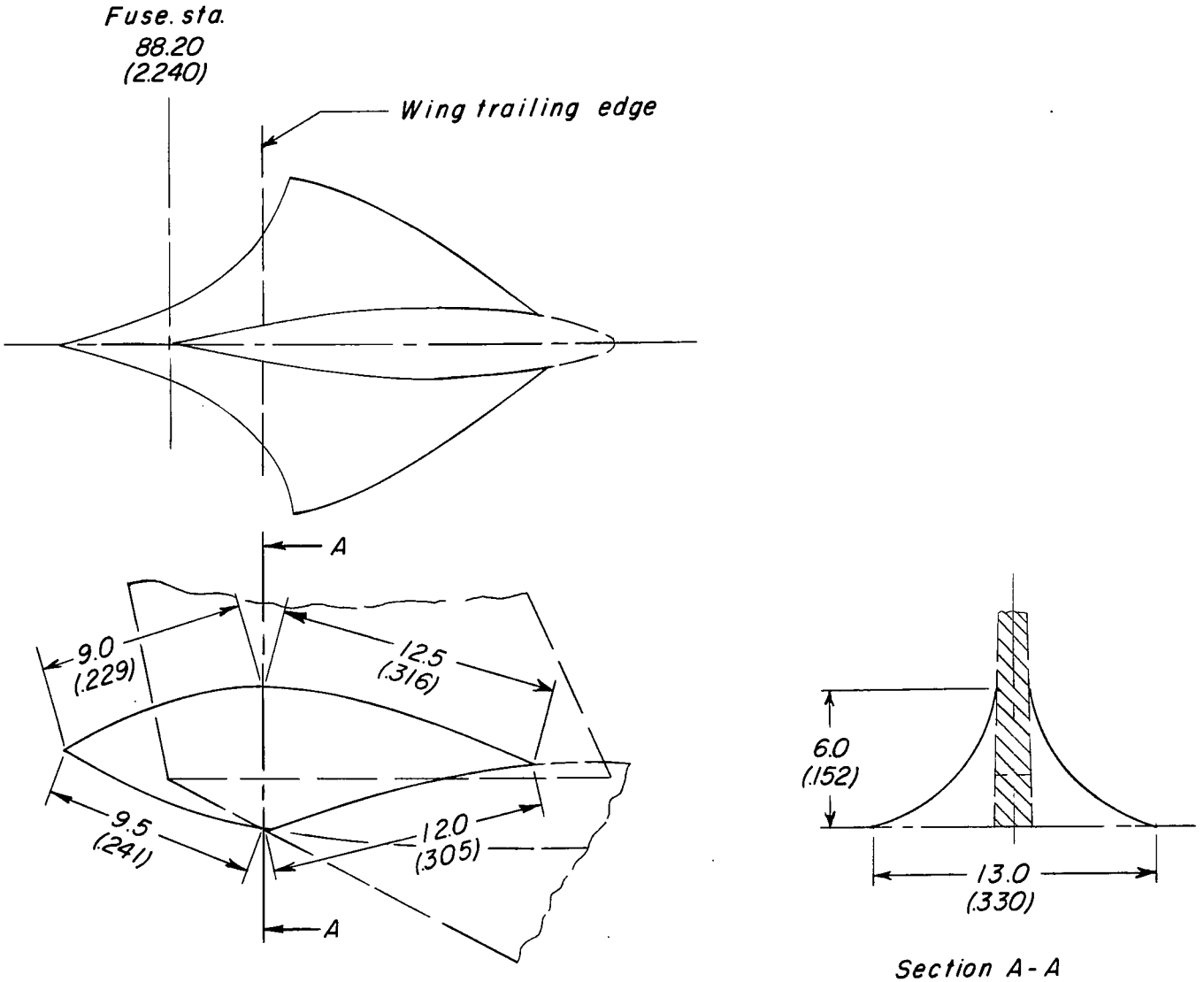

(e) Fairing 5.

Figure 8.- Continued.

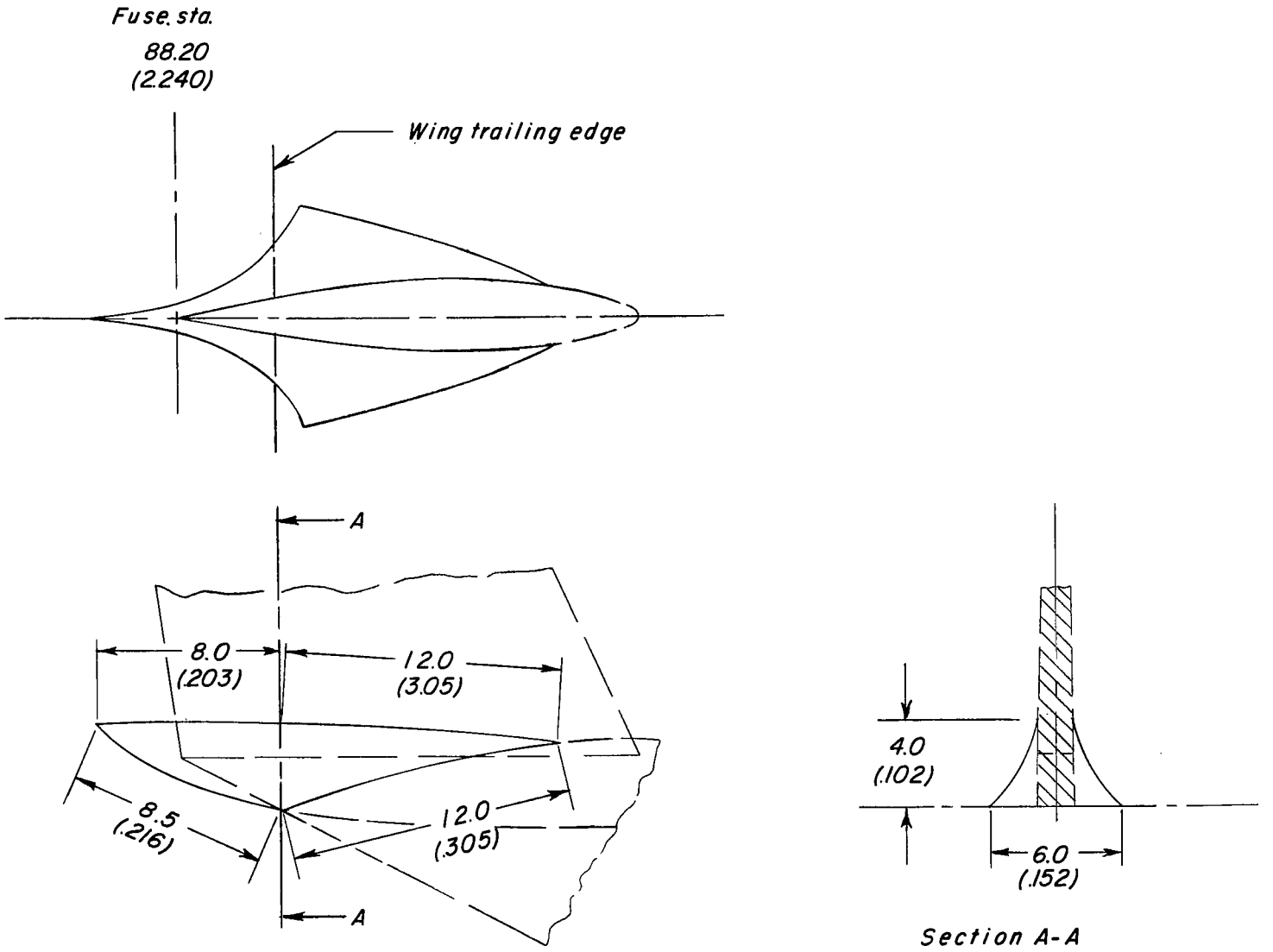

(f) Fairing 6.

Figure 8.- Concluded.

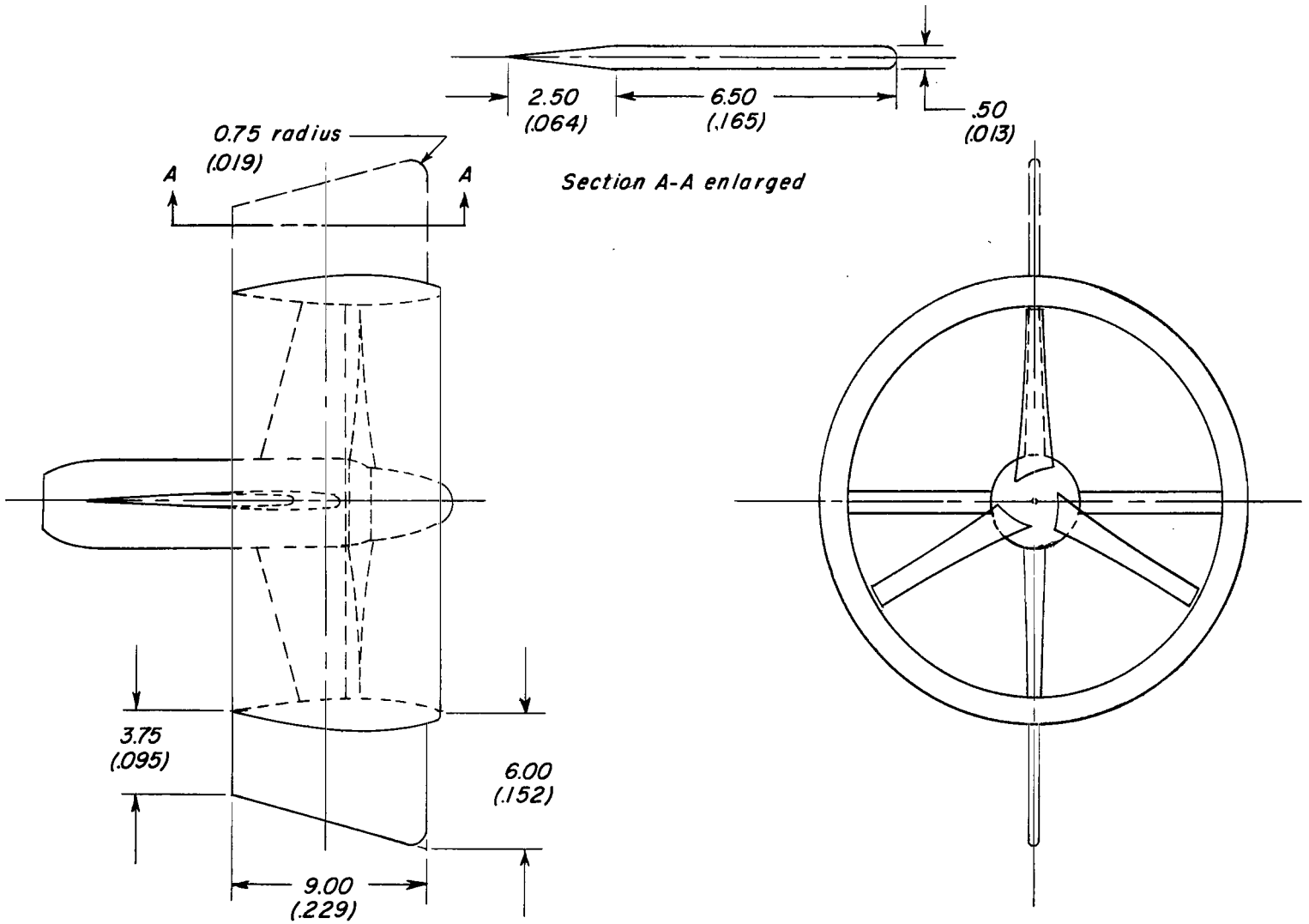

Figure 9.- Vertical fins used on rear ducts. (Dimensions given first in inches and parenthetically in meters.)

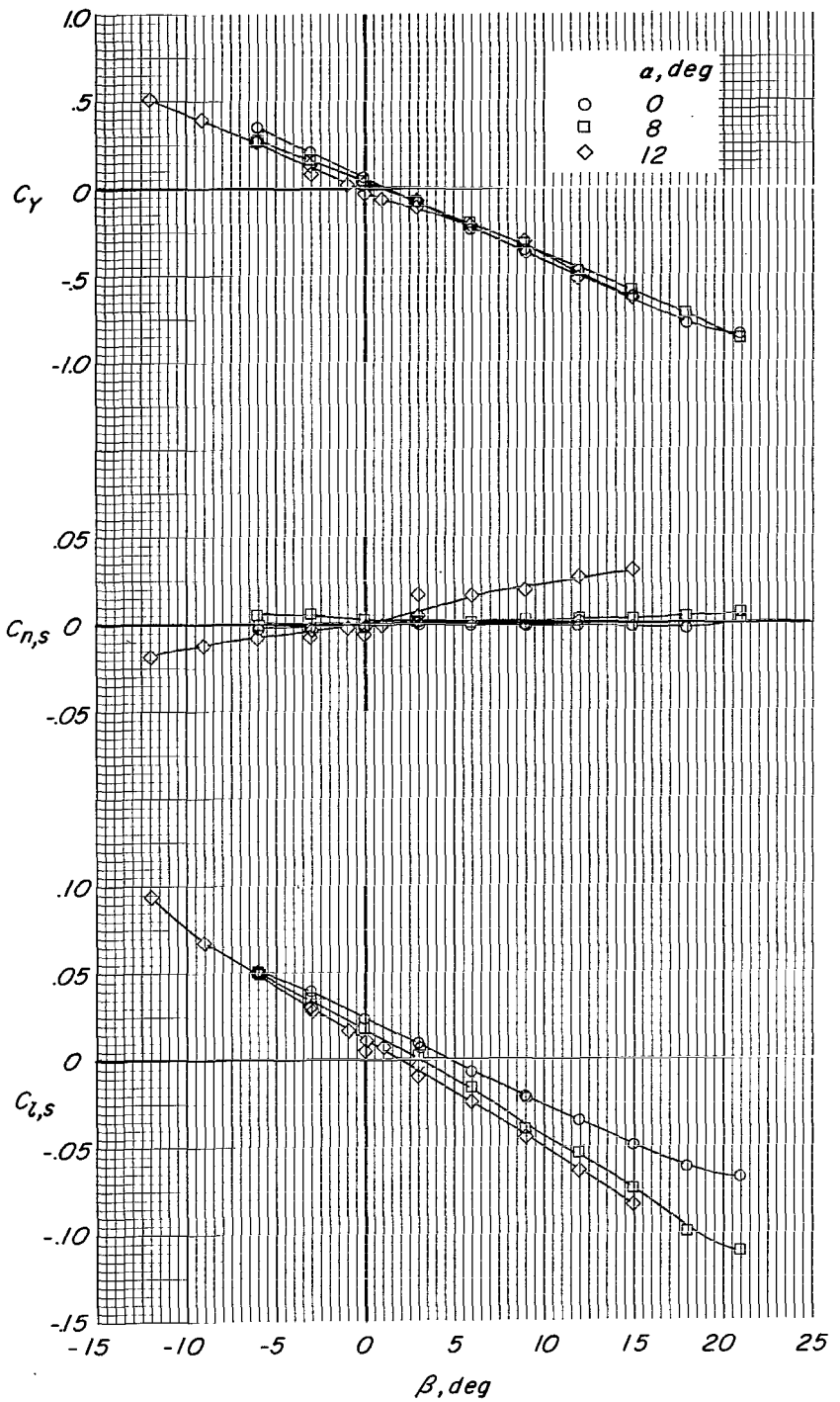

Figure 10.- Effect of angle of attack on sideslip characteristics with vertical tail 1. $\delta_{D,F} = 5^0$; $\delta_{D,R} = 0^0$; $\delta_{V,F} = \delta_{V,R} = 0^0$; vertical fins off; H_2; $i_t = -10^0$; $C_T = 0$; propellers off.

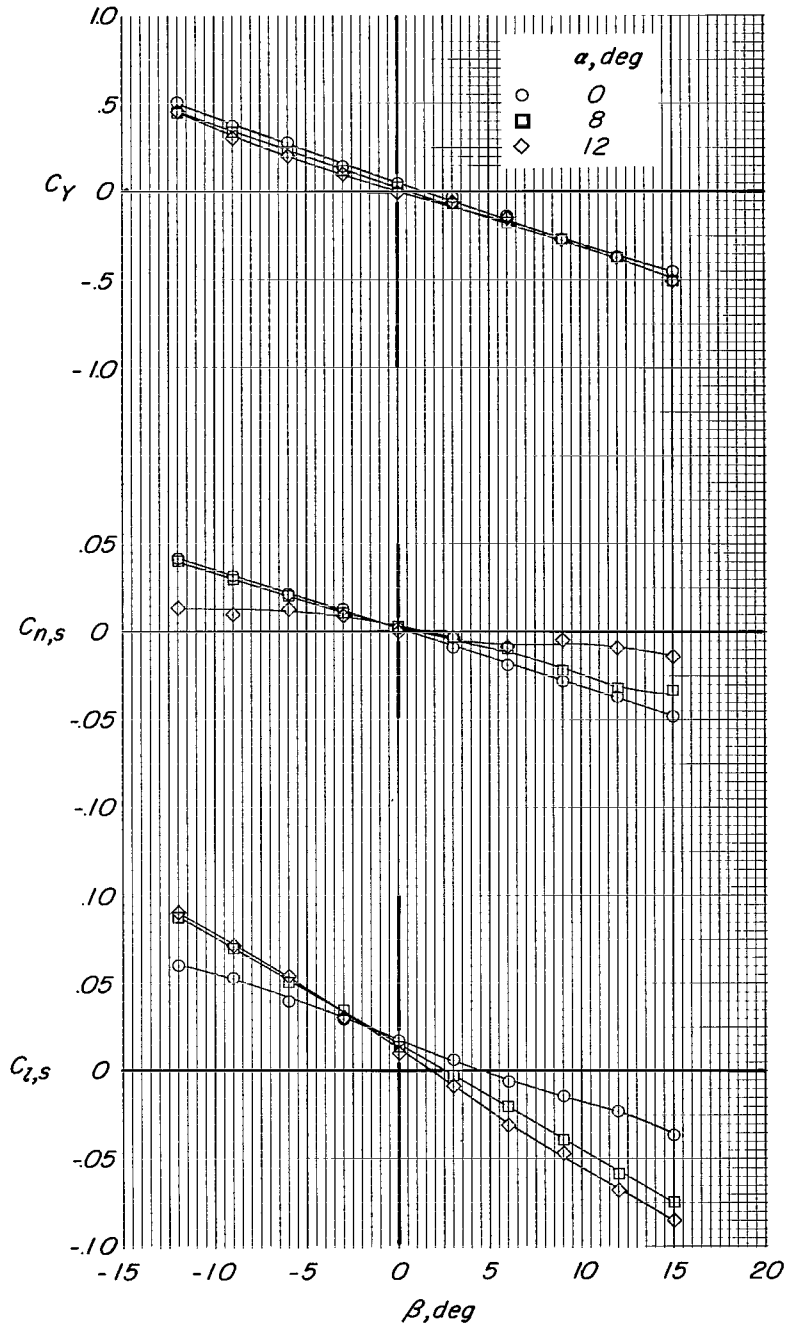

(a) $C_T = 0$; propellers off.

Figure 11.- Effects of angle of attack and power on sideslip characteristics with vertical tail off. $\delta_{D,F} = 5^0$; $\delta_{D,R} = 0^0$; $\delta_{V,F} = \delta_{V,R} = 0^0$; vertical fins off; H_1.

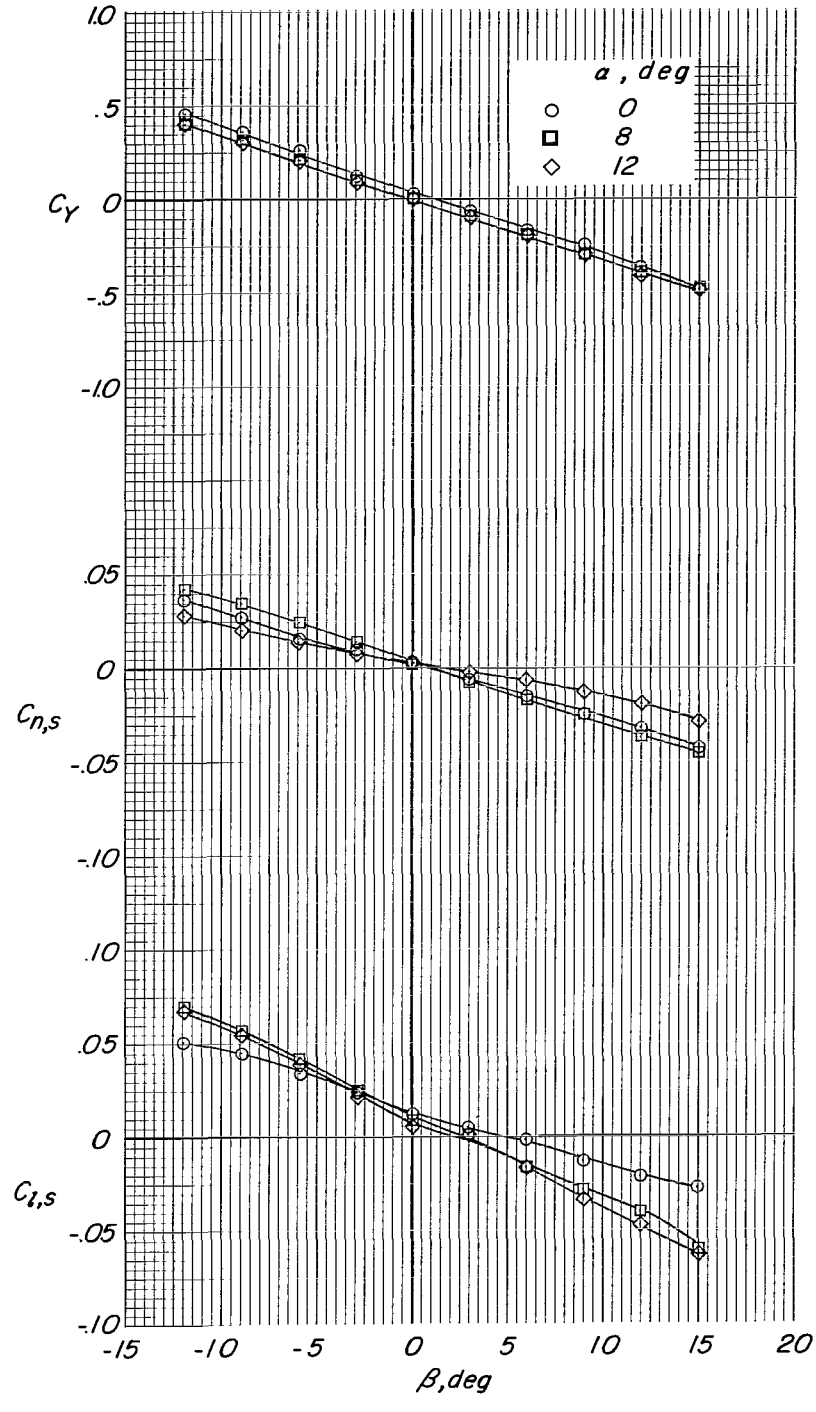

(b) $C_T \approx 0$; propellers windmilling.

Figure 11.- Continued.

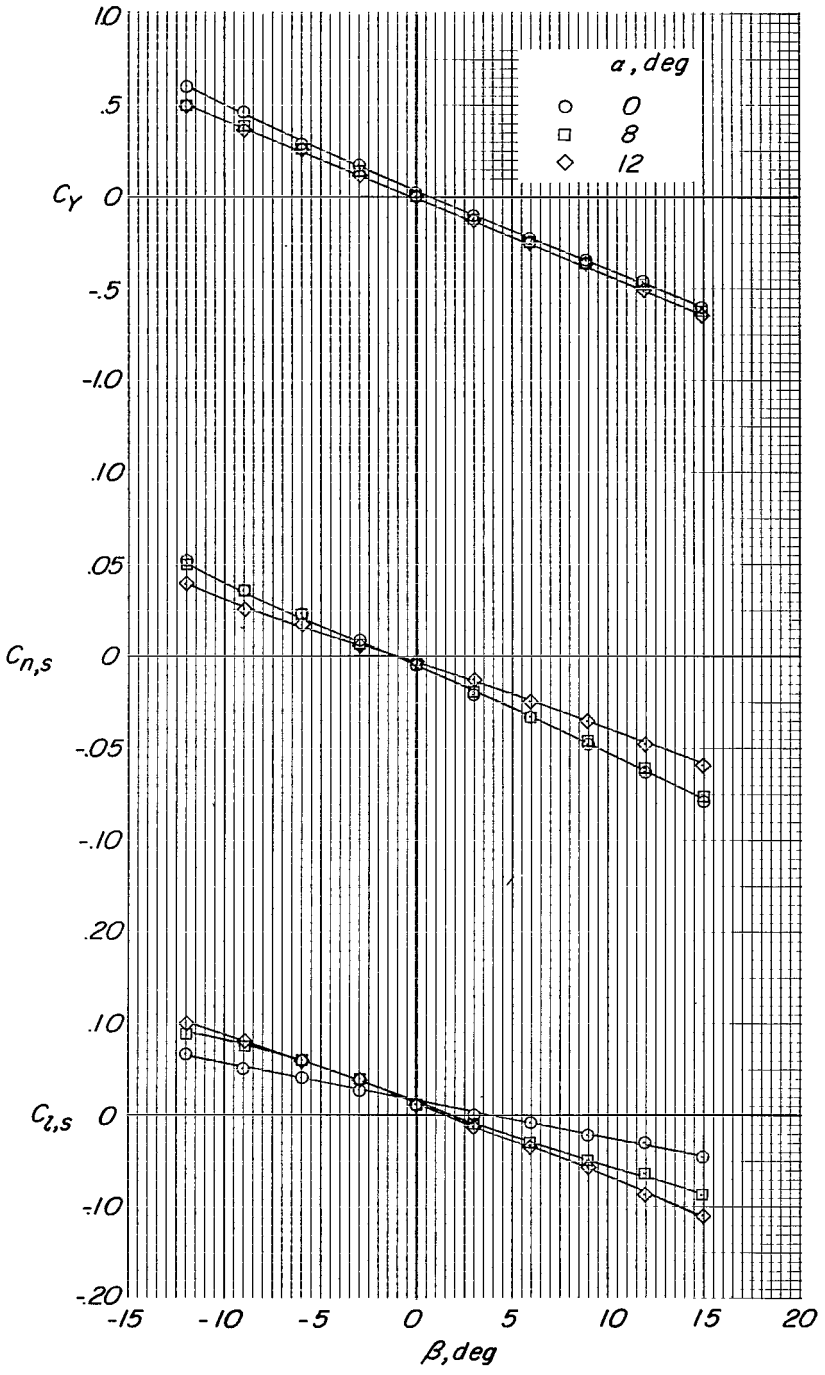

(c) C_T = 0.80.

Figure 11.- Concluded.

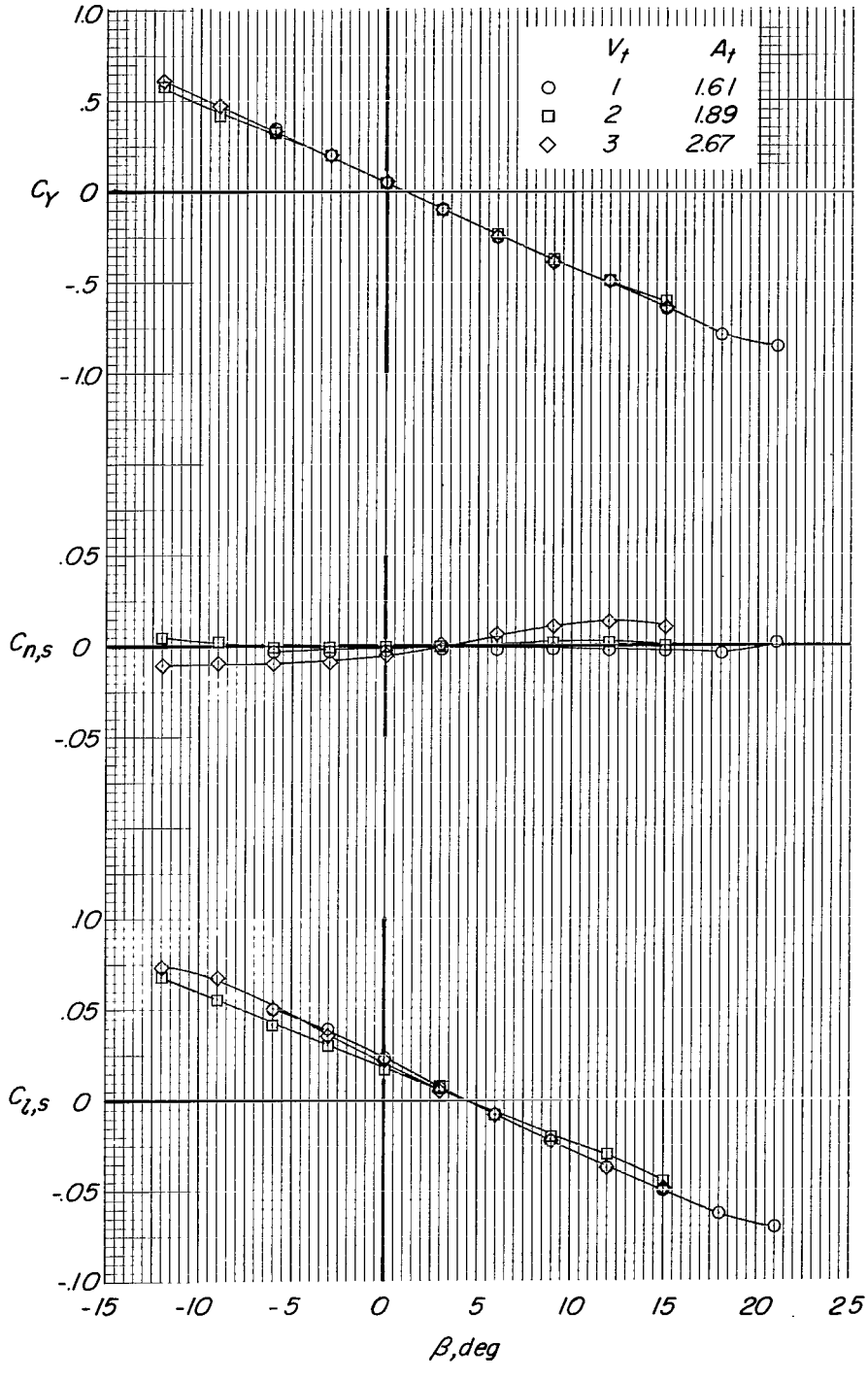

Figure 12.- Effect of size and aspect ratio of vertical tail on sideslip characteristics. $\alpha = 0^0$; $\delta_{D,F} = 5^0$; $\delta_{D,R} = 0^0$; $\delta_{V,F} = \delta_{V,R} = 0^0$; vertical fins off; $C_T = 0$; propellers off; H_1; $i_t = 0^0$.

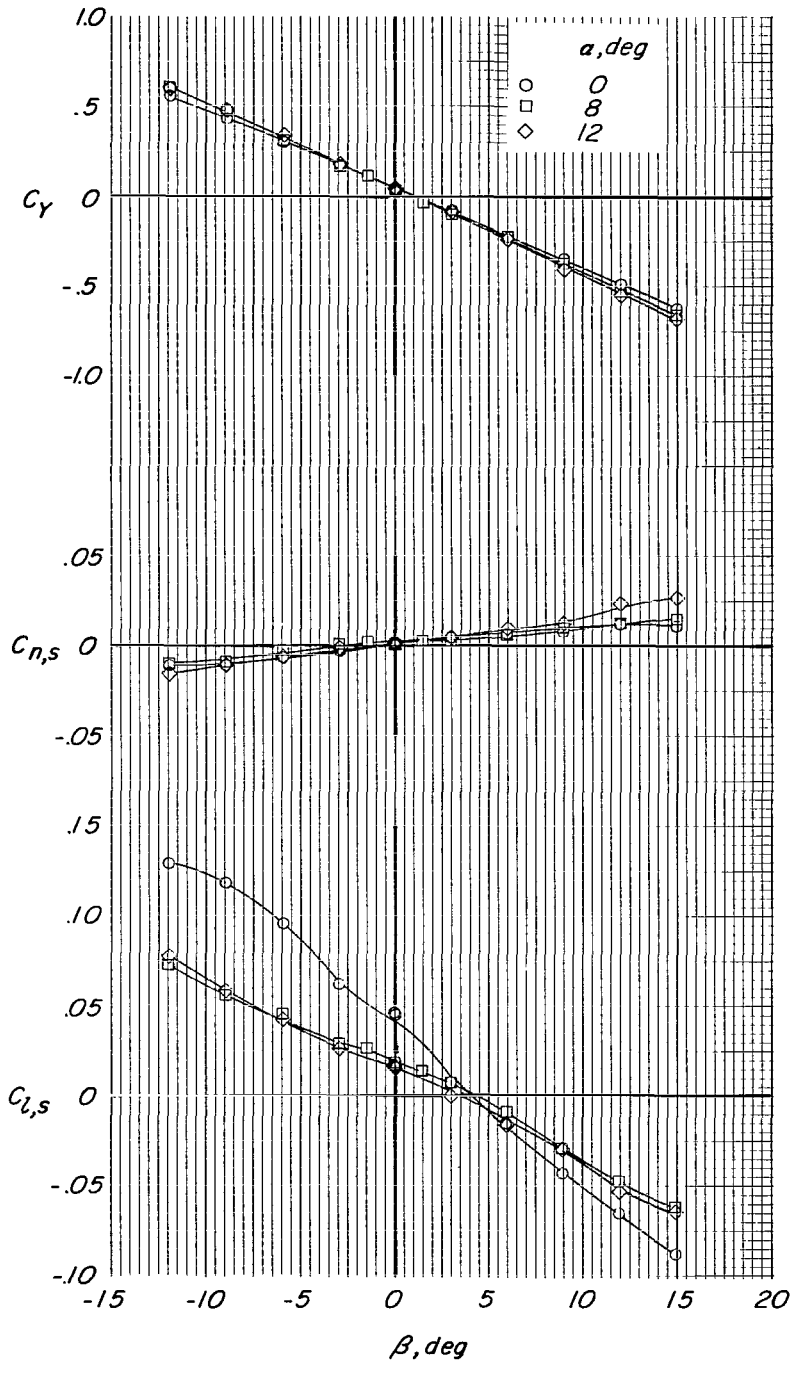

(a) $C_T \approx 0$; propellers windmilling.

Figure 13.- Effects of power and angle of attack on sideslip characteristics. $\delta_{D,F} = 0^0$; $\delta_{D,R} = -5.25^0$; $\delta_{V,F} = \delta_{V,R} = 0^0$; vertical tail 3; vertical fins off; H_1; $i_t = 0^0$.

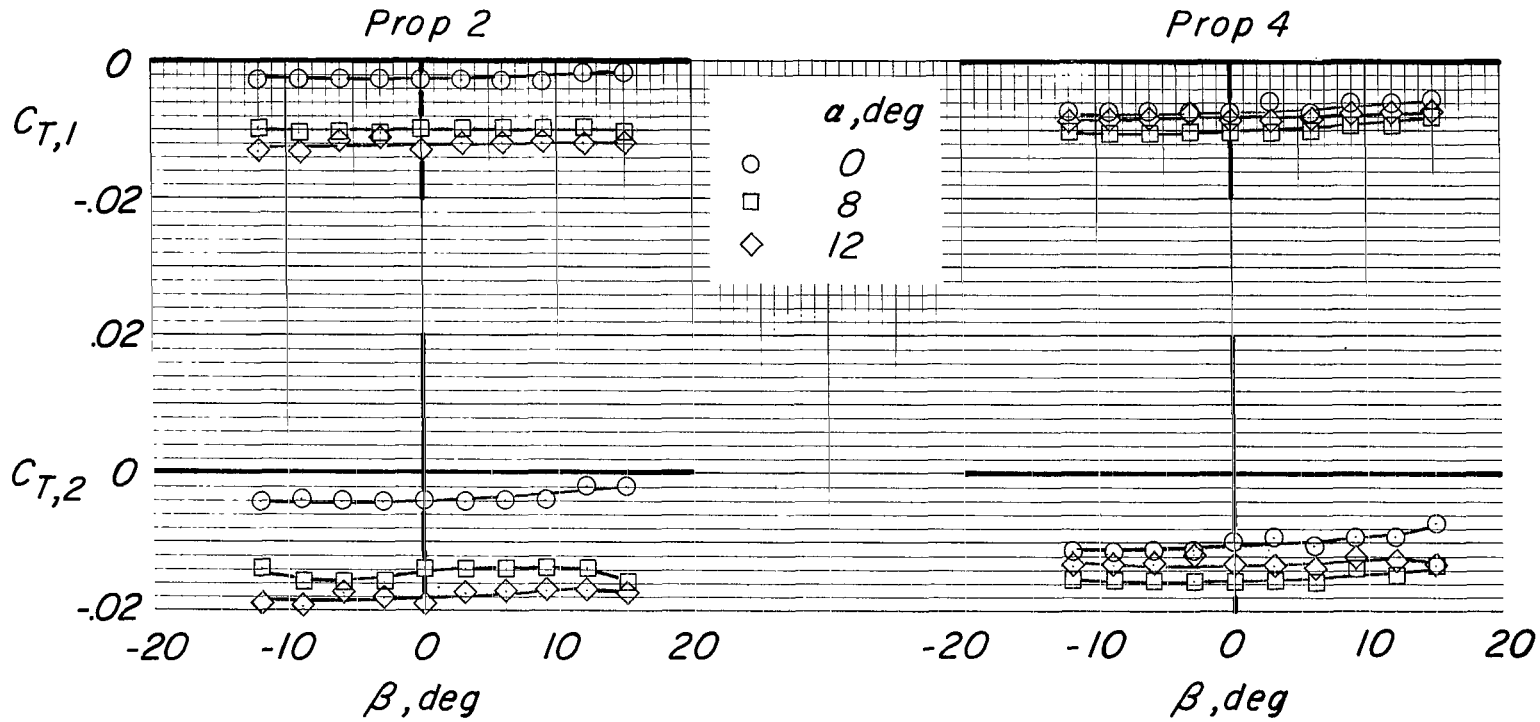

(a) Concluded.

Figure 13.- Continued.

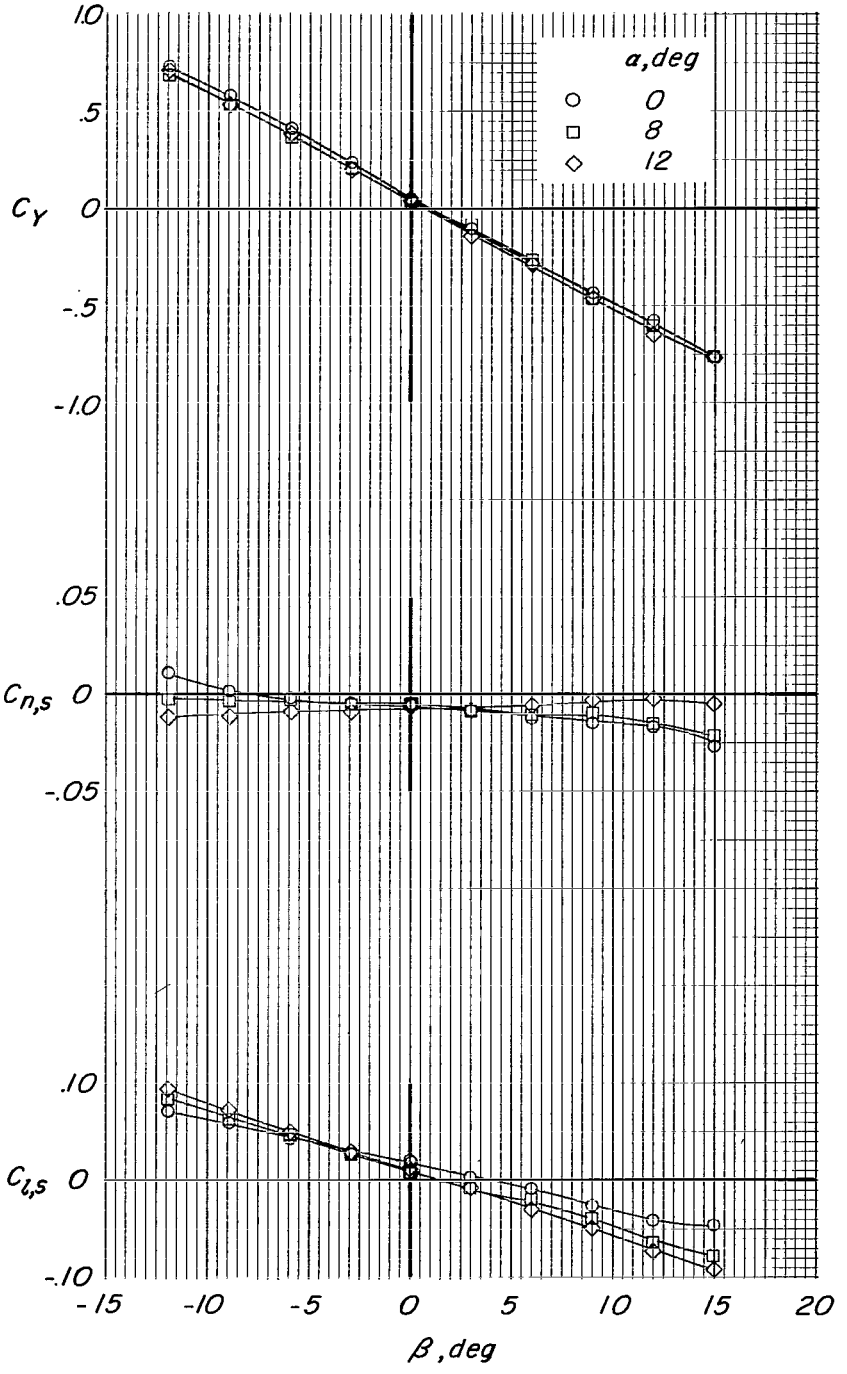

(b) $C_T = 0.80$.

Figure 13.- Continued.

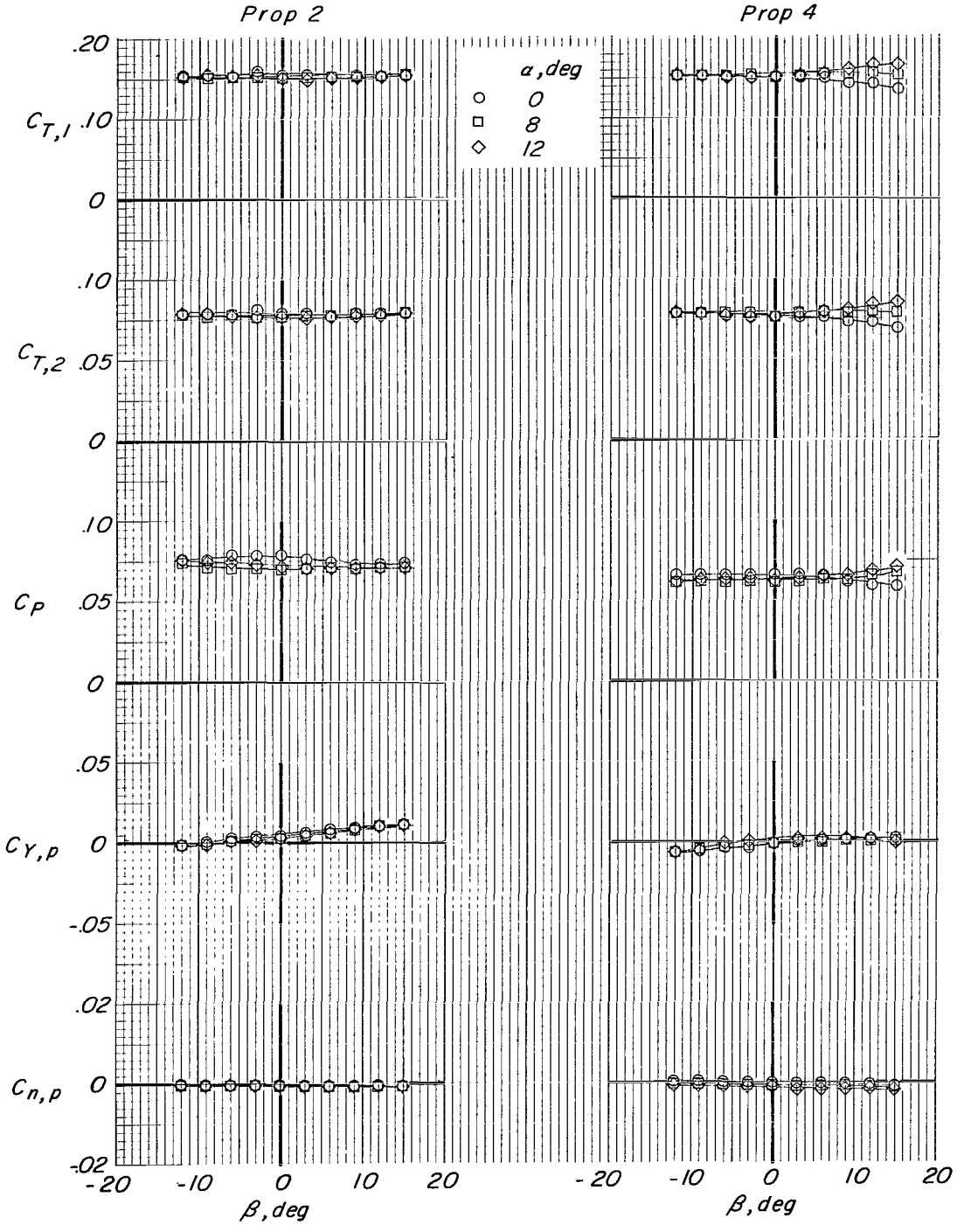

(b) Concluded.

Figure 13.- Concluded.

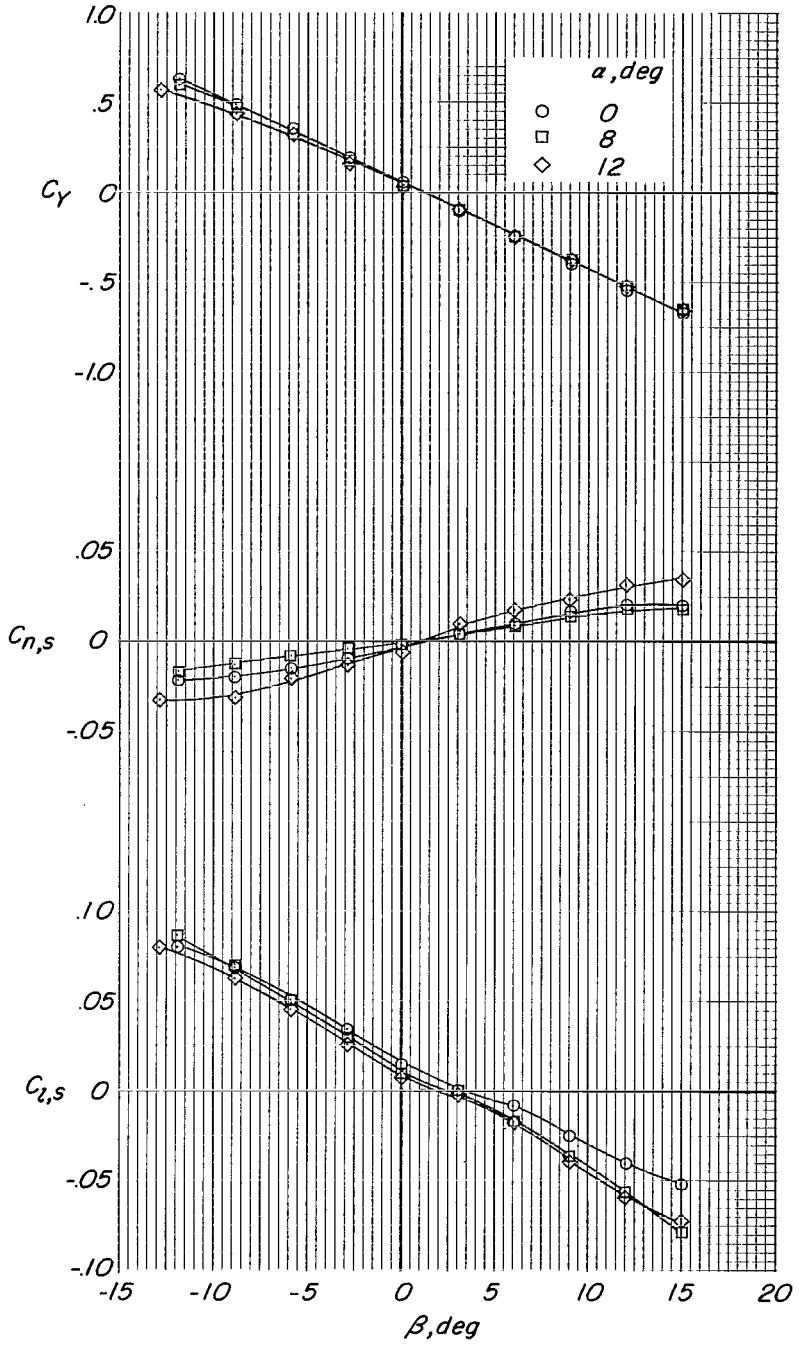

(a) $C_T \approx 0$; propellers windmilling.

Figure 14.- Effects of angle of attack and power on sideslip characteristics with vertical tail 3 and tail-wing fairing 1. $\delta_{D,F} = 5^0$; $\delta_{D,R} = 0^0$; $\delta_{V,F} = \delta_{V,R} = 0^0$; vertical fins off; H_1; $i_t = 0^0$.

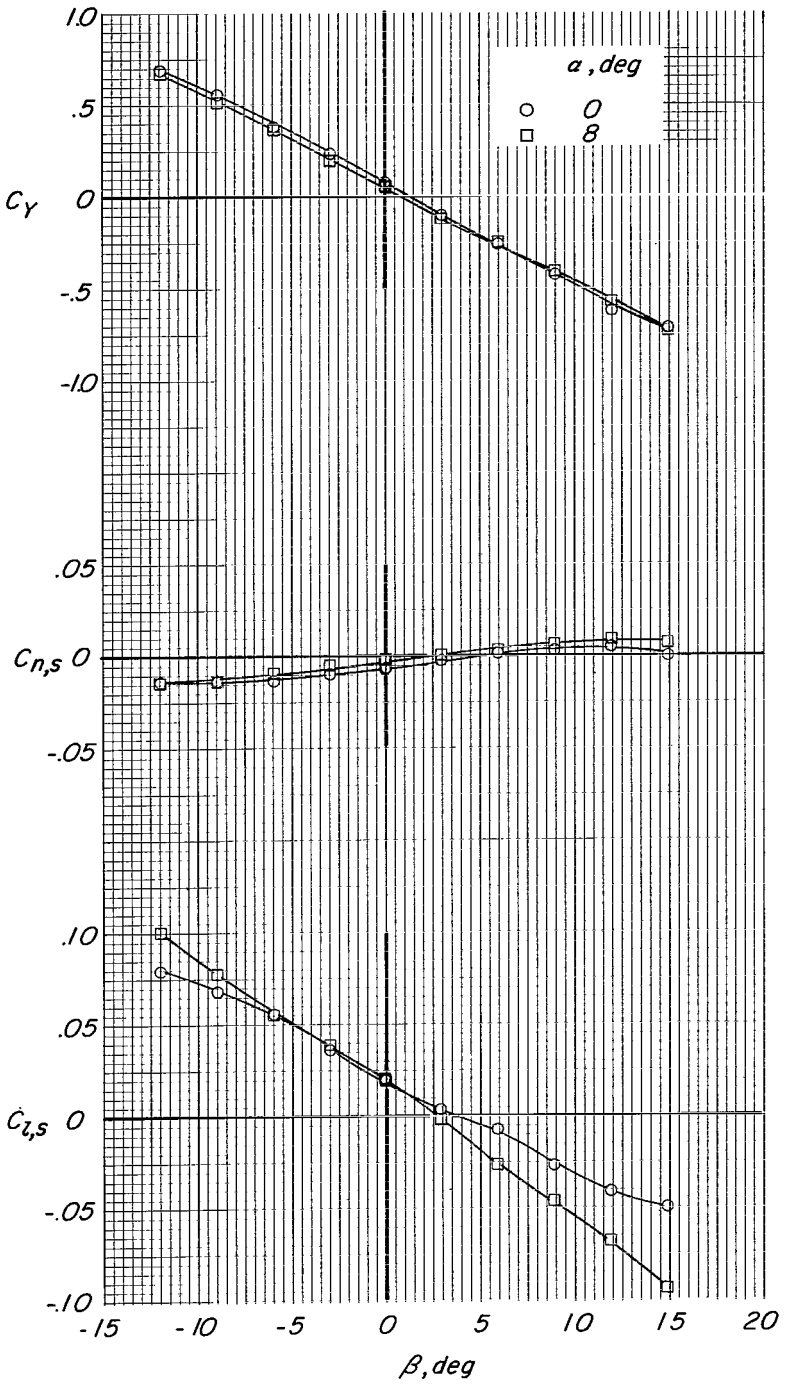

(b) C_T = 0.40.

Figure 14.- Continued.

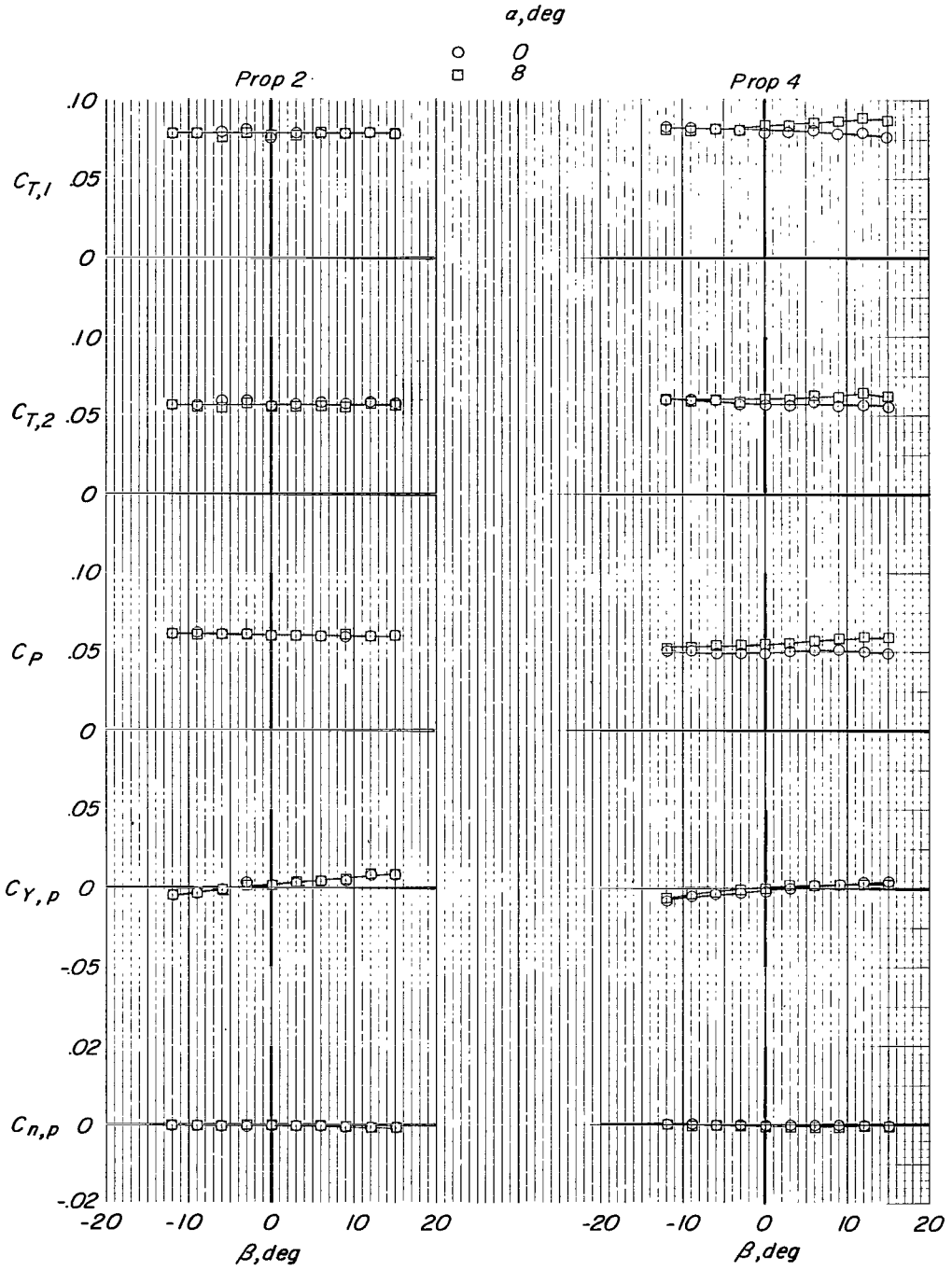

(b) Concluded.

Figure 14.- Continued.

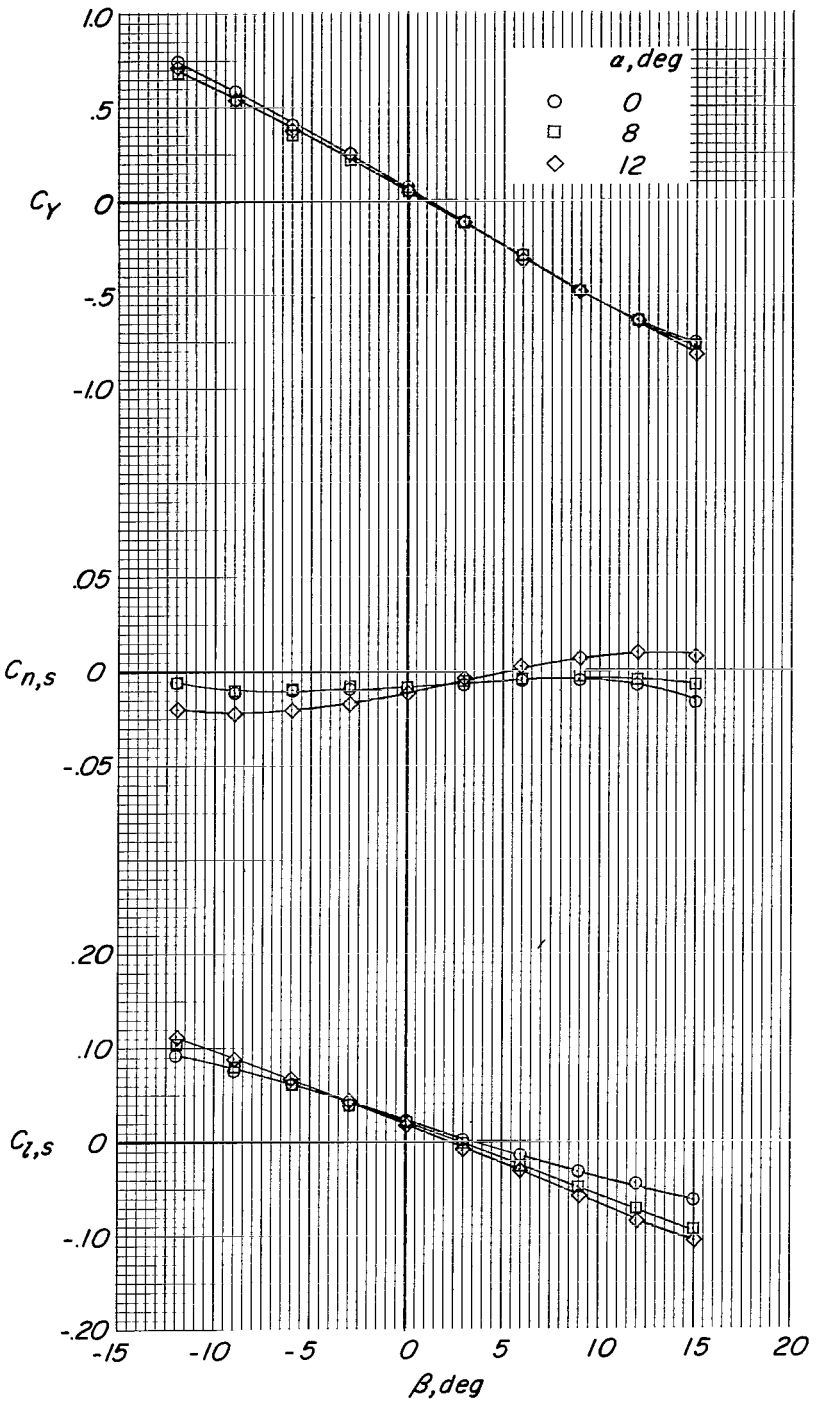

(c) C_T = 0.80.

Figure 14.- Continued.

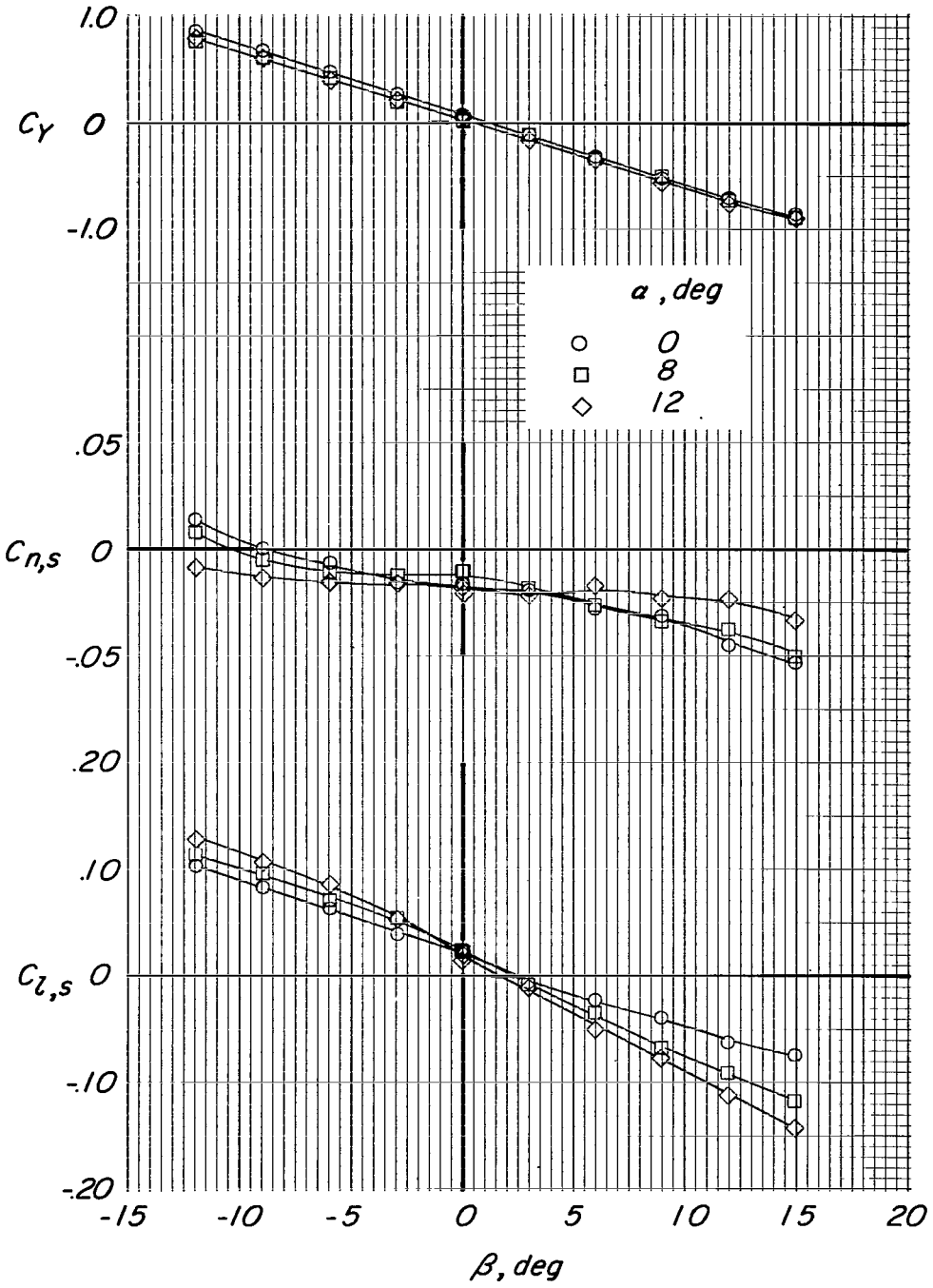

(d) C_T = 2.1.

Figure 14.- Continued.

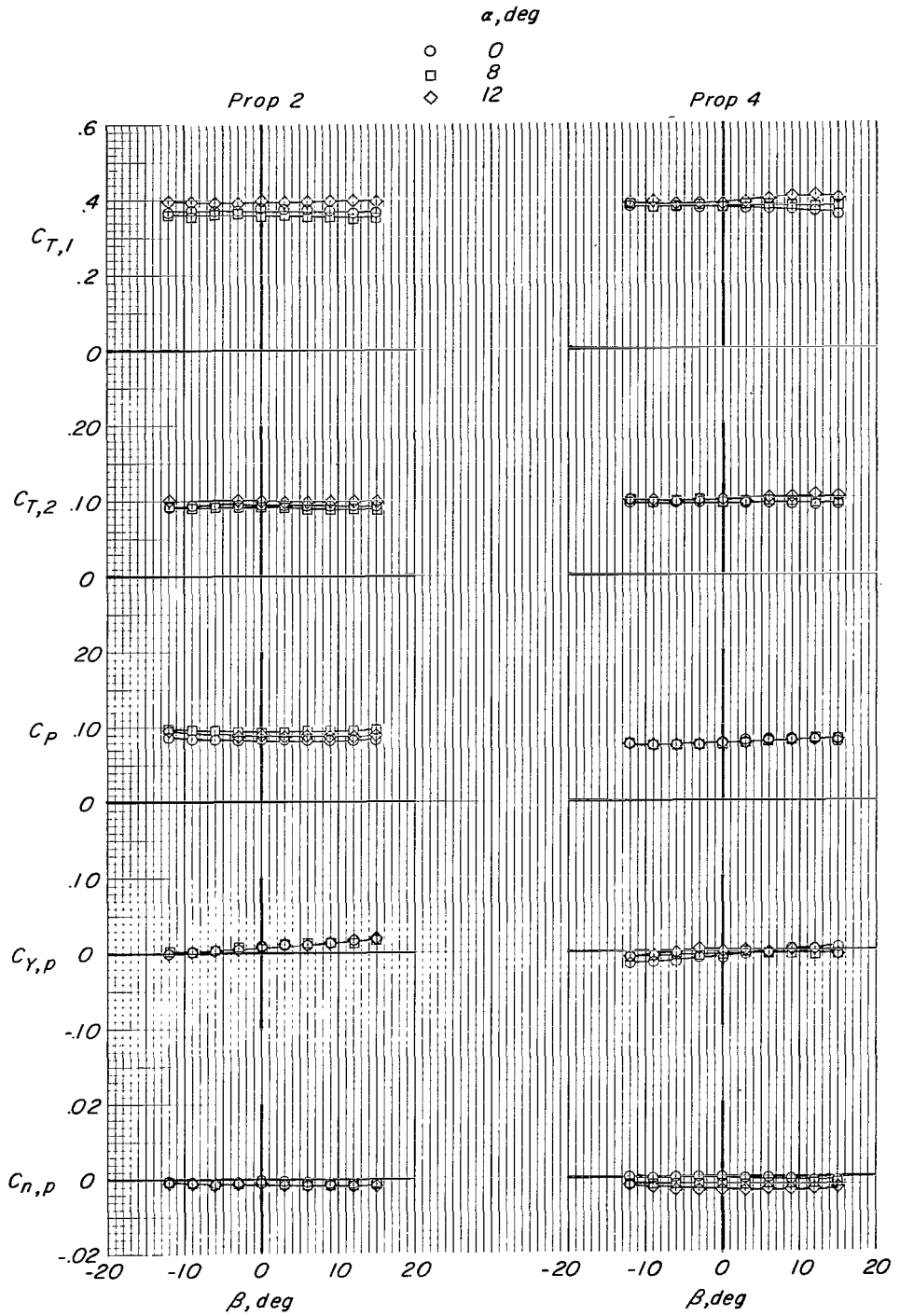

(d) Concluded.

Figure 14.- Concluded.

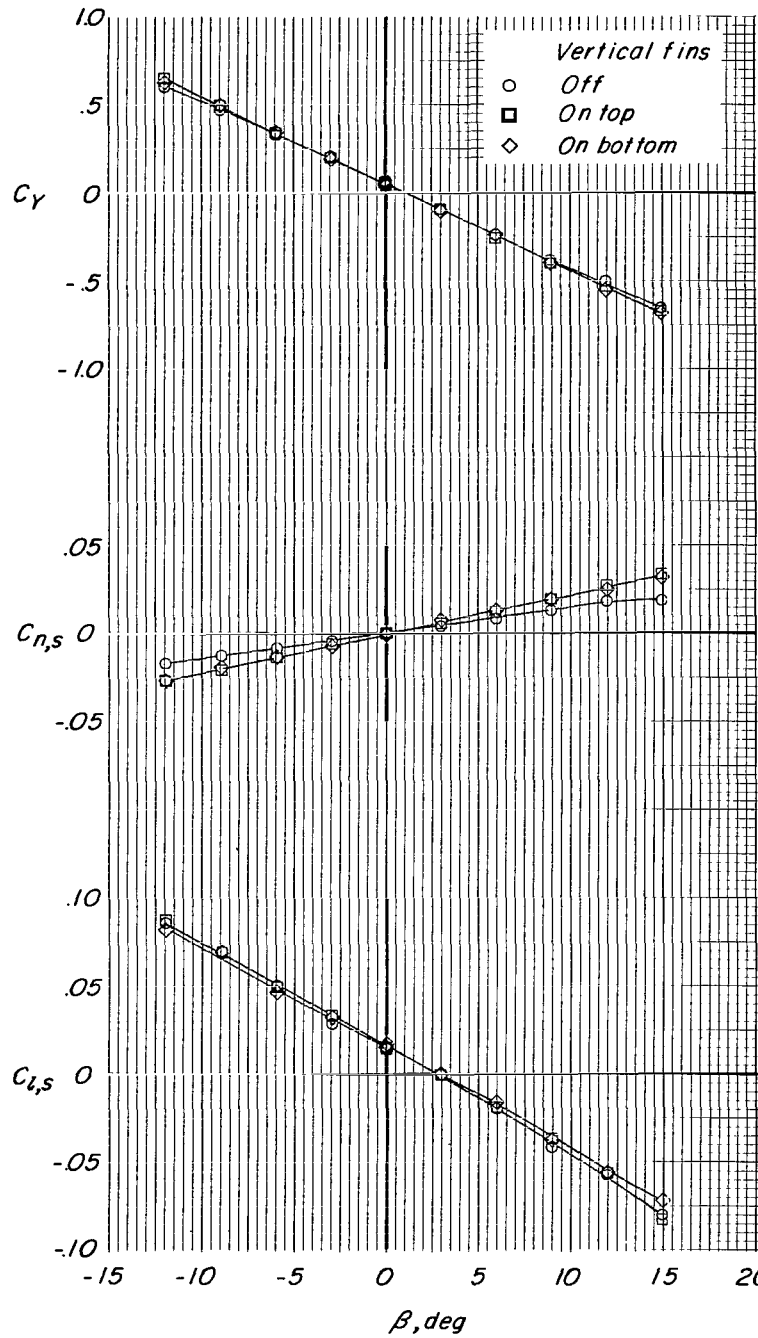

(a) $C_T \approx 0$; propellers windmilling.

Figure 15.- Effect of vertical fins and power on sideslip characteristics. $\alpha = 8^0$; $\delta_{D,F} = 5^0$; $\delta_{D,R} = 0^0$; $\delta_{V,F} = \delta_{V,R} = 0^0$; vertical tail 3; tail-wing fairing 1; H_1; $i_t = 0^0$.

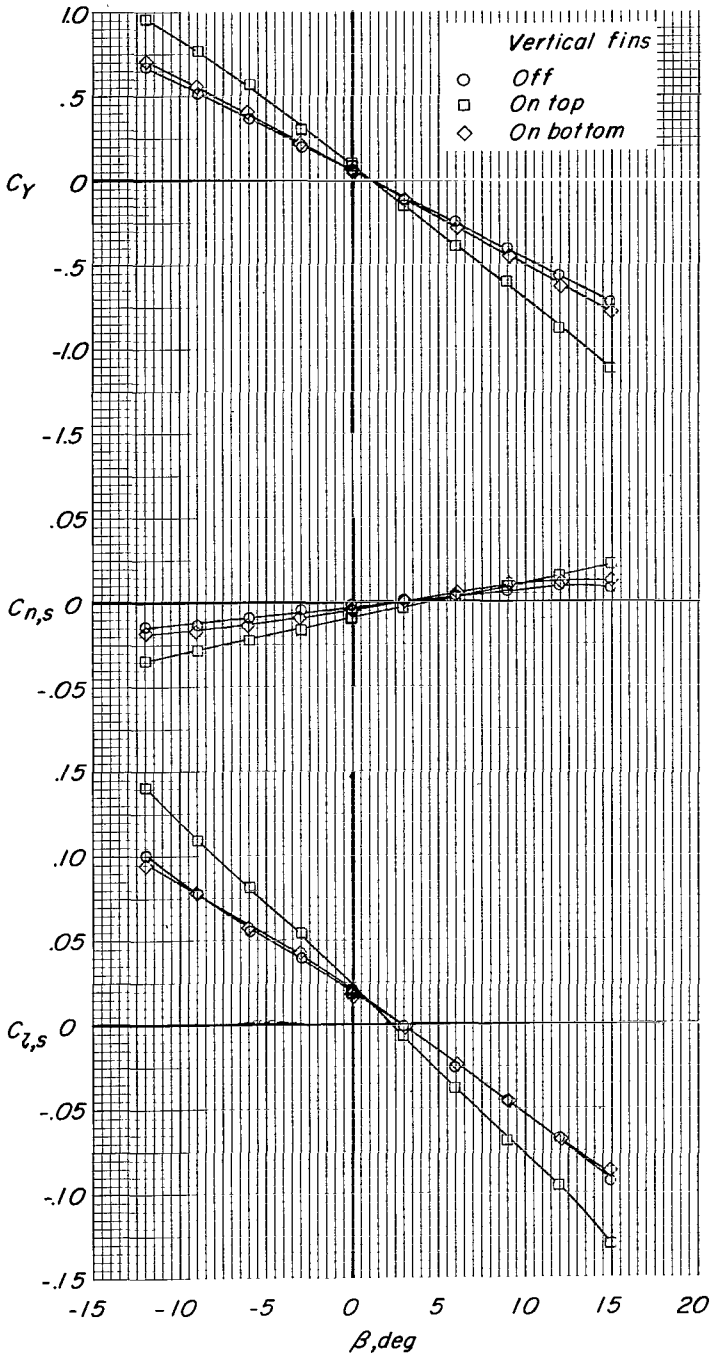

(b) $C_T = 0.40$.

Figure 15.- Continued.

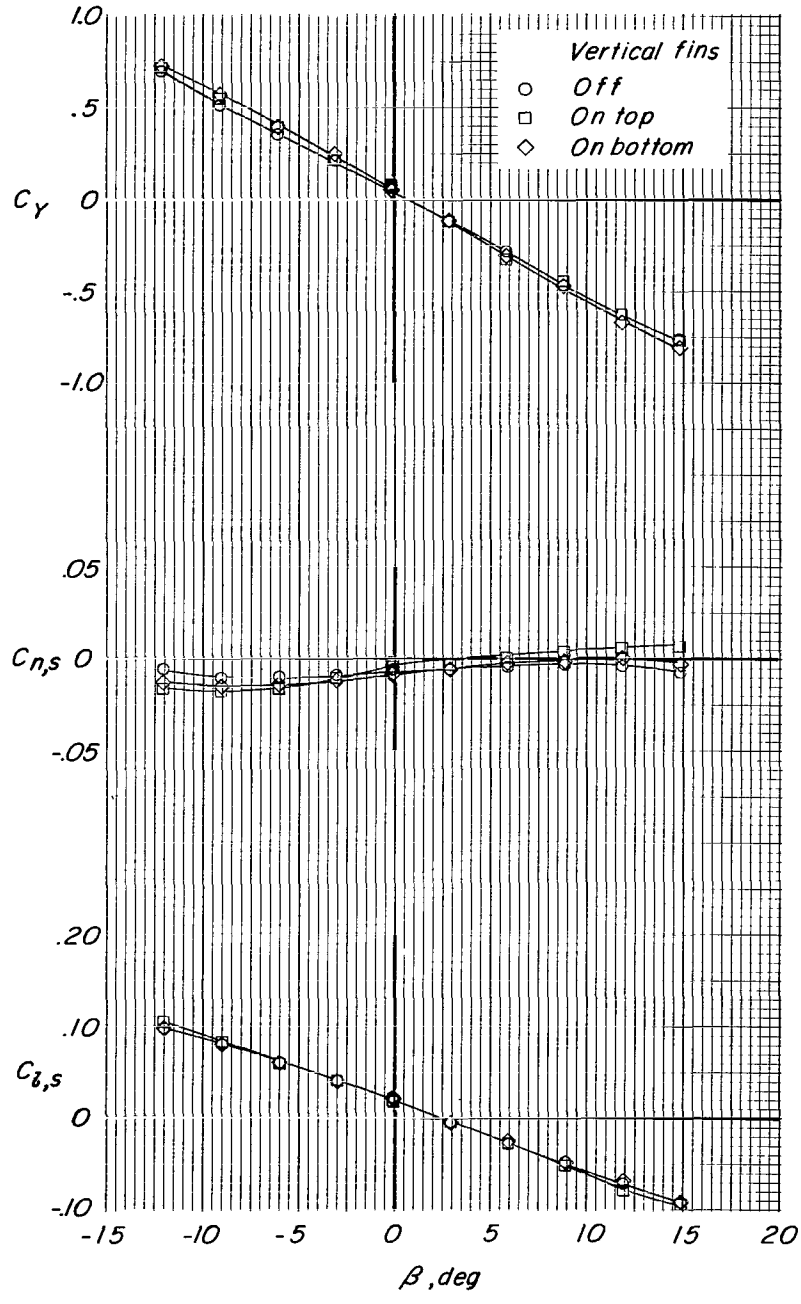

(c) $C_T = 0.80$.

Figure 15.- Continued.

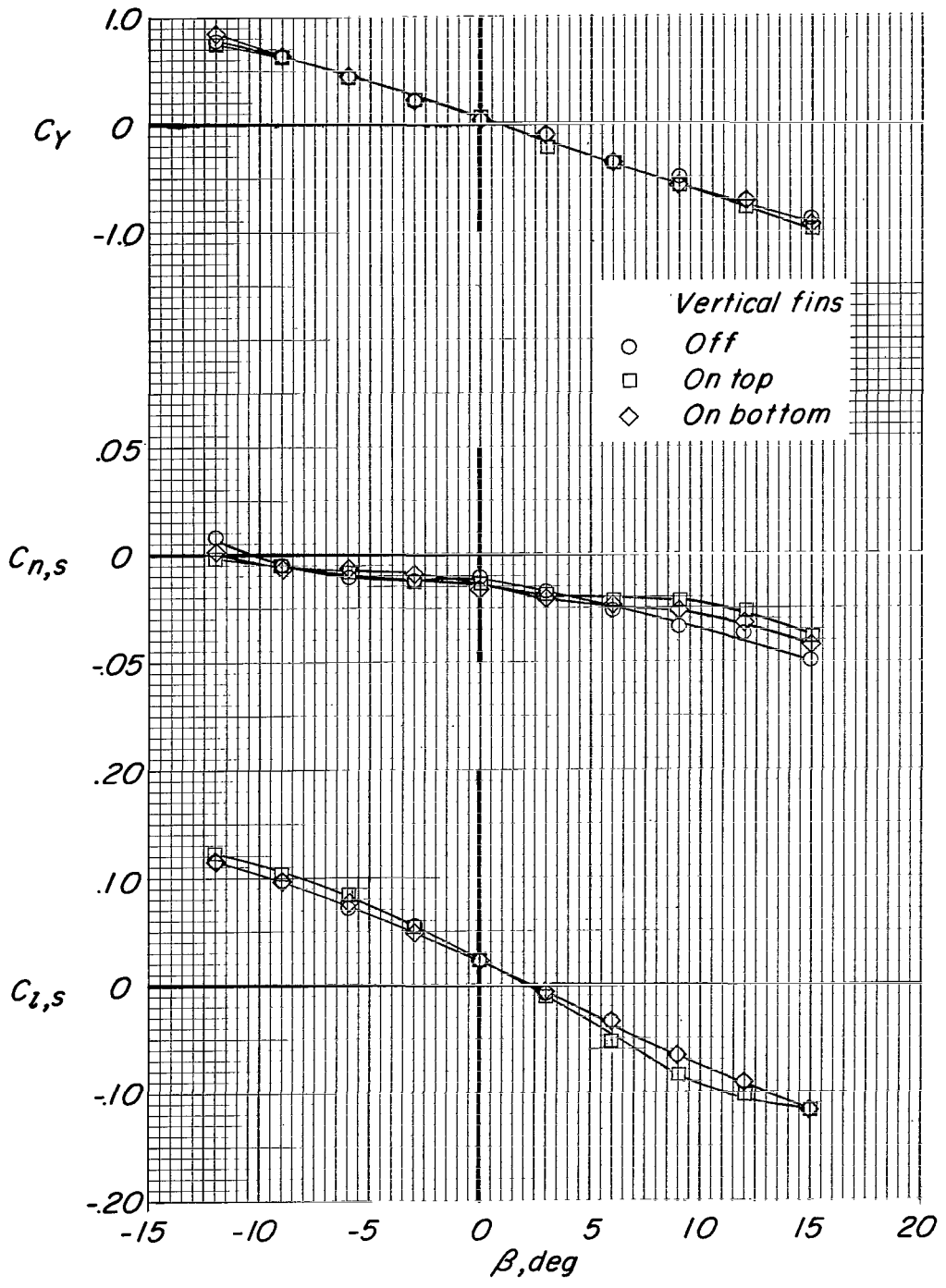

(d) C_T = 2.1.

Figure 15.- Concluded.

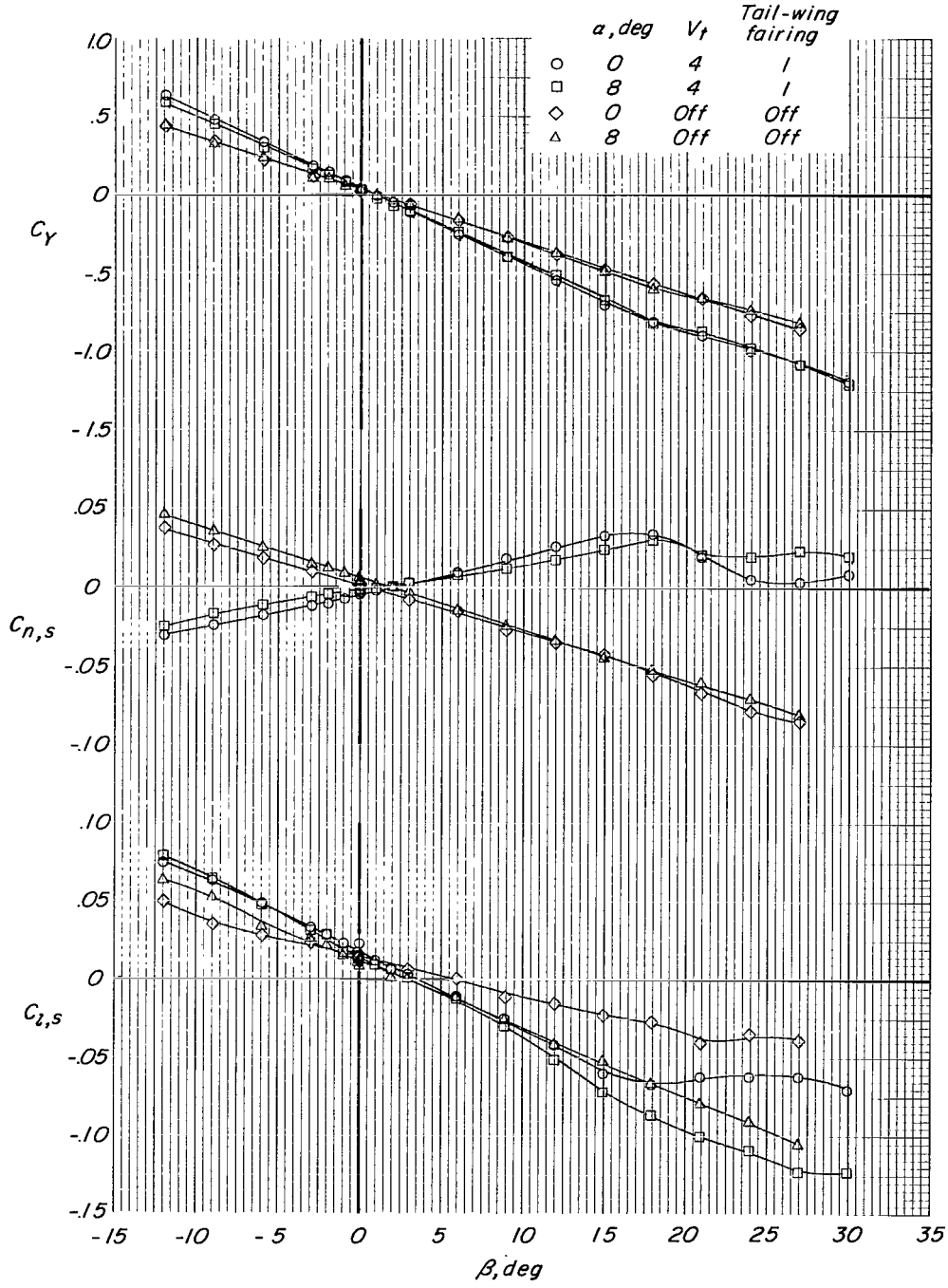

(a) $C_T \approx 0$; propellers windmilling.

Figure 16.- Effects of vertical tail 4 and power on sideslip characteristics. $\delta_{D,F} = 2^0$; $\delta_{D,R} = -3^0$; $\delta_{V,F} = \delta_{V,R} = 0^0$; H_2; $i_t = 0^0$.

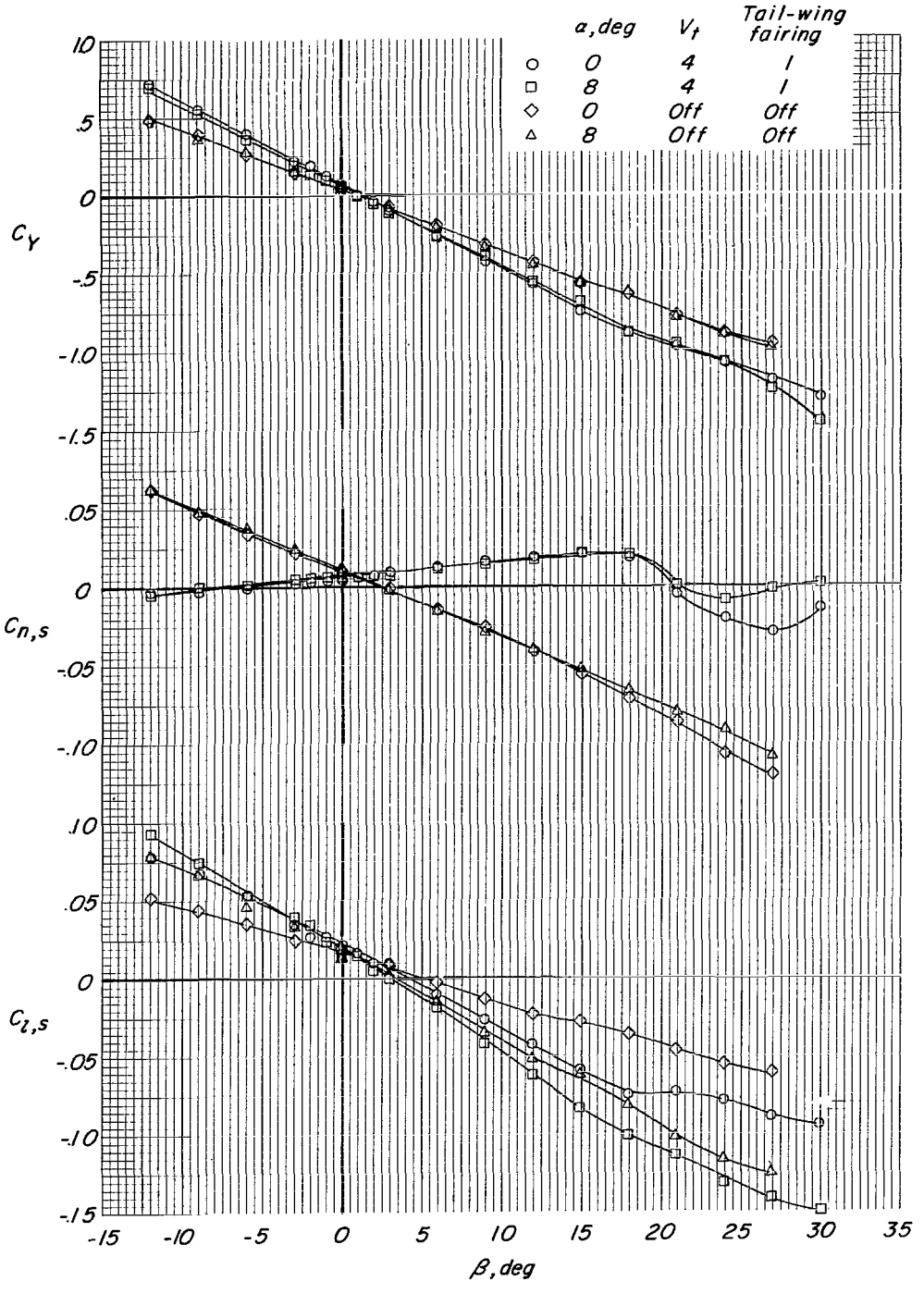

(b) C_T = 0.40.

Figure 16.- Continued.

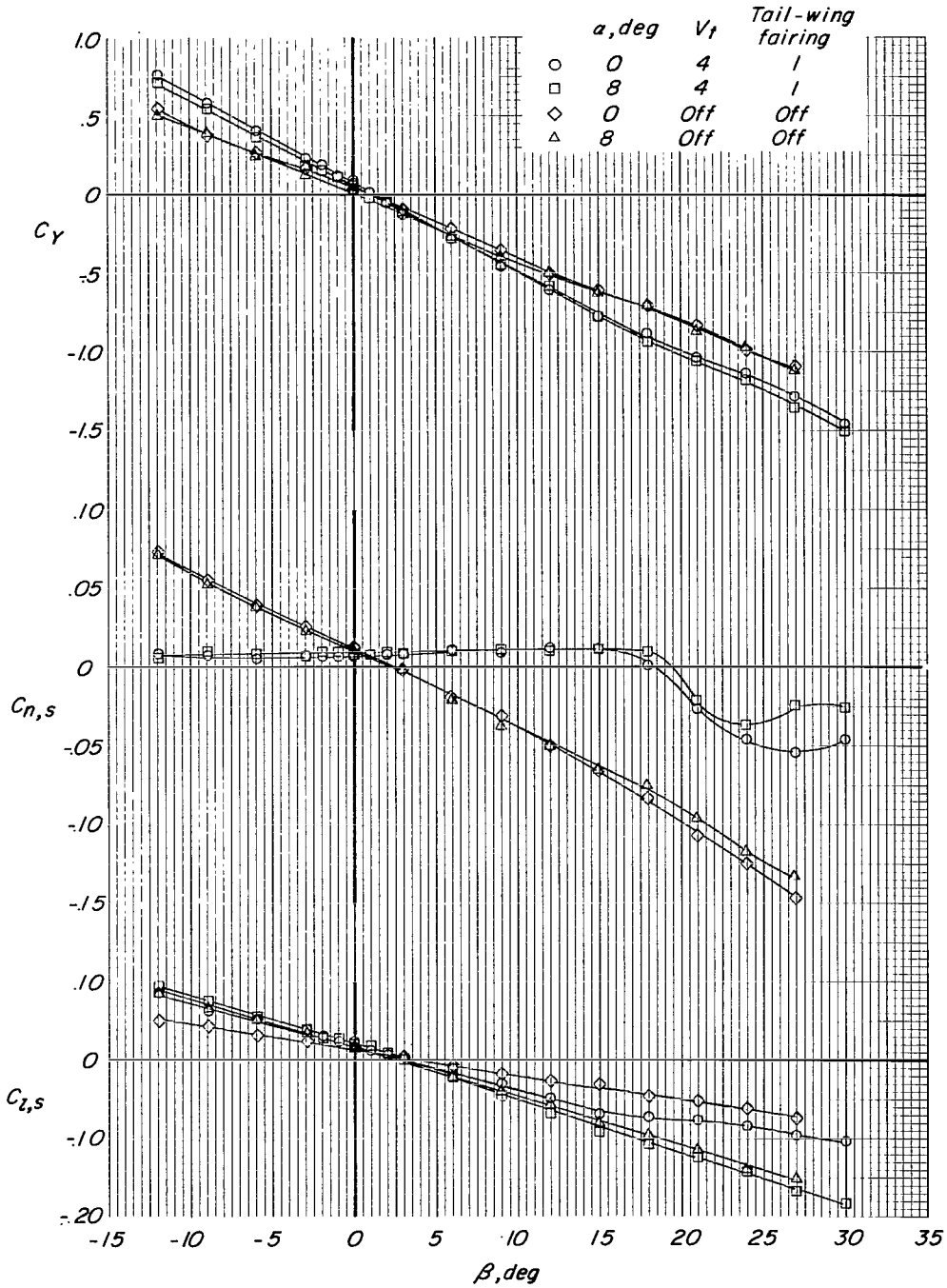

(c) C_T = 0.80.

Figure 16.- Continued.

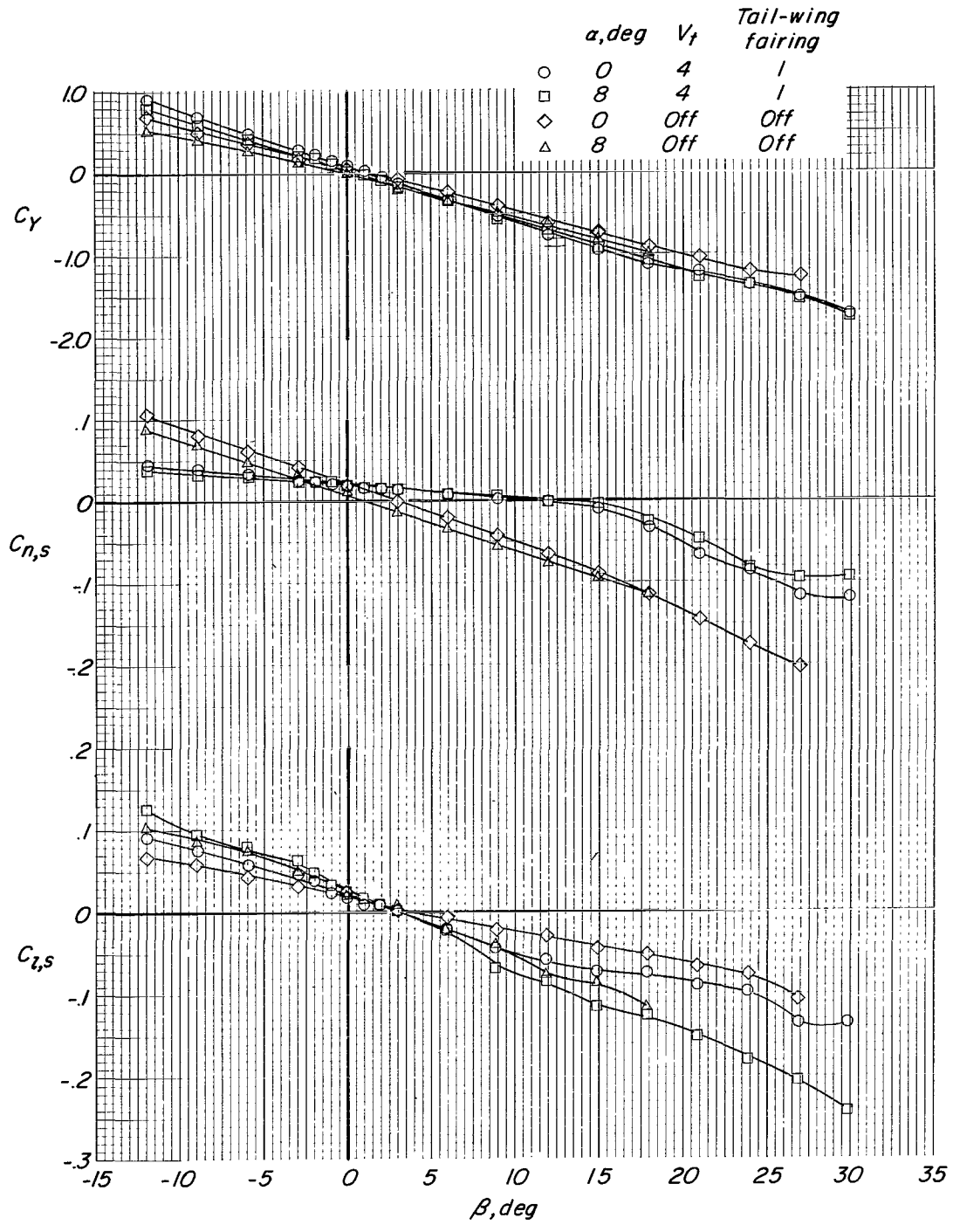

(d) C_T = 2.1.

Figure 16.- Concluded.

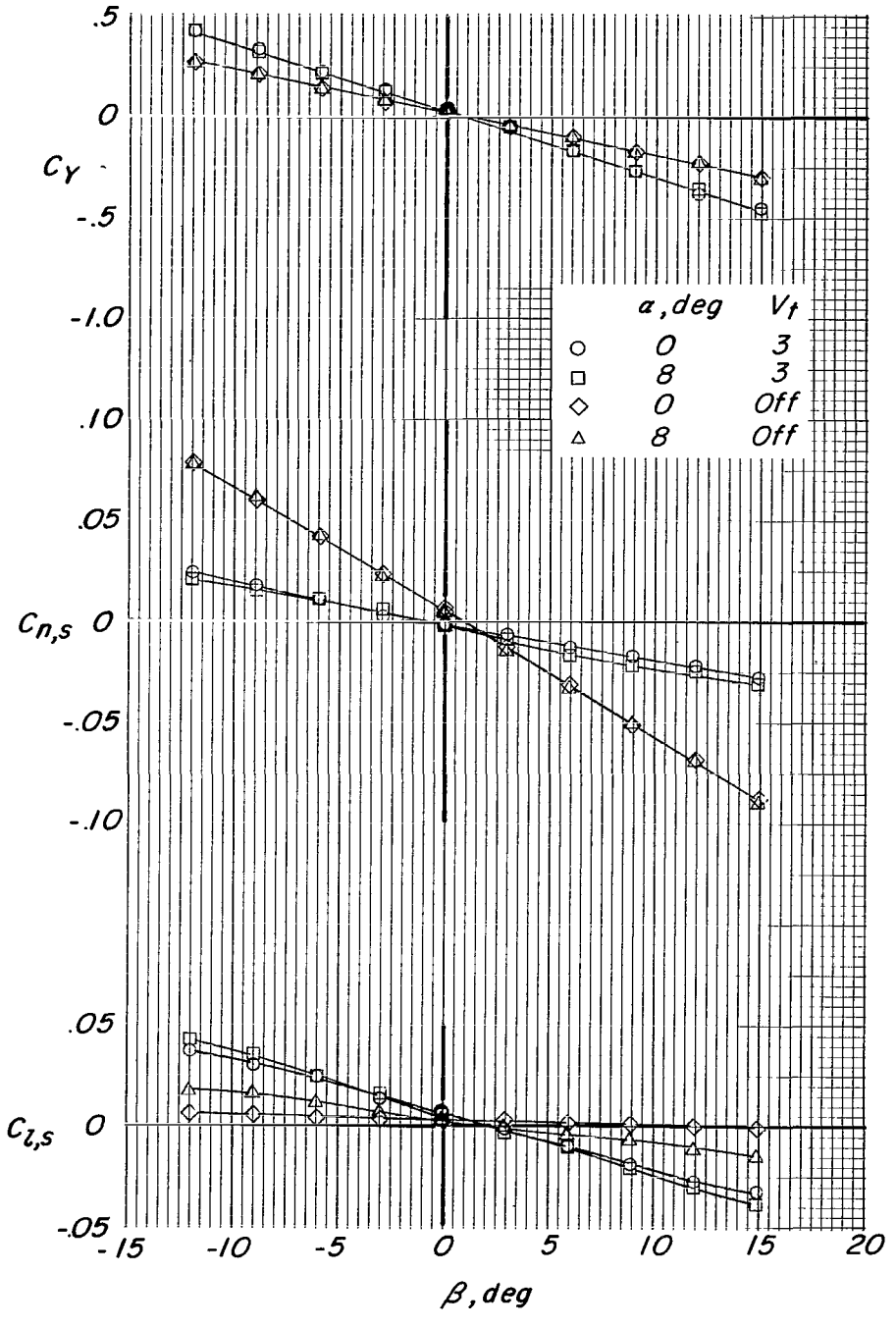

(a) $C_T \approx 0$; propellers windmilling.

Figure 17.- Effect of vertical tail and angle of attack on sideslip characteristics of model with rear ducts and wing removed. $\delta_{D,F} = 5^0$; $\delta_{V,F} = 0^0$.

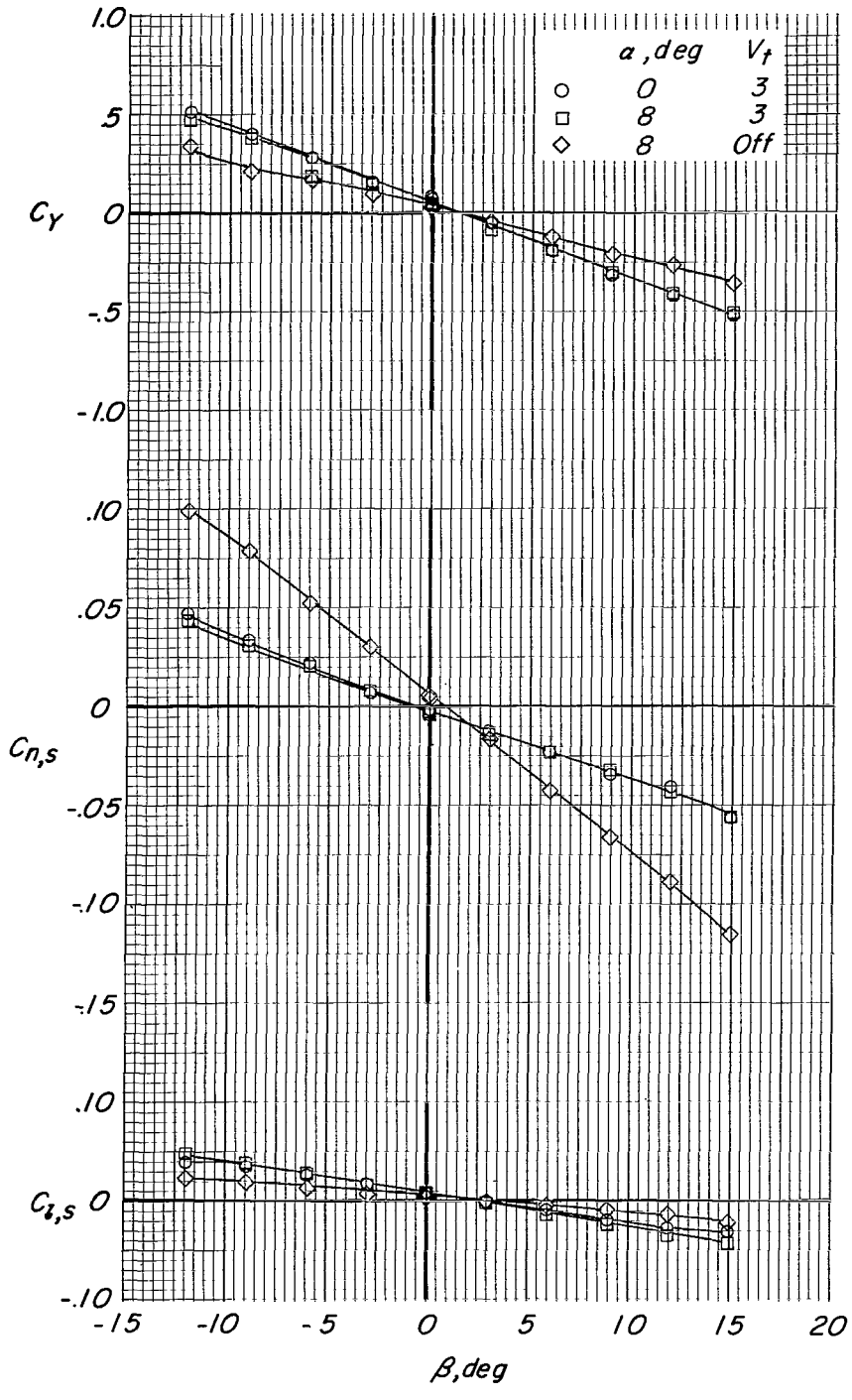

(b) $C_T = 0.80$.

Figure 17.- Concluded.

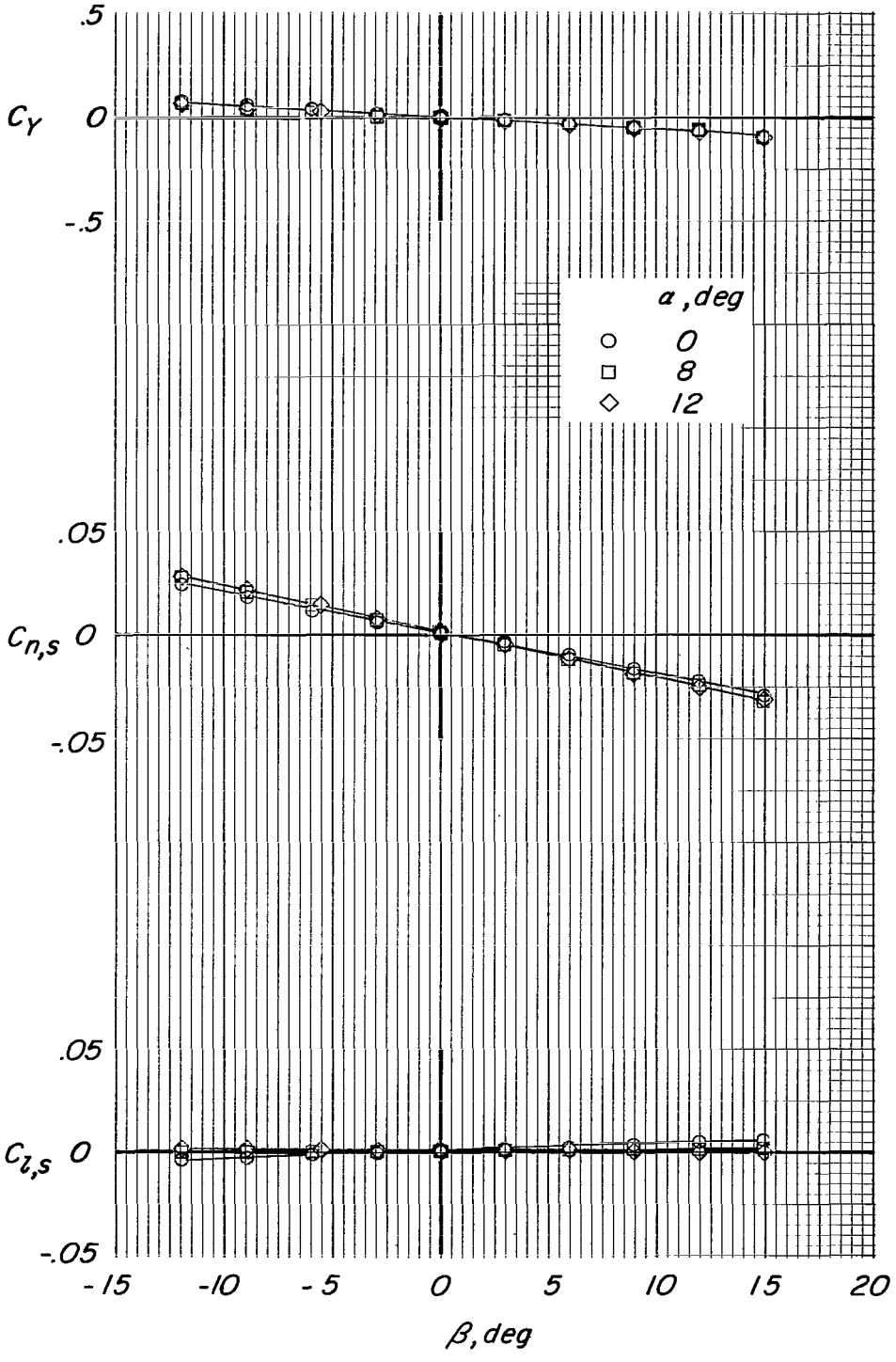

Figure 18.- Fuselage-alone characteristics in sideslip. $C_T = 0$; $q = 10$ lbf/ft^2 (478.8 N/m^2).

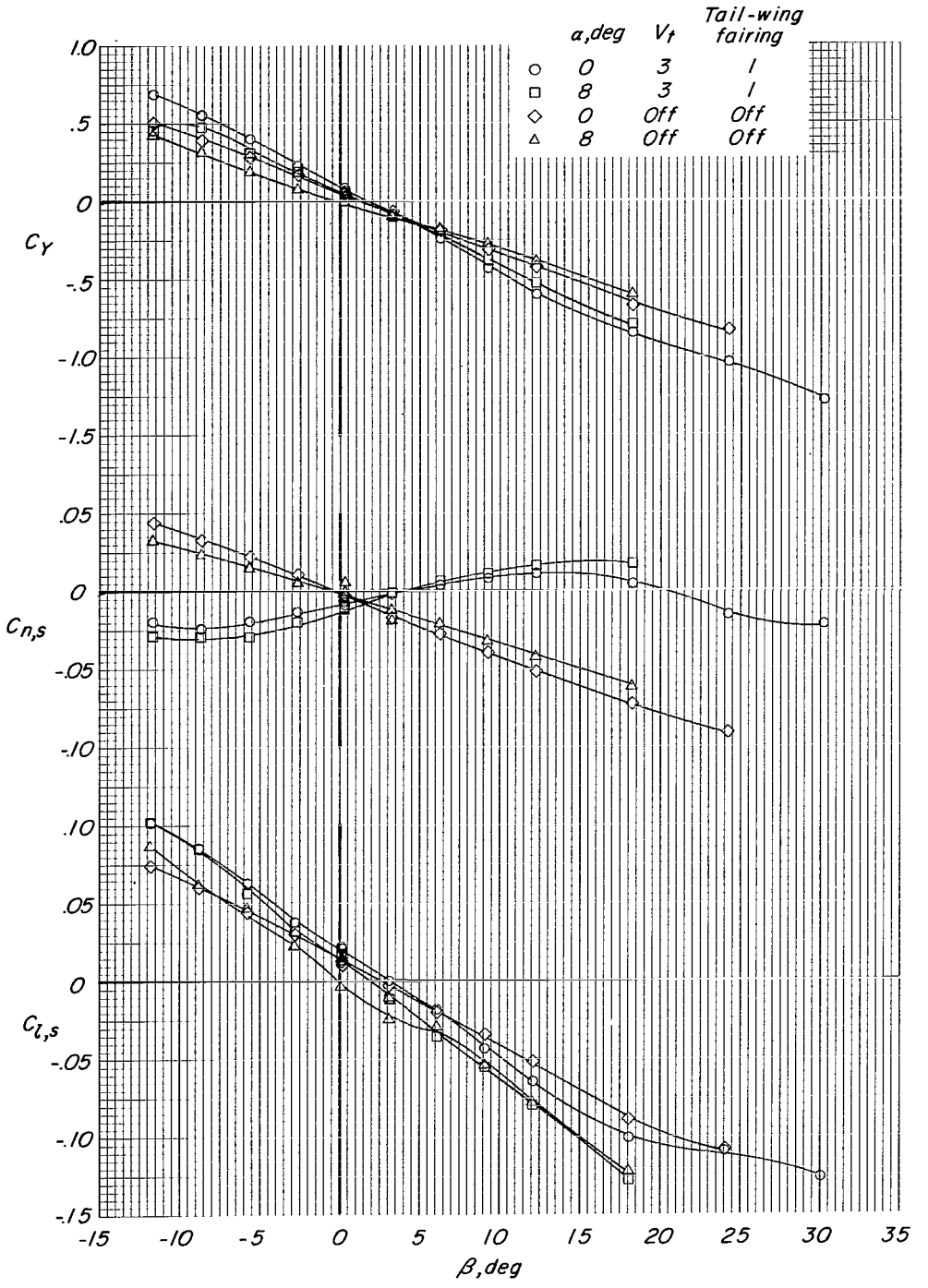

(a) $C_T = 0.40$; $\delta_{D,F} = \delta_{D,R} = 15^0$.

Figure 19.- Effect of vertical tail 3 on sideslip characteristics in transition-speed range. Modified duct lips; $\delta_{V,F} = \delta_{V,R} = 0^0$; H_1; $i_t = 0^0$.

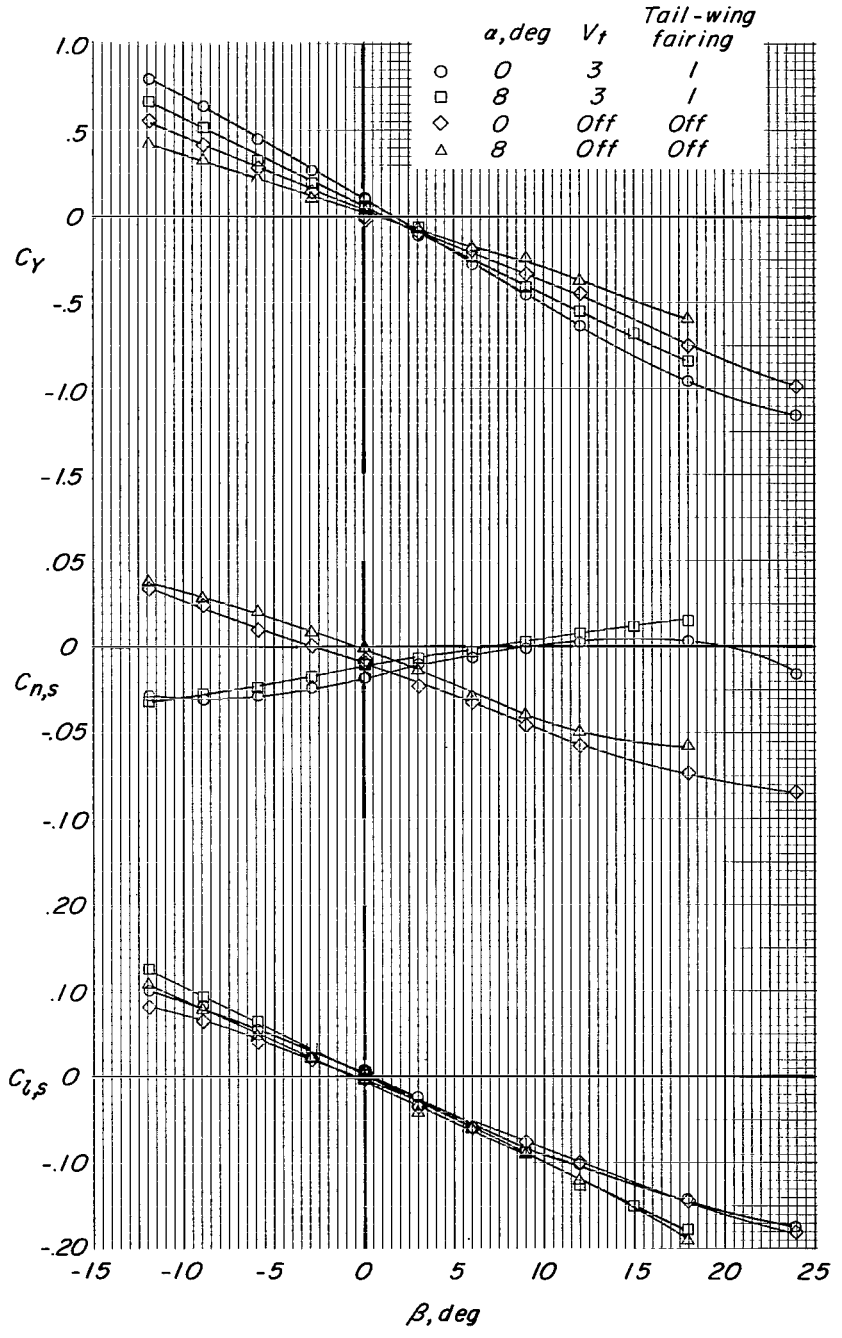

(b) $C_T = 0.80$; $\delta_{D,F} = \delta_{D,R} = 30^o$.

Figure 19.- Continued.

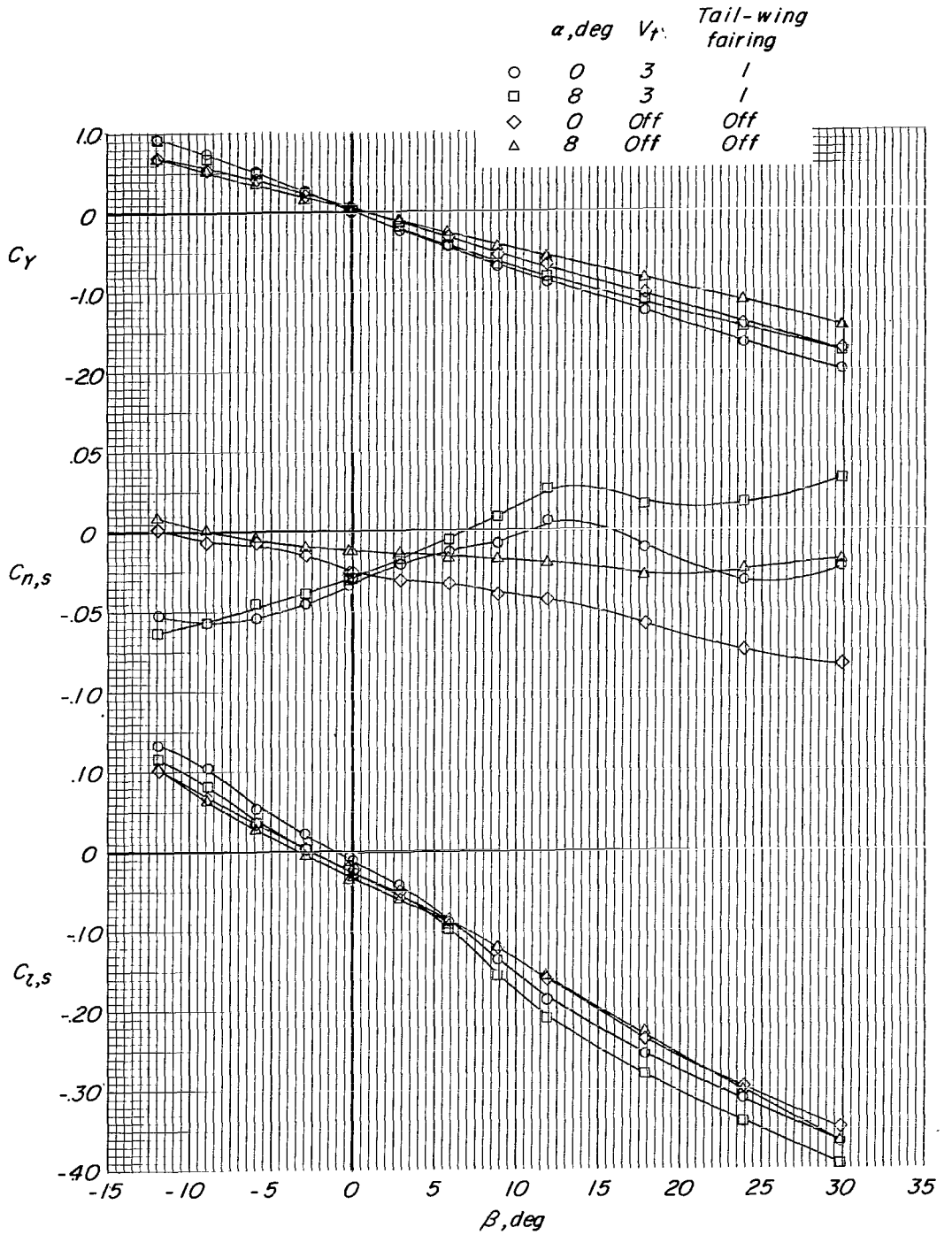

(c) $C_T = 2.1$; $\delta_{D,F} = \delta_{D,R} = 45^o$.

Figure 19.- Continued.

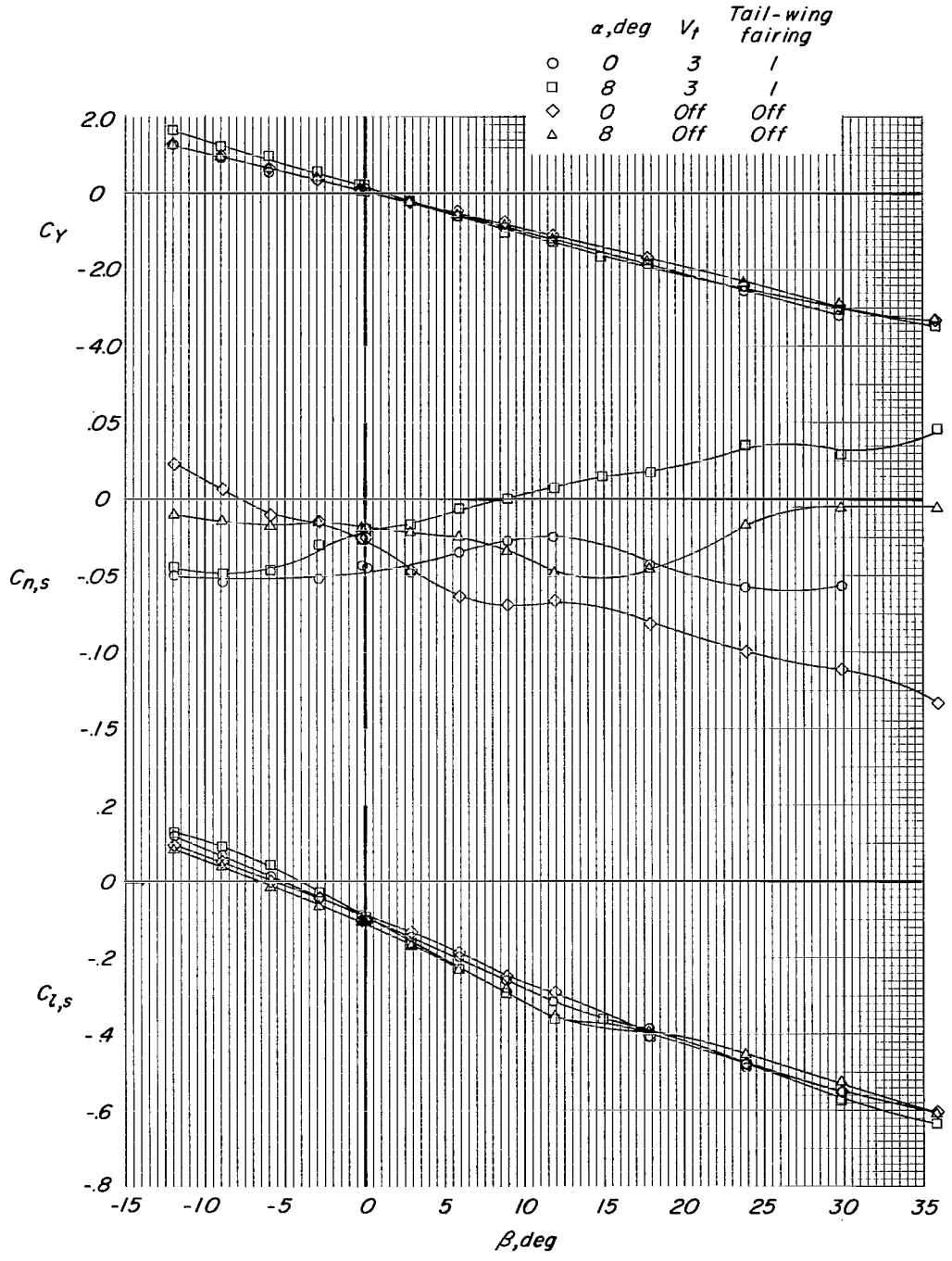

(d) $C_T = 7.1$; $\delta_{D,F} = \delta_{D,R} = 60^0$.

Figure 19.- Continued.

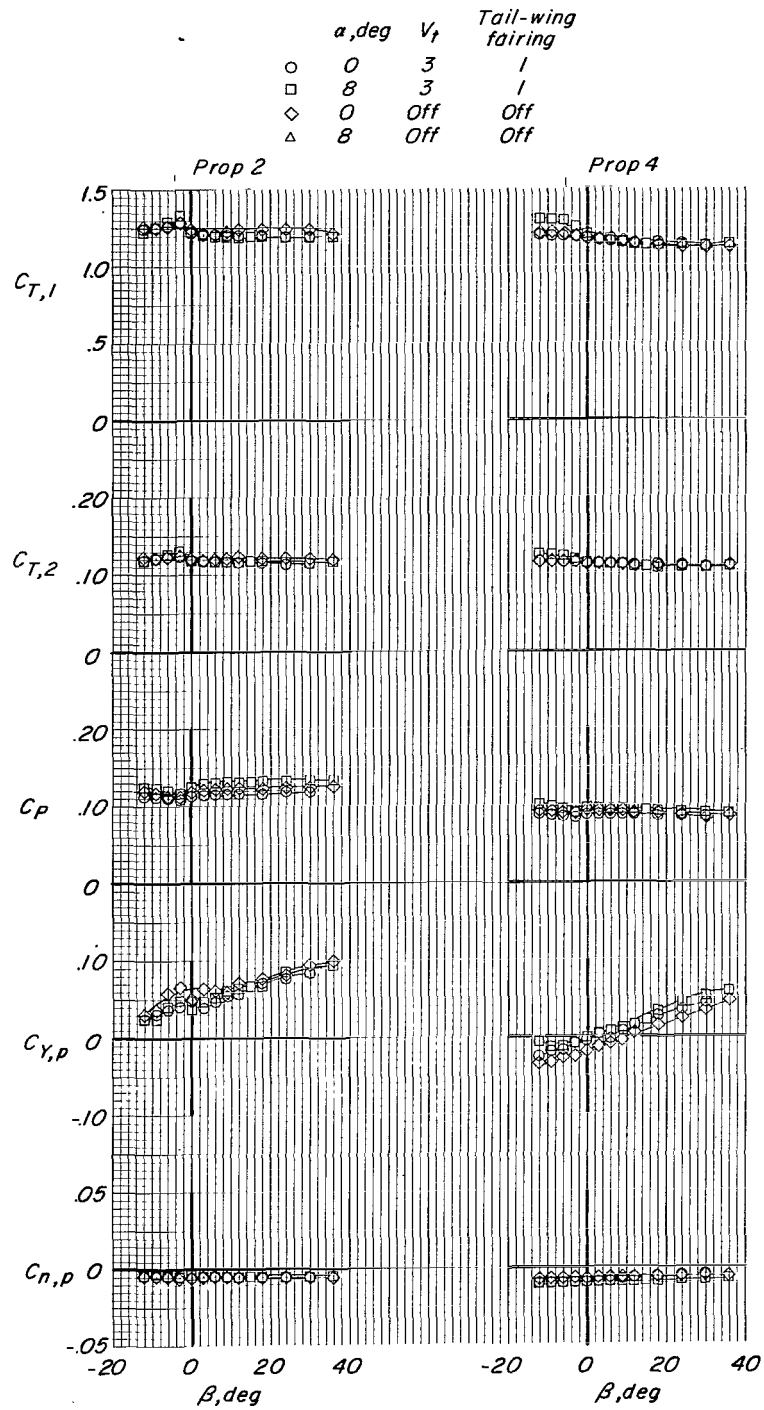

(d) Concluded.

Figure 19.- Continued.

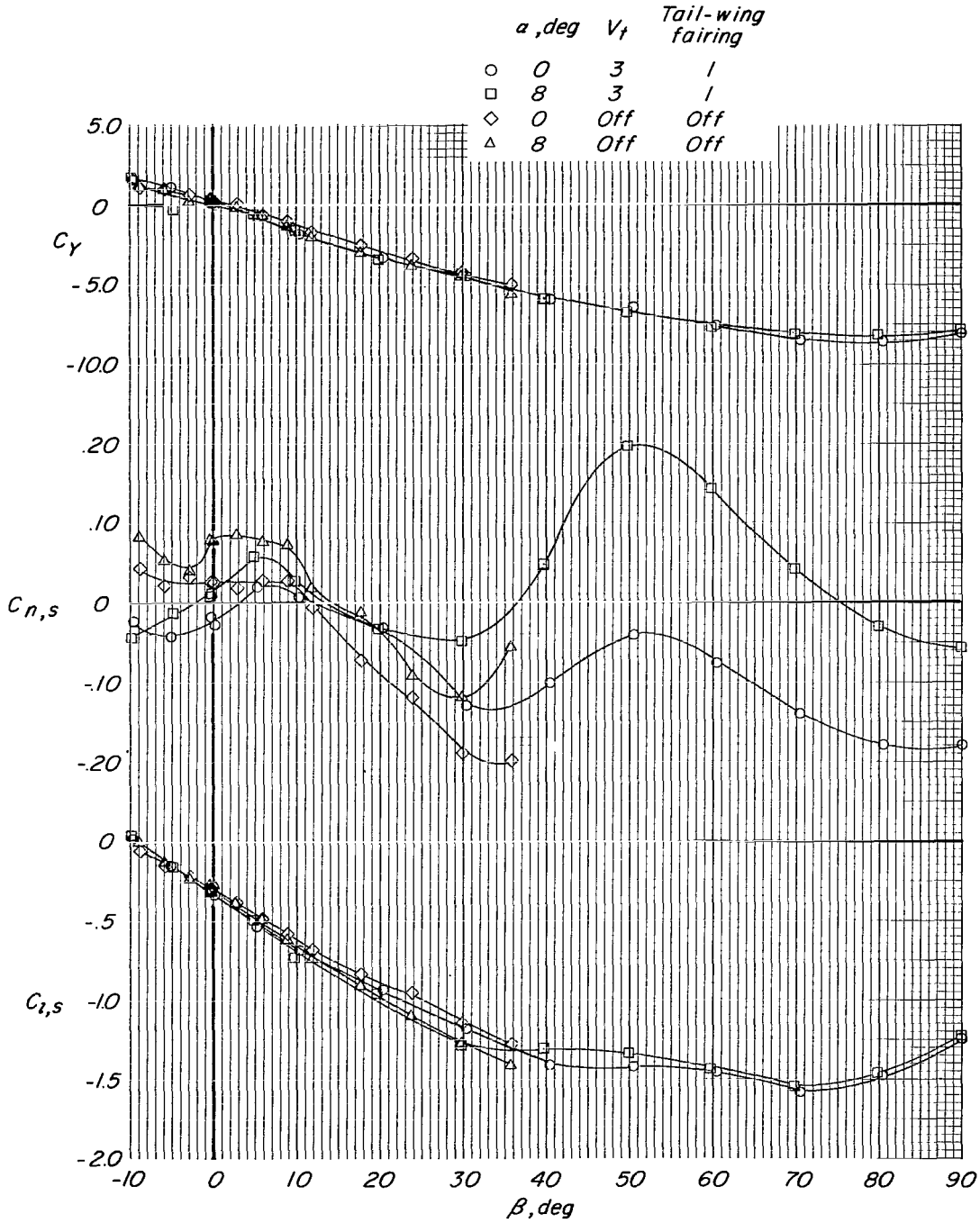

(e) $C_T = 25.0$; $\delta_{D,F} = \delta_{D,R} = 75^0$.

Figure 19.- Continued.

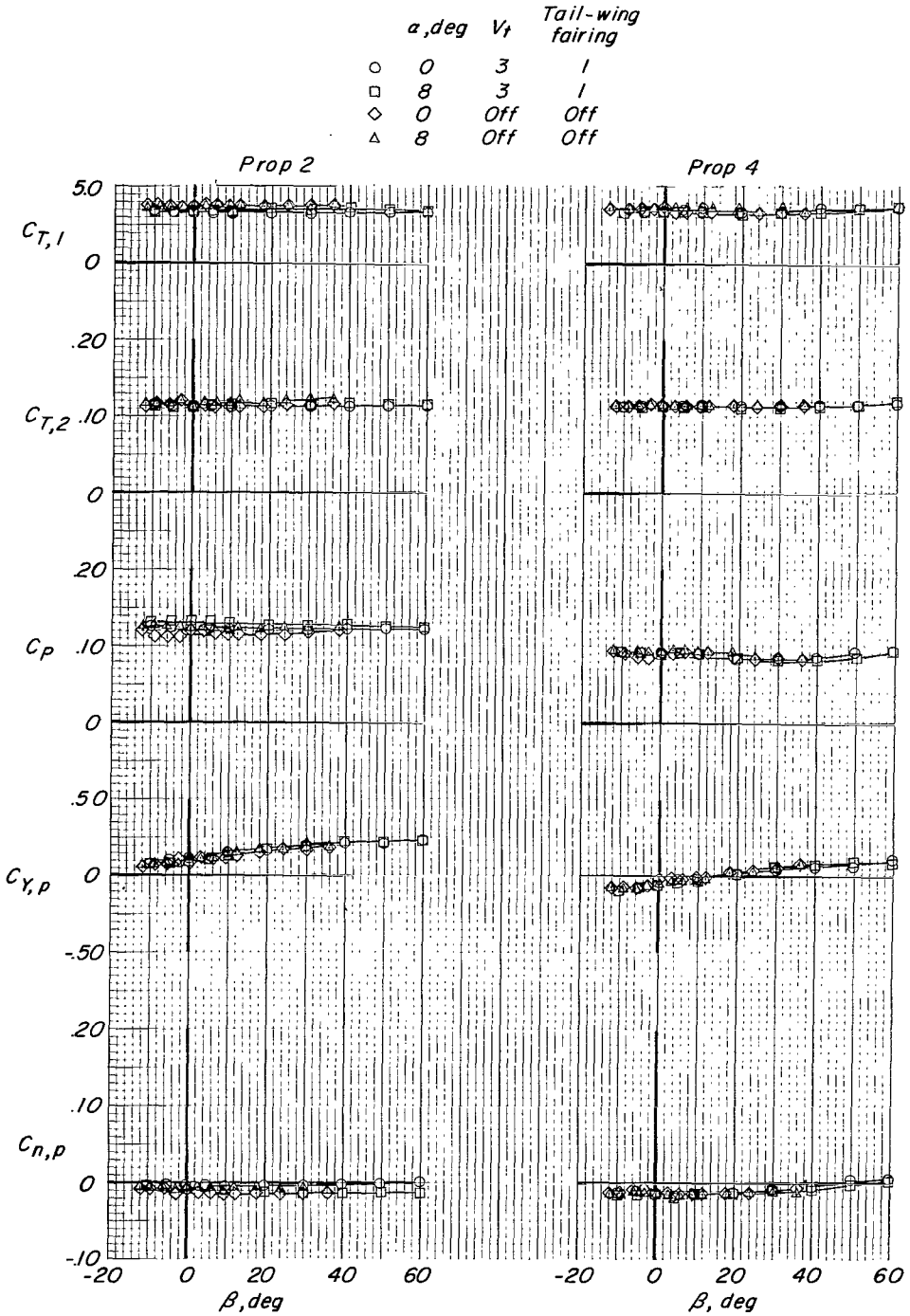

(e) Concluded.

Figure 19.- Continued.

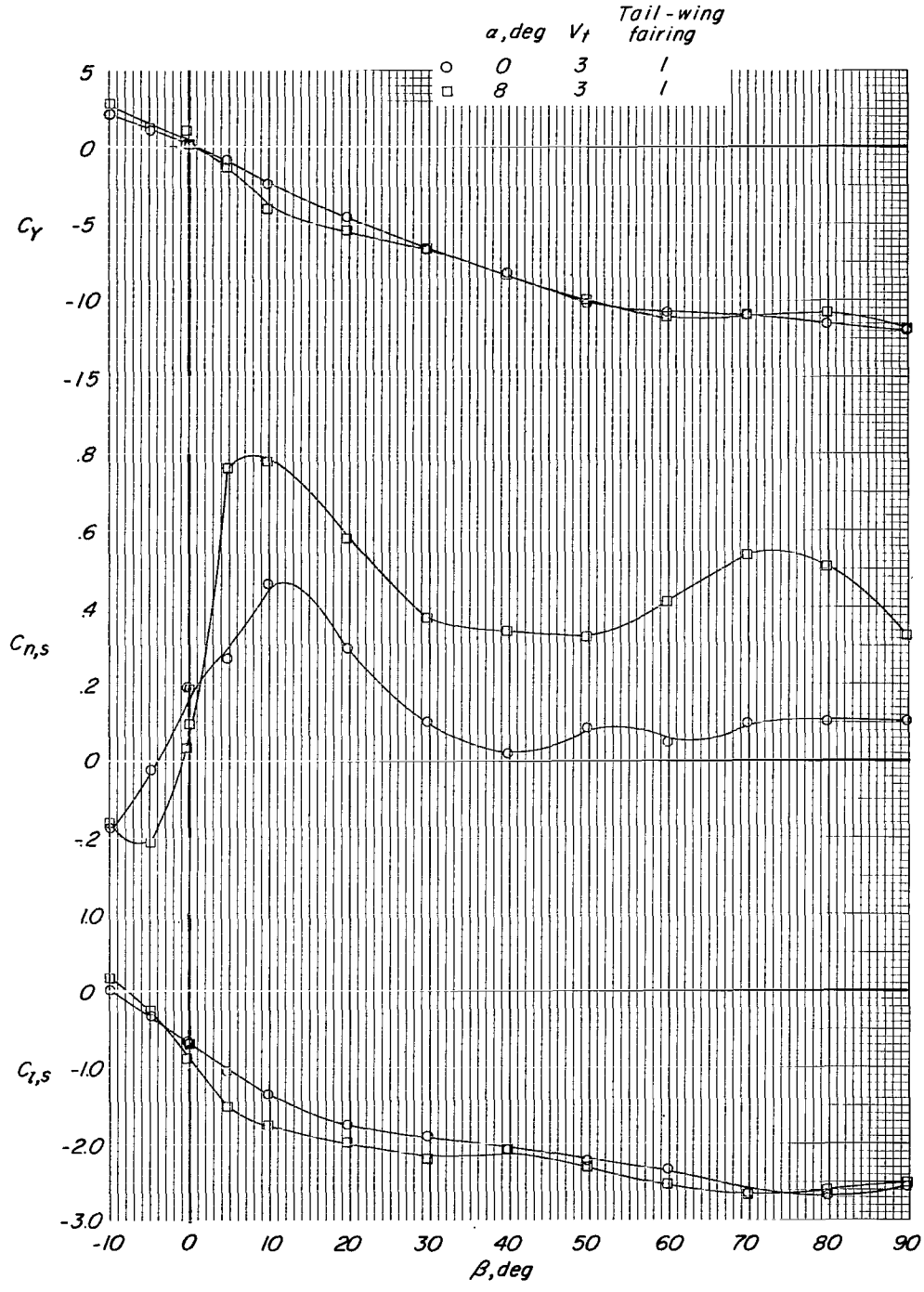

(f) $C_T = 60.0$; $\delta_{D,F} = \delta_{D,R} = 90^\circ$.

Figure 19.- Continued.

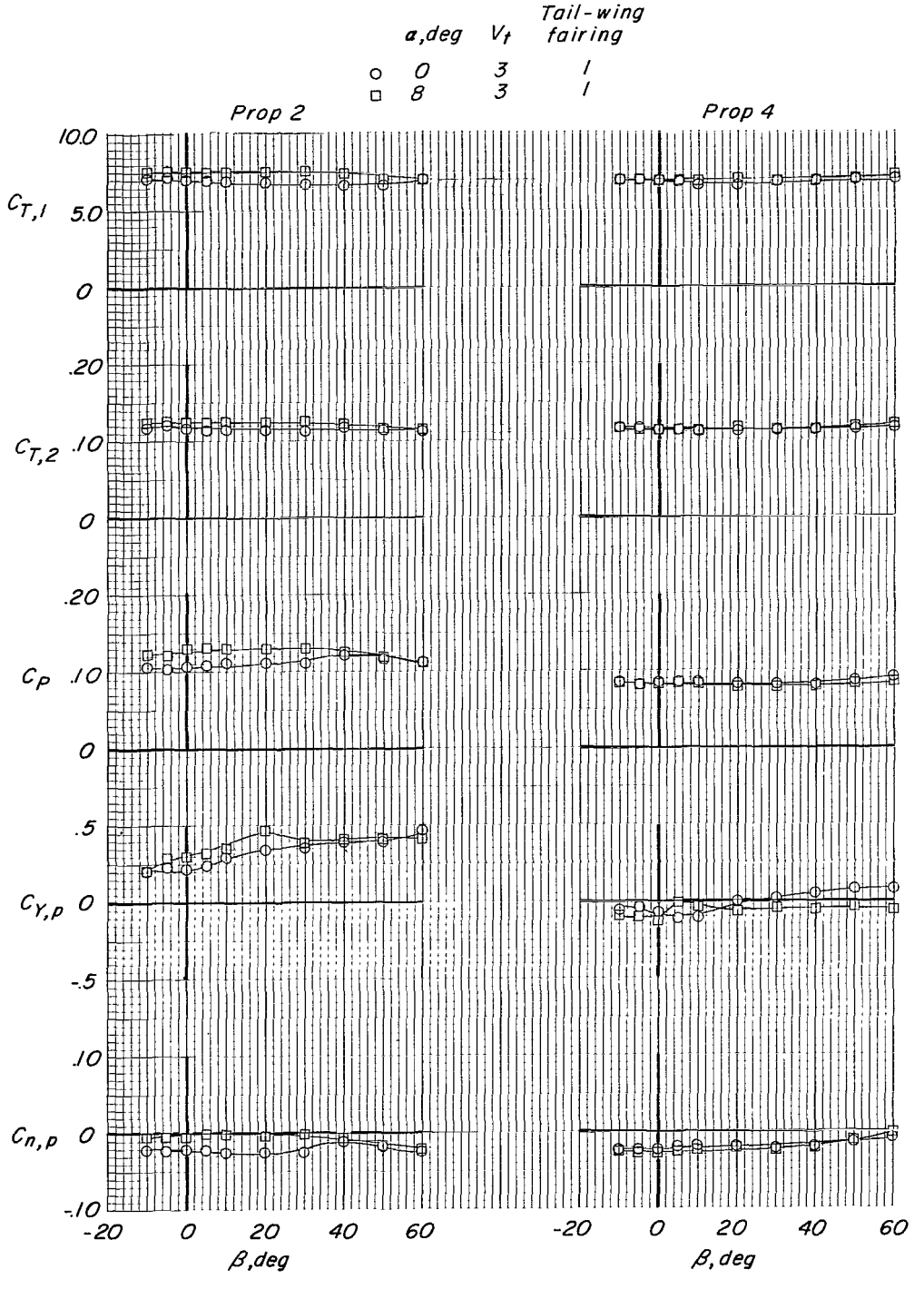

(f) Concluded.

Figure 19.- Concluded.

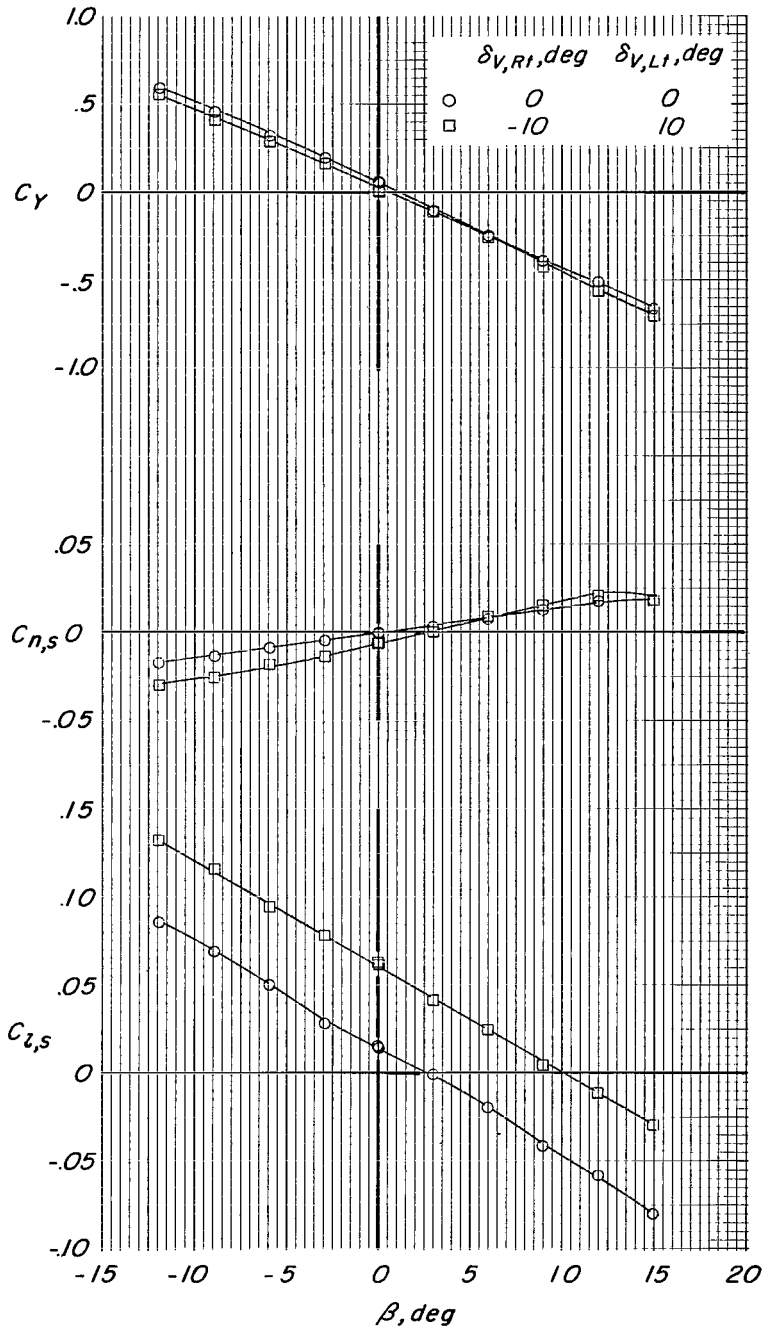

(a) $\alpha = 8^0$; $C_T \approx 0$; propellers windmilling.

Figure 20.- Effect of elevons (vanes) for roll control with angle of sideslip. $\delta_{D,F} = 5^0$; $\delta_{D,R} = 0^0$; vertical tail 3; tail-wing fairing 1; H_1; $i_t = 0^0$.

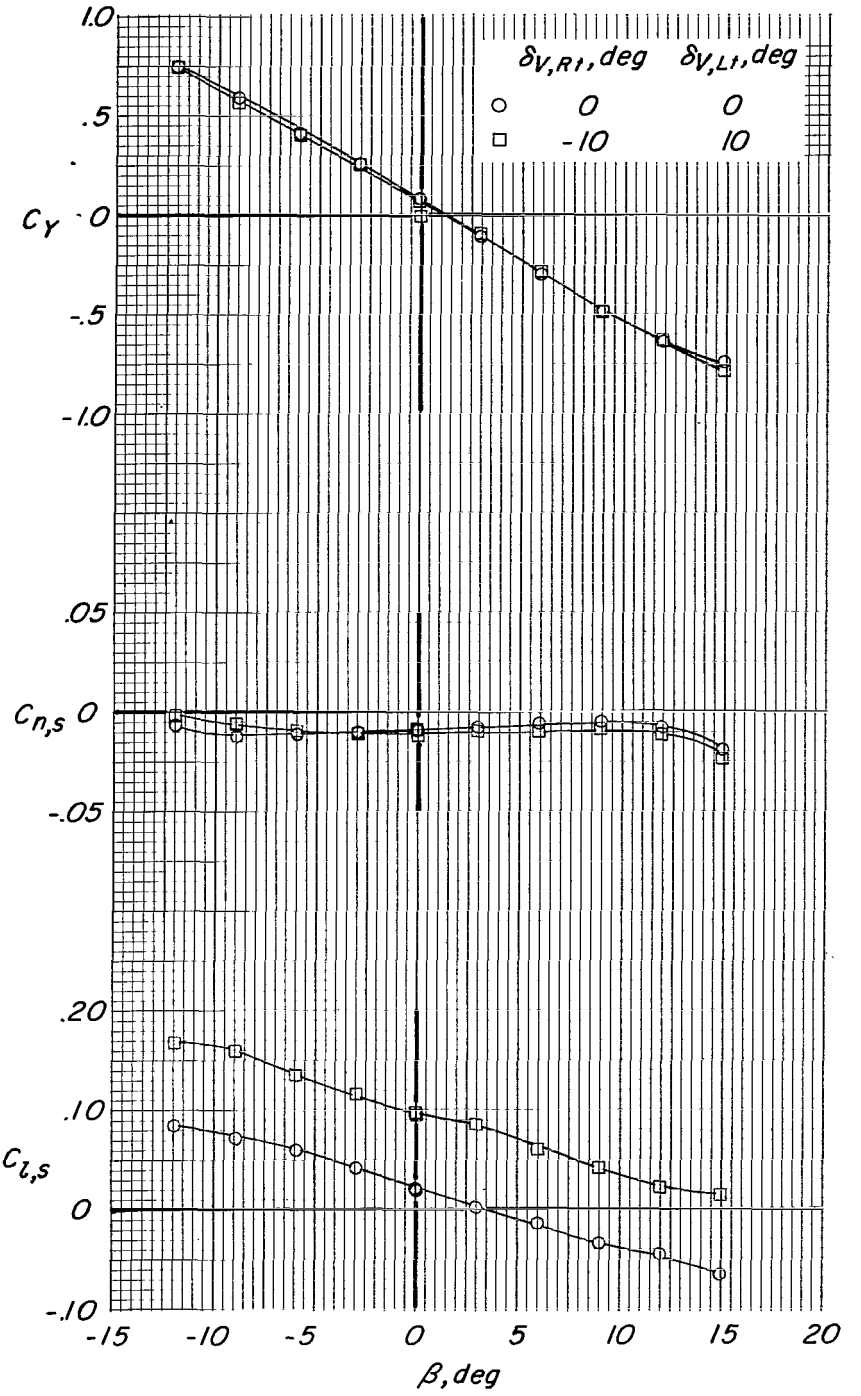

(b) $\alpha = 0^0$; $C_T = 0.80$.

Figure 20.- Concluded.

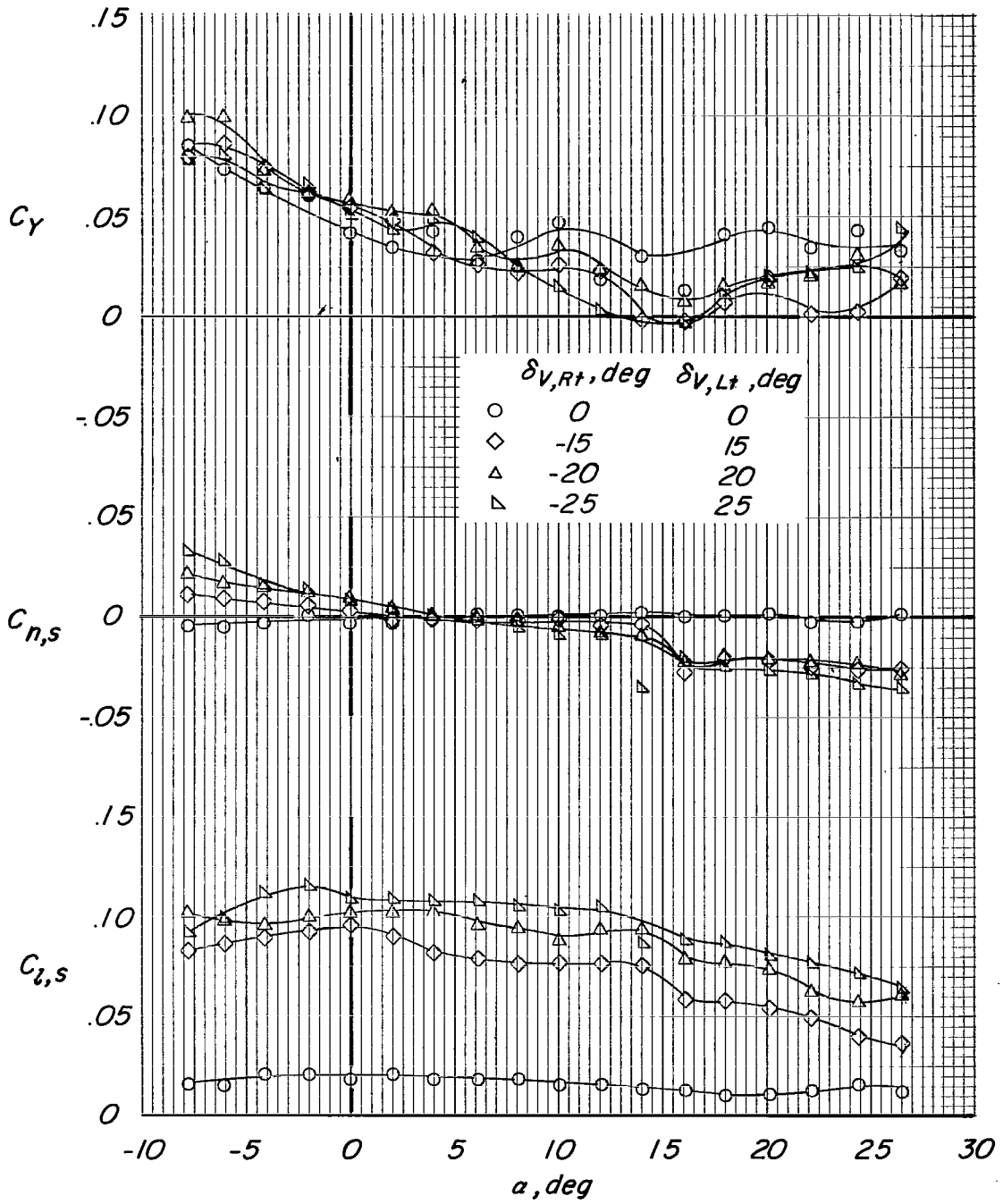

(a) $C_T \approx 0$; propellers windmilling.

Figure 21.- Effect of elevons (vanes) for roll control through angle-of-attack range. $\delta_{D,F} = 2^0$; $\delta_{D,R} = -3^0$; vertical tail 4; tail-wing fairing 1; H_2; $i_t = 0^0$.

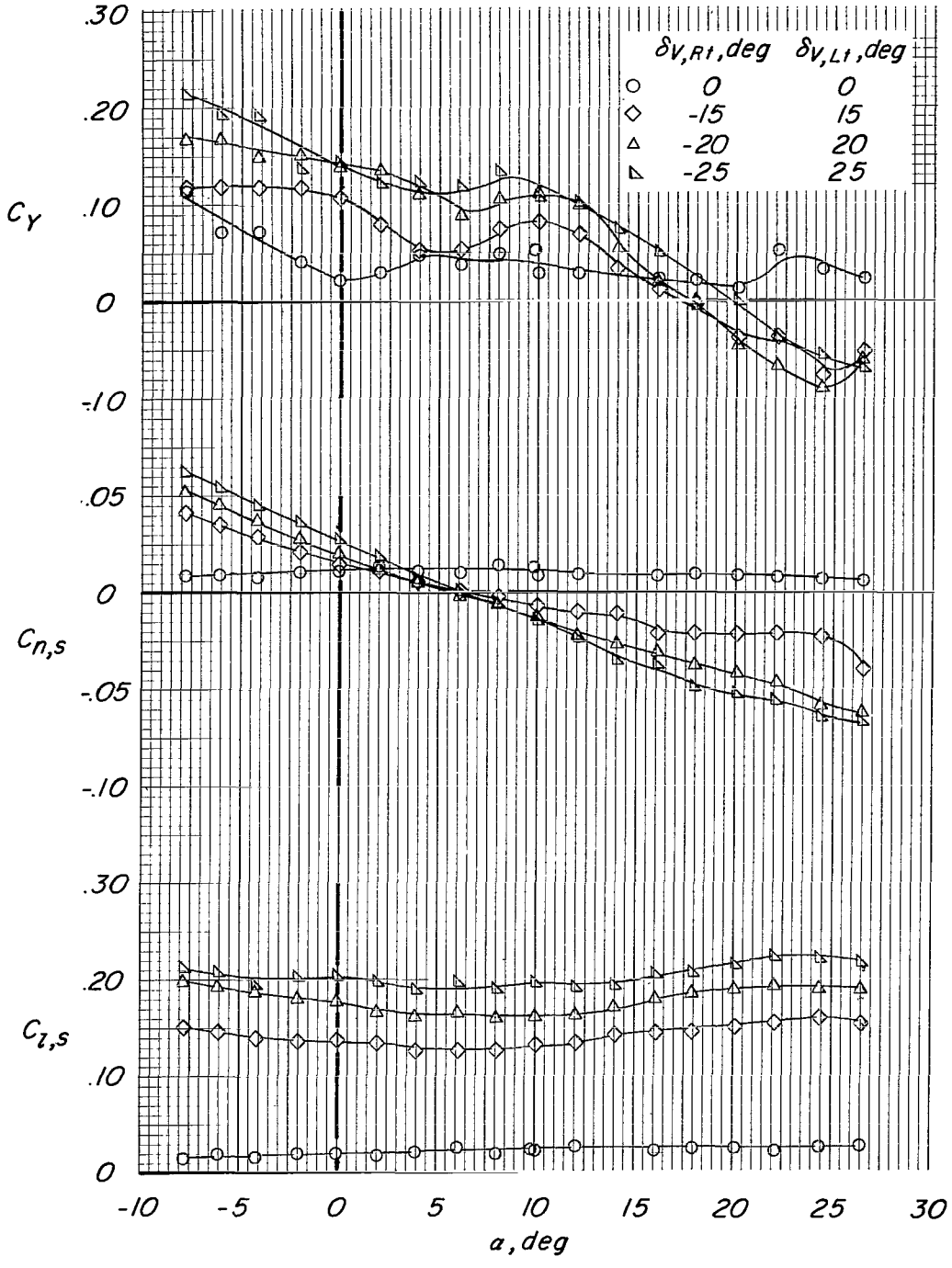

(b) $C_T = 0.80$.

Figure 21.- Continued.

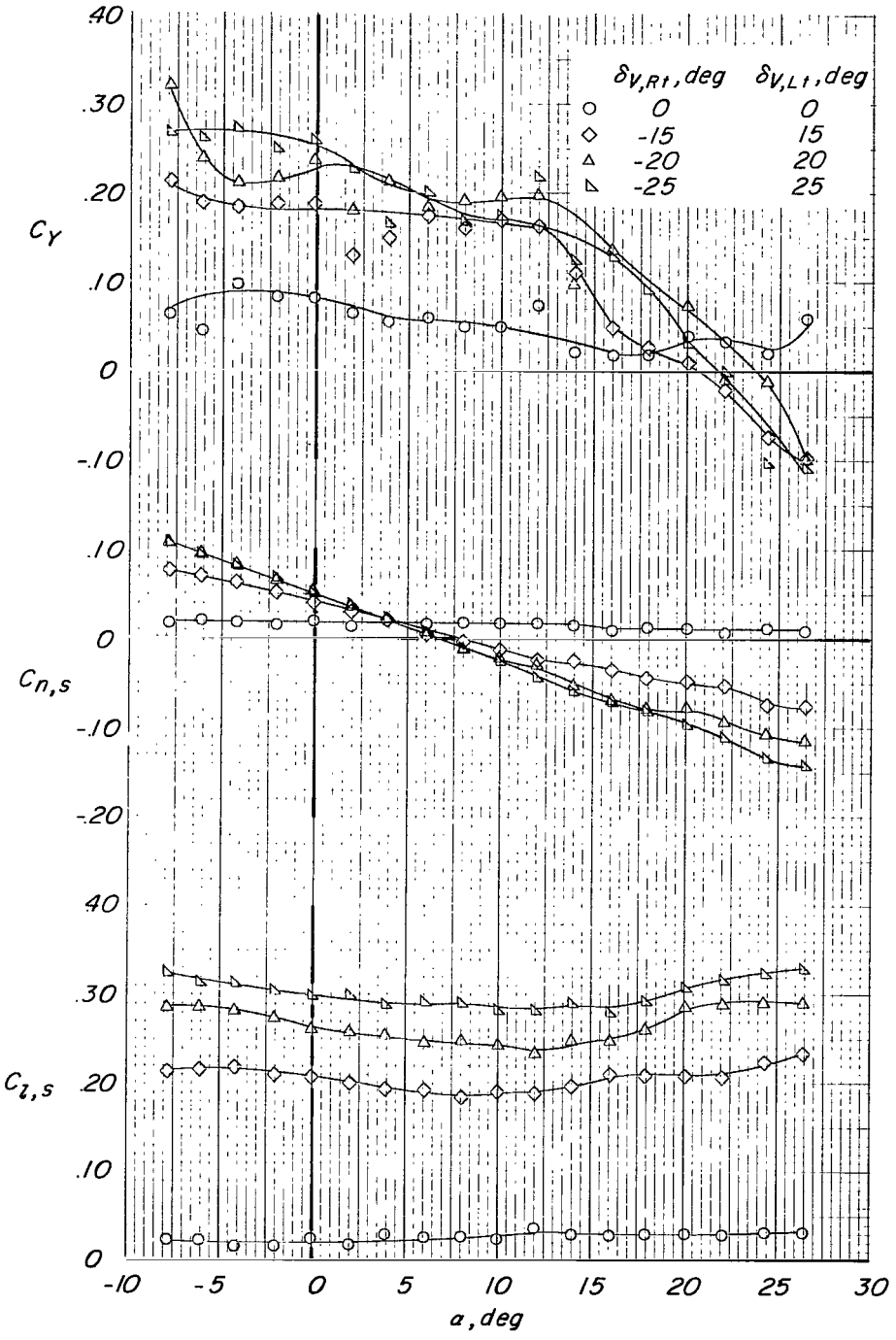

(c) $C_T = 2.1$.

Figure 21.- Concluded.

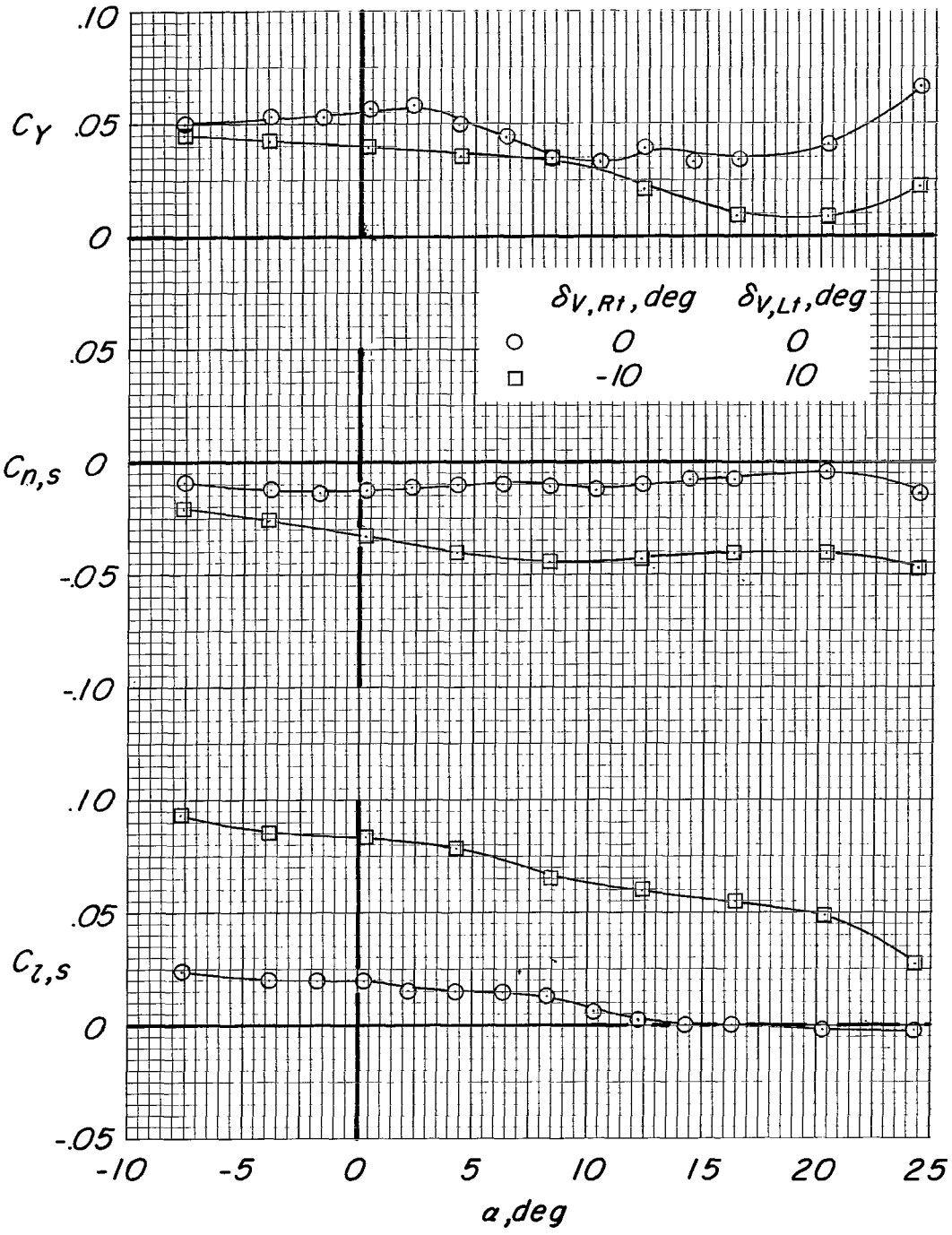

(a) $C_T = 0.40$; $\delta_{D,F} = \delta_{D,R} = 15^0$.

Figure 22.- Effect of vanes for roll and yaw control through the transition-speed range. Tail-wing fairing 1; modified duct lips; vertical tail 3; H_1; $i_t = 0^0$.

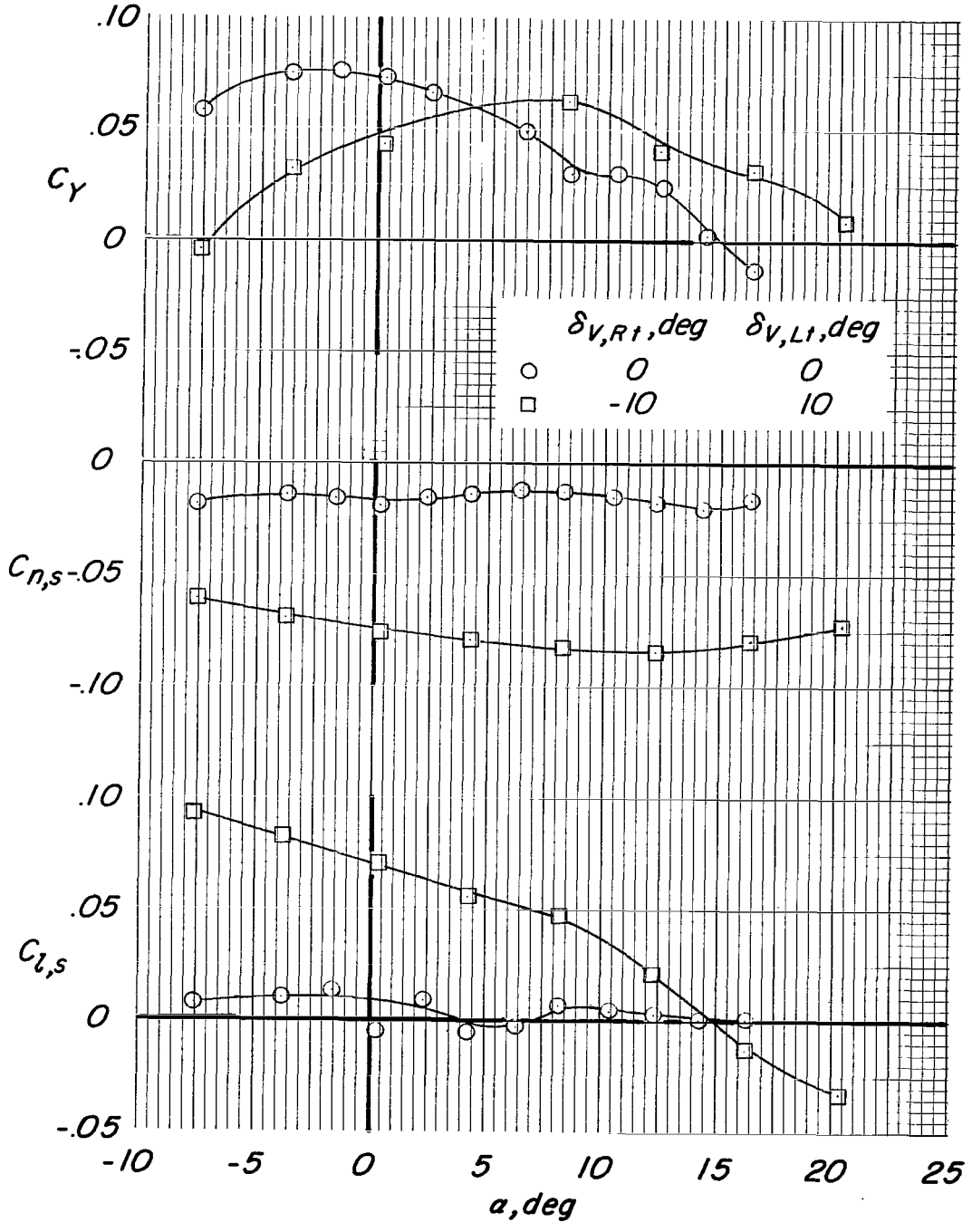

(b) $C_T = 0.80$; $\delta_{D,F} = \delta_{D,R} = 30^o$.

Figure 22.- Continued.

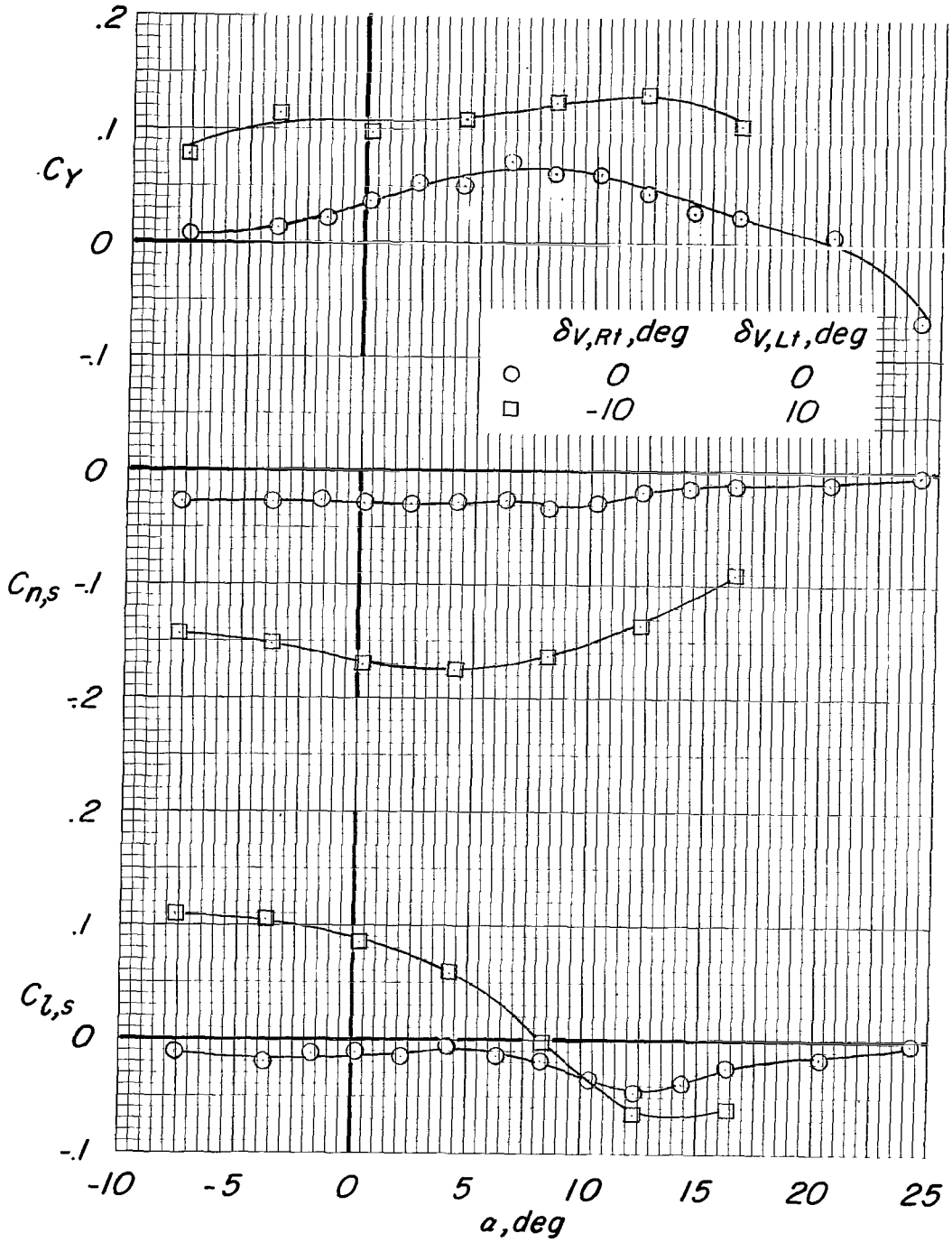

(c) $C_T = 2.1$; $\delta_{D,F} = \delta_{D,R} = 45^0$.

Figure 22.- Continued.

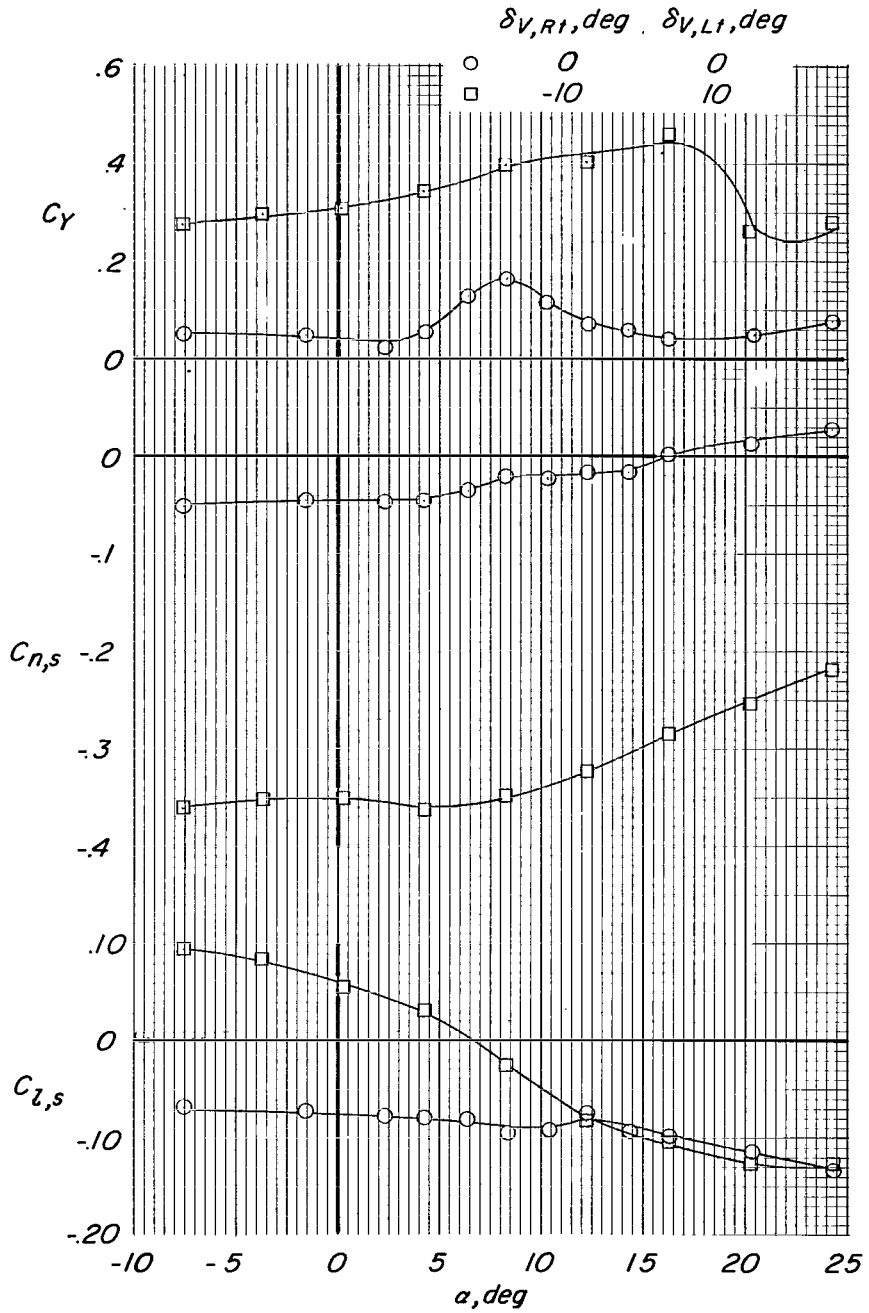

(d) $C_T = 7.1$; $\delta_{D,F} = \delta_{D,R} = 60^0$.

Figure 22.- Continued.

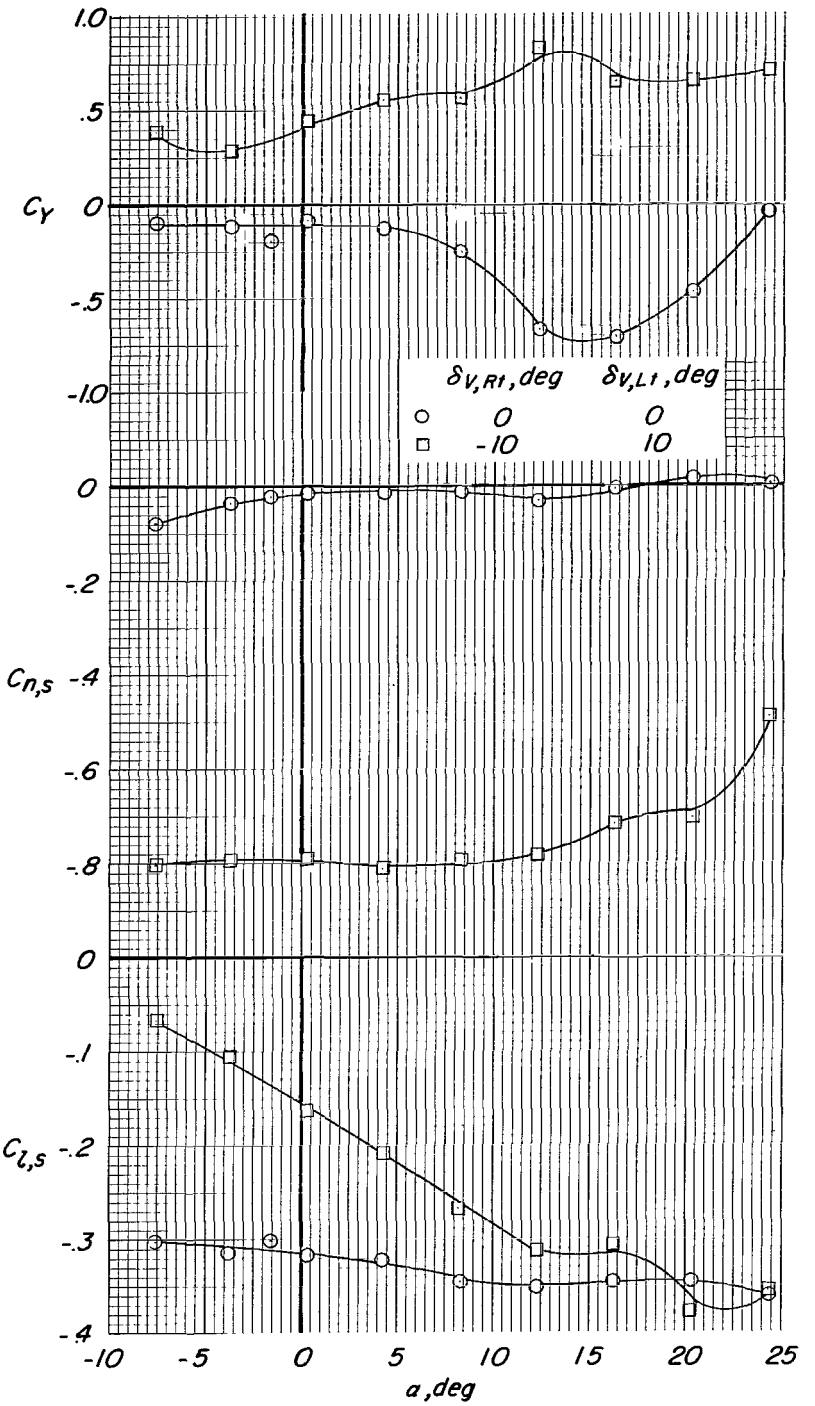

(e) $C_T = 25.0$; $\delta_{D,F} = \delta_{D,R} = 75^0$.

Figure 22.- Continued.

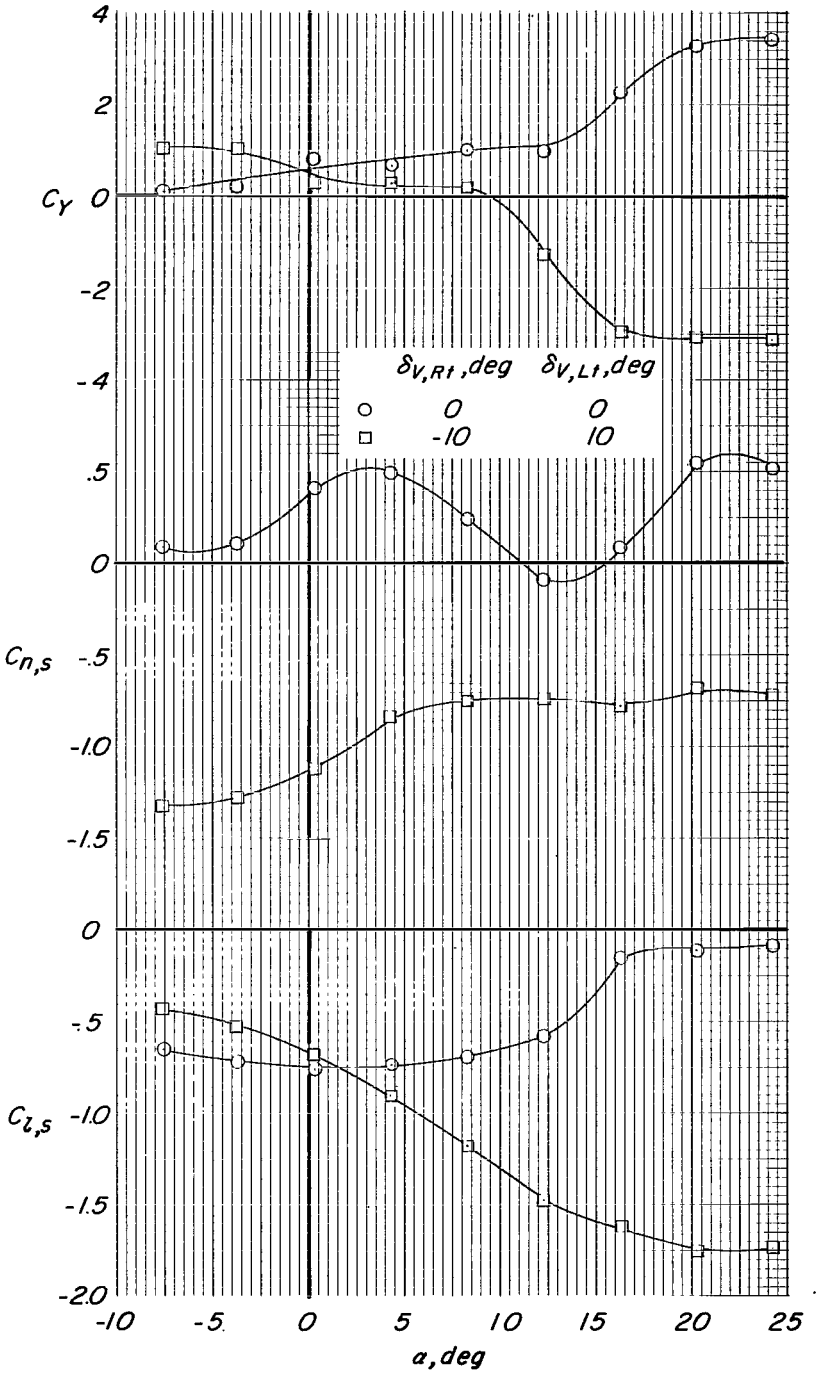

(f) $C_T = 60.0$; $\delta_{D,F} = \delta_{D,R} = 90^0$.

Figure 22.- Continued.

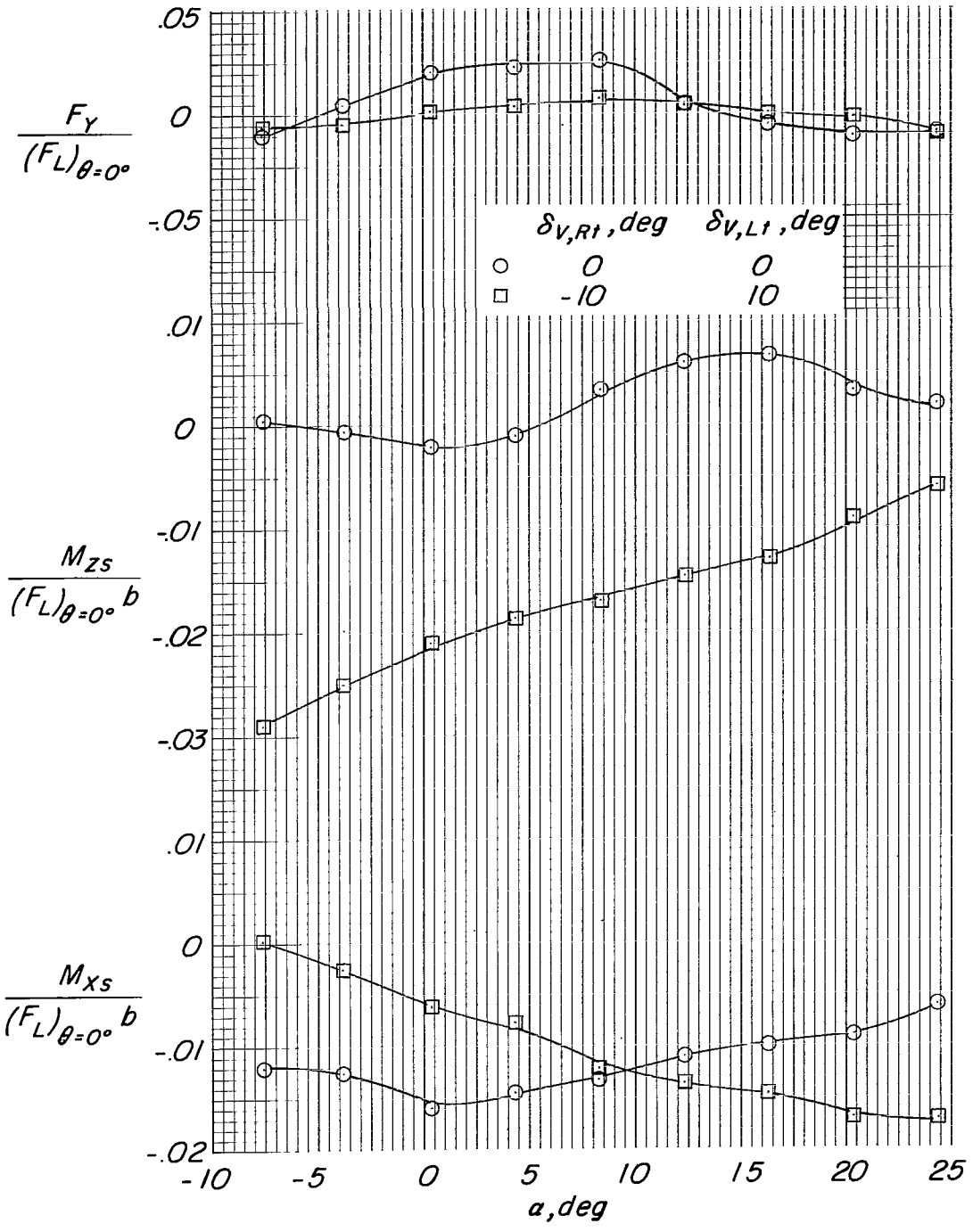

(g) $C_T = \infty$; $\delta_{D,F} = \delta_{D,R} = 90^U$.

Figure 22.- Concluded.

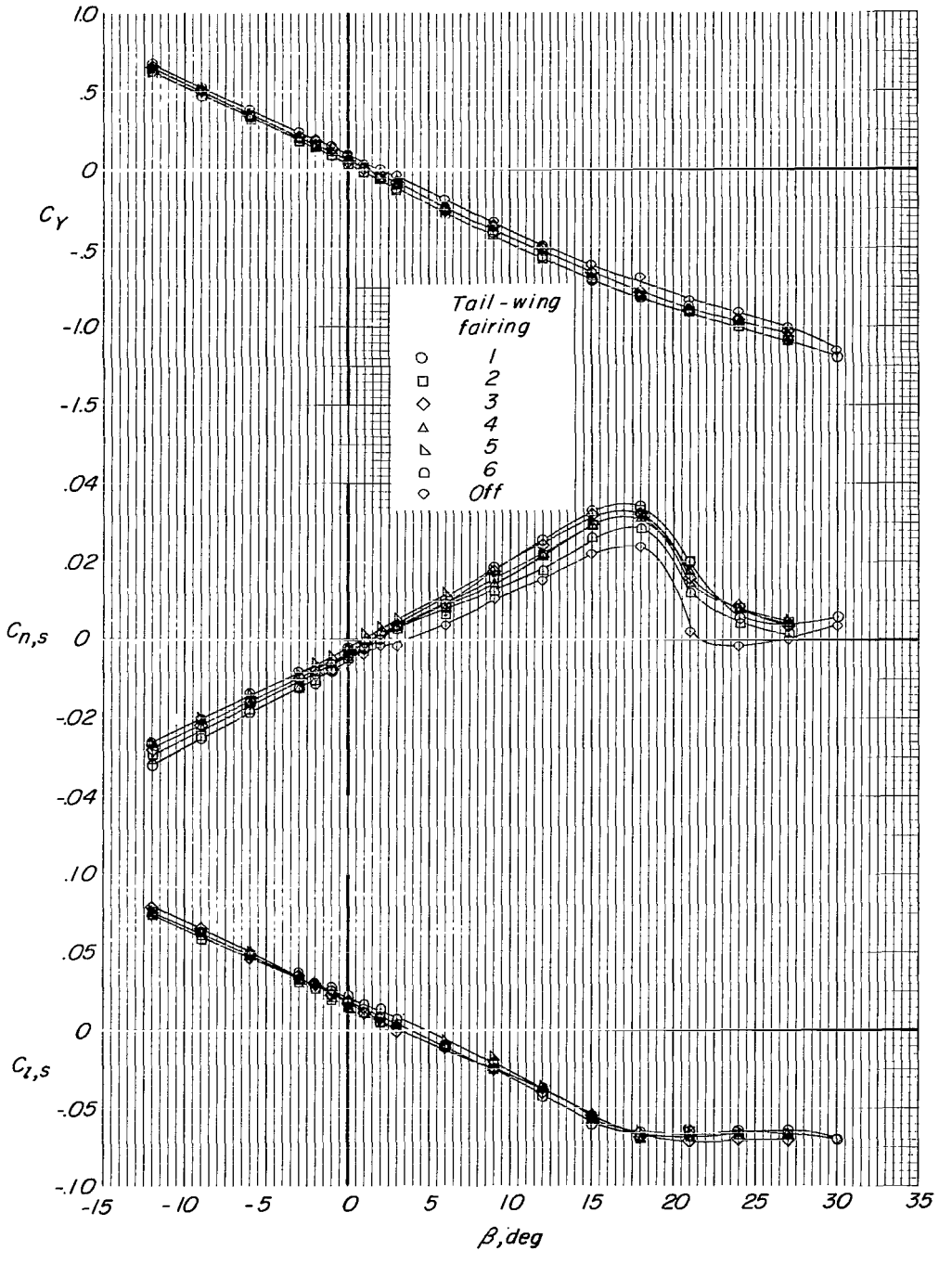

(a) $\alpha = 0^0$.

Figure 23.- Effect of tail-wing fairing size and shape on sideslip characteristics. $\delta_{D,F} = 2^0$; $\delta_{D,R} = -3^0$; $\delta_{V,F} = \delta_{V,R} = 0^0$; vertical tail 4; H_2; $i_t = 0^0$; propellers windmilling.

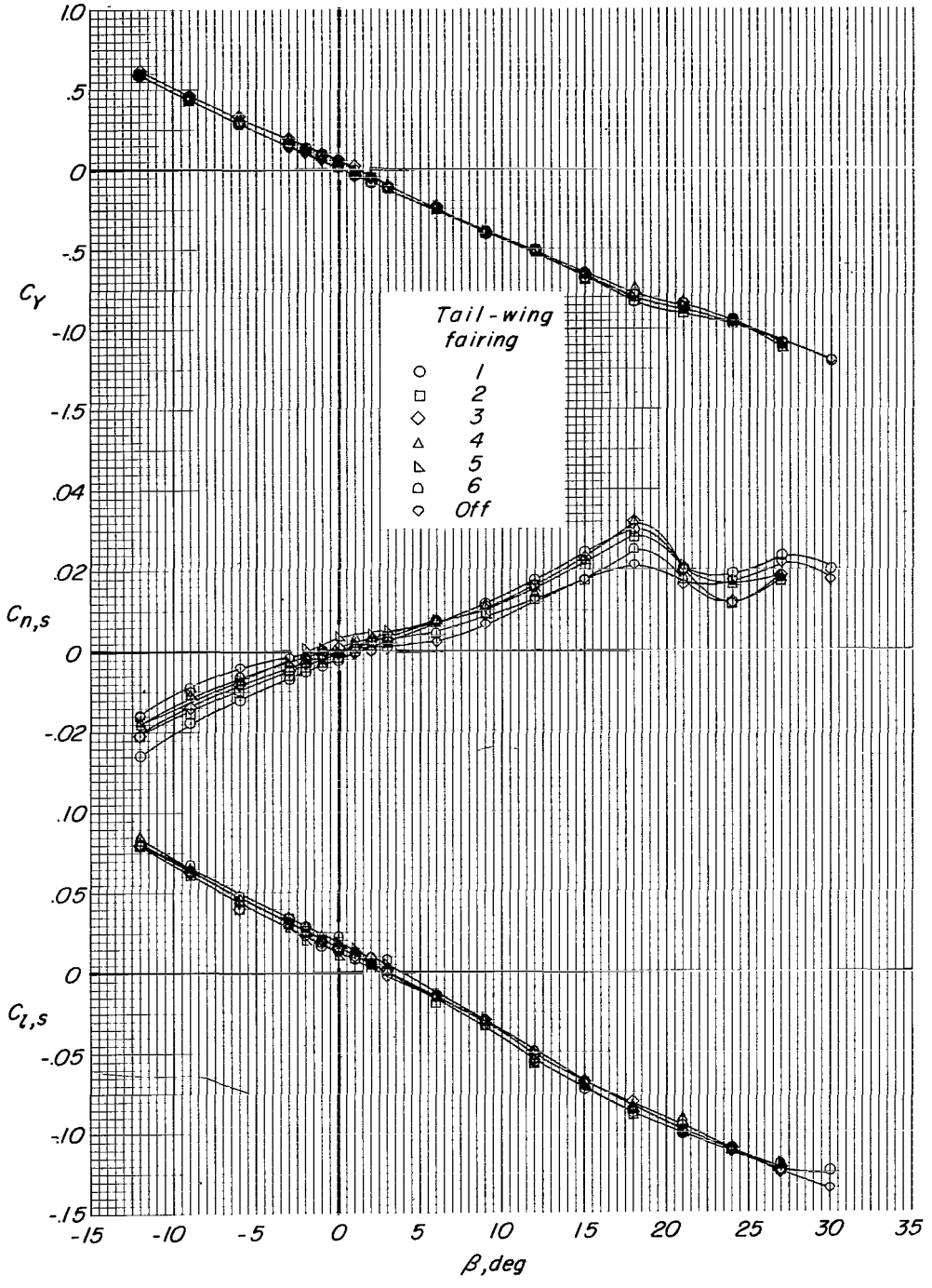

(b) $\alpha = 8^{\circ}$.

Figure 23.- Concluded.

NASA-Langley, 1968 — 2 L-5582